POLITECNICO DI TORINO
Repository ISTITUZIONALE

Limiting factors for planar solid oxide fuel cells under different trace compound concentrations

Original
Limiting factors for planar solid oxide fuel cells under different trace compound concentrations / Papurello, D., Lanzini, A., Drago, D., Leone, P., Santarelli, M.. - In: ENERGY. - ISSN 0360-5442. - 95:(2016), pp. 67-78. [10.1016/j.energy.2015.11.070]

Availability:
This version is available at: 11583/2648242 since: 2016-09-12T15:54:58Z

Publisher:
Elsevier Ltd

Published
DOI:10.1016/j.energy.2015.11.070

Terms of use:

This article is made available under terms and conditions as specified in the corresponding bibliographic description in the repository

Publisher copyright
Elsevier postprint/Author's Accepted Manuscript

© 2016. This manuscript version is made available under the CC-BY-NC-ND 4.0 license http://creativecommons.org/licenses/by-nc-nd/4.0/.The final authenticated version is available online at: http://dx.doi.org/10.1016/j.energy.2015.11.070

(Article begins on next page)

19 November 2026

Limiting factors for planar solid oxide fuel cells under different trace compound concentrations

1 *Davide Papurello*[*], *Andrea Lanzini, Davide Drago, Pierluigi Leone, Massimo Santarelli*

2 *Department of Energy (DENERG), Politecnico di Torino, Corso Duca degli Abruzzi, 24, 10129, Turin, Italy.*

3 *Corresponding author. Tel.:+393402351692. *Email address*: davide.papurello@polito.it

Abstract

The present work investigates the performance of anode supported solid oxide fuel cells under the influence of different trace compounds. Electrochemical impedance spectroscopy (EIS) has been used to deconvolute the impedance spectra of an SOFC in order to identify the main losses. The impact of single and double contaminants on the SOFC performance has also been investigated. Typical biogas trace contaminants, obtained after a clean-up stage, such as sulfur, chlorine, aromatic compounds and siloxanes, have been taken into consideration. The results show how the ohmic contribution is almost independent of the H_2S concentration. H_2S acts mainly on the polarization losses and especially on the mass transport resistance. The impact of HCl on the SOFC performance is mainly connected to the charge transfer process. D4, as the model compound for siloxanes, already acts on SOFC performance at ppb(v) levels. The polarization losses have been influenced the most, and the largest increase has been recorded for the low frequency term, R_{low}, related to the mass transport resistance for naphthalene and toluene. H_2S, introduced with other contaminants, causes the instantaneous deterioration of the SOFC performance and the more the types of contaminants co-fed to the SOFC, the larger the initial anode degradation.

Keywords

Trace compounds, Biogas, SOFC, anode based fuel cell, Electrochemical Impedance Spectroscopy (EIS), Nyquist diagram.

Nomenclature

ASC, Anode Supported Cell;

ASR, Area Specific Resistance;

CPE, Constant Phase Element;

DIR, Direct Internal Reforming;

EIS, Electrochemical Impedance Spectroscopy;

FU, Fuel Utilization;

OCV, Open Circuit Voltage;

OFMSW, Organic Fraction of Municipal Solid Waste;

POx, Partial Oxidation;

ppb(v), parts per billion by volume;

ppm(v), parts per million by volume;

Re, ohmic resistance;

Rp, polarization resistance;

S/C, Steam to Carbon ratio;

SOFC, Solid Oxide Fuel Cell;

TCE, Tetrachloroethylene;

TOFC, TOpsoe Fuel Cell;

TPB, Three Phase Boundary;

VOCs, Volatile Organic Compounds;

WGS, Water Gas Shift;

WWTPs, Waste Water Treatment Plants.

Introduction

Among all the different fuel cells that are available, Solid Oxide Fuel Cells (SOFCs) can be considered as the most flexible energy generators in relation to fuel selections [1][2][3]. SOFC systems offer electrical efficiencies of more than 50%, even for small-case units with low calorific fuels [1][4]. Various types of fuels can be adopted, from fossil fuels to biogenous fuels [5][3][1][6][7]. The possible fossil fuels for SOFCs include kerosene, gasoline, natural gas, coal gas and liquid petroleum gas. Fuels from renewable matrices, mostly biogas, are appropriate for high temperature fuel cell energy production. Biogenous fuels, with respect to fossil fuels, allow the global warming potential impact to be reduced in order to meet EU 20-20-20 requirements. The

54 European climate and energy change protocol, EU 20-20-20, incorporates these points in order to
55 reduce the energy demand from fossil fuels that are not renewable, and to increase the exploitation
56 of resources that are already distributed locally [5][8]. However, these practical fuels contain minor
57 constituents as impurities. These impurities are mainly volatile organic compounds (VOCs), which
58 are contained in a biogas mixture that originates from the dry anaerobic digestion of the organic
59 fraction of municipal solid waste (OFMSW) [9]. As reported by Papurello et al., (2014, 2015,
60 2015(1)), a gas cleaning section is mandatory to feed a SOFC generator due to the stringent VOC
61 requirements currently in force, which are especially rigorous as far as sulfur, chlorine and siloxane
62 compounds are concerned [1,10,11]. Sigot et al., (2015) have provided another example of sulfur
63 and siloxane removal for biogas conversion in a solid oxide fuel cell [12] in which the SOFC
64 tolerance limits for trace contaminants have been matched with already available gas cleaning
65 technologies. Sasaki et al., (2011) investigated the chemical degradation of SOFCs with trace
66 compounds through long-term poisoning tests of up to 3000 h, in which microstructural
67 observations were considered [5]. H_2S, PH_3, Cl_2 and D_5 were among the trace compounds that
68 Sasaki et al., (2011) investigated, together with their effect on an NiScSz anode based fuel cell. The
69 compounds with the most detrimental effects on SOFC performance are H_2S, HCl and siloxanes
70 [5,13–18]. As reported by Haga et al. (2008), D5 was selected as the model compound for
71 siloxanes, and 10 ppm(v) was demonstrated to be fatal for SOFCs [19]. No studies have been
72 conducted on siloxanes at ultra-low concentrations, even though they seem to have an important
73 influence on cell performances at the ppm(v) level [20]. In order to conduct a detailed investigation
74 into the effect of VOCs on the performance of SOFCs, proper testing and modeling tools have to be
75 identified, especially considering the remarkable growth in SOFC pilot plant applications [1].

76 These following methods have been used to detect the performance limiting factors of an in-
77 operating fuel cell. A powerful method adopted to analyze fuel cell operation and diagnostics is
78 electrochemical impedance spectroscopy (EIS) [21–27]. The use of EIS analysis as a diagnosis tool

is well known at a laboratory level. EIS analysis could be adopted for the on-line diagnostics of operating fuel cell stacks in order to follow and to investigate the SOFC performance of real machines. The other possible methods that could be used as alternatives to investigate cell performance losses could be detrimental for cell operation. For instance, if I-V curve analysis is adopted for the evaluation of the area specific resistance (ASR) for each test condition, detrimental problems could arise related to the current density variation and these could compromise the integrity of the entire test. Leone et al., (2013) conducted an interesting study on the limiting factors for a planar SOFC under different flow and temperature conditions with EIS analysis [27]. The EIS analysis of a fuel cell is carried out under transient and almost equilibrium conditions in order to avoid causing rapid changes in the current [23,26–31] . Two possible conditions can be selected: an open circuit voltage (OCV) or a current density value. In the latter case, polarization of the cell becomes an independent variable. The potential difference between the thermodynamic open circuit potential and the operational potential is the polarization or the overpotential of a fuel cell [32]. This voltage loss is a function of the current density, and it mainly depends on the processes that occur during fuel cell operation. It is generally difficult to interpret the obtained impedance diagrams. For this reason, a specific method is adopted for the EIS spectra deconvolution to separate the ASR value into the different contributions that describe the cell losses related to the cell functional layers [23,28–31]. Three main potential losses [33] can be recognized and connected to: (i) the ohmic resistances of the materials and interfaces due to the transport of ions and electrons through the materials; (ii) concentration polarizations that are caused by the resistance to fuel and oxidant mass transport through the electrodes; (iii) activation polarizations related to the electrochemical reactions of the electrolyte/electrodes. With these techniques, impedance diagrams can at least provide a breakdown of the total loss (ASR). The ASR value can be divided into ohmic resistance, Re, measured at high frequency, and polarization resistance, Rp, measured at medium and low frequencies, reflecting losses due to chemical, electrochemical, and transport processes.

The goal of this work was to investigate cell performance losses related to the different trace compound concentrations contained in a biogenous fuel adopting an EIS analysis.

Materials and methods

A simulated gas mixture representing different fuel conditions has been considered with different trace compounds. Experiments were performed with nickel-based anode supported solid oxide fuel cells (ASC). Three circular planar type seal-less anode supported cells were used. The tested cells have a diameter of 80 mm and a screen printed cathode of 78 mm:

1. the ASC700 cell (SOFCpower, Italy) consists of a 240-260 µm porous Ni/8YSZ anode support, a 8-10 µm dense electrolyte YSZ and a 50-60 µm porous GDC/LSCF cathode bilayer;
2. the ASC4 cell (H.C. Starck, Germany) consists of a 465-555 µm porous NiO/YSZ anode support with a 5-10 µm NiO/YSZ porous active layer, a 4-6 µm dense electrolyte YSZ and a 2.4 µm YDC blocking layer plus a 30-60 µm porous LSCF cathode layer;
3. the TOFC cell (Topsoe fuel cell, Denmark) consists of a porous Ni/8YSZ anode support, a dense electrolyte YSZ and a porous CGO/LSCF cathode bilayer.

The design of SOFC supported anodes has been extensively investigated over the last few years because of their relatively easy of manufacturing and potentially high power density. Moreover, the cathode material of LSCFs has been investigated for intermediate temperature SOFC applications [23,28–33] and a polarization resistance of 0.018 Ωcm^2 has been shown at 750 °C as well as relative stability (400% of increased polarization resistance in 700 h) [34].

Planar SOFCs have been used for the experimental test session. They were fed with synthetic biogas and syngas obtained by mixing pure gas feeds from CH_4, CO_2, CO, N_2 and H_2 cylinders (Siad, Italy). A variable concentration of trace compounds was added to the fuel stream. If it is not explicitly reported the trace compound was added to the fuel mixture and the EIS analysis was conducted after a stabilization time within 2 h. An extensive experimental campaign was scheduled

and the details are reported in Table 1. The experiments were performed by varying the fuel composition and the trace compound concentrations in order to investigate SOFC losses.

Pollutant test	Conc. Range (ppm(v))	Cell adopted	H_2 (ml min^{-1})	CO (ml min^{-1})	CO_2 (ml min^{-1})	CH_4 (ml min^{-1})	N_2 (ml min^{-1})	H_2O (ml min^{-1})	H_2O (g h^{-1})	T (°C)	FU	Fuel condition
H_2S high conc.	0.84-6.4	ASC700	151.5	136.4	68.2	15.2	386.4	60.2	2.9	750	30.0	Syngas
H_2S high conc.	0.8-6.7	ASC4	250	0	41.7	62.5	0	124.5	6	750	20.9	DIR 50% biogas
H_2S low conc.	0.078-0.174	ASC4	250	0	41.7	62.5	0	124.5	6	750	20.9	DIR 50% biogas
HCl	1-1000	ASC700	348	133.7	62.1	5		136.5	6.58	750	29.9	biogas reformate
D4	0.11-1.92	TOFC	348	133.7	62.1	5		136.5	6.58	750	20.8	biogas reformate
C_7H_8	3.8-24.2	ASC700	151.5	136.4	68.2	15.2	386.4	269.8	13	750	30.0	Syngas
$C_{10}H_8$	0-9.3	ASC700	151.5	136.4	68.2	15.2	386.4	269.8	13	750	30.0	Syngas
C_2H_2	371.2	ASC700	250	0	42	63	0	0.0	0	750	20.8	POx 50% biogas
H_2S	1.34	ASC700	250	0	42	63	0	0.0	0	750	20.8	POx 50% biogas
H_2S +C_2Cl_4	0-4/1.7-0	ASC700	151.5	136.4	68.2	15.2	386.4	269.8	13	750	30.0	Syngas
H_2S +C_2H_2	1.34/371.2	ASC700	250	0	42	63	0	0.0	0	750	20.8	POx 50% biogas
H_2S + C_7H_8	4/3.7	ASC700	151.5	136.4	68.2	15.2	386.4	269.8	13	750	30.0	Syngas

Table 1 – Test conditions.

The oxidant flow (air) at the cathode side was 0.5 Nl min^{-1} during the start-up and shut-down procedures, otherwise it was fixed at 1.2 Nl min^{-1} for all the performed experiments. The fuel gas mixtures, contained in certified gas bottles (Siad spa, Italy), were fed to the anode and regulated by means of mass flow controllers (Bronkhorst, The Netherlands). All the cells were first activated with hydrogen. The fuel mixture was restored to clean conditions after each poisoning phase with the trace compound of interest. Four gas mixtures were adopted for the experimental tests:

1. A syngas mixture, used to represent a wood gasification plant.
2. A direct internal reforming case (DIR 50%), used to represent a mixture of biogas reformed internally with steam (50% vol.-electrochemical), while the remaining part was reformed externally.
3. A partial oxidation case (POx 50%), used to represent a biogas mixture reformed internally with air (50% vol.-electrochemical), while the remaining part was reformed externally.

4. A biogas reformate case, used to represent a biogas mixture completely reformed externally in a steam reformer with a steam-to-carbon (S/C) ratio equal to 2.

The electrochemical characterization of the fuel cell was carried out with an electronic load (Kikusui Electronics Corp., Japan) in conjunction with an additional power supply in current-following mode (Delta Elektronica, The Netherlands). Electrochemical impedance spectroscopy analyses were performed using a GAMRY FC350 in the 10 Hz to 300 kHz range. The oven temperature was kept constant at 750 °C. Temperature control was provided by a thermocouple placed in the center of the anodic ceramic housing, 1 mm from the anode surface. The seal-less cell arrangement was adopted to allow the excess fuel and oxidant in the outer border of the cell to combust. Nickel and platinum double meshes were used for current collection at the anode and cathode electrodes, respectively.

Results

The electrochemical impedance analysis results are reported in this section. The analysis focused on a more detailed investigation of cell performance, which was affected by the trace compounds through the deconvolution of the impedance spectrum. The Nyquist diagrams that were obtained for the different measurement conditions are also reported. The behavior of the cell was simulated by means of the equivalent electrical circuit shown in figure 1, and the impedance data were analyzed at different trace compound concentrations. The equivalent circuit is constituted by the ohmic resistance, Re and two parallel combinations of a resistance and a constant phase element, CPE [25]. The polarization resistance, Rp, is obtained by summing the R_{high} and R_{low} resistances. The first term is related to the electrochemical processes that take place at the electrodes, whereas the second contribution accounts for the mass transport phenomena [35].

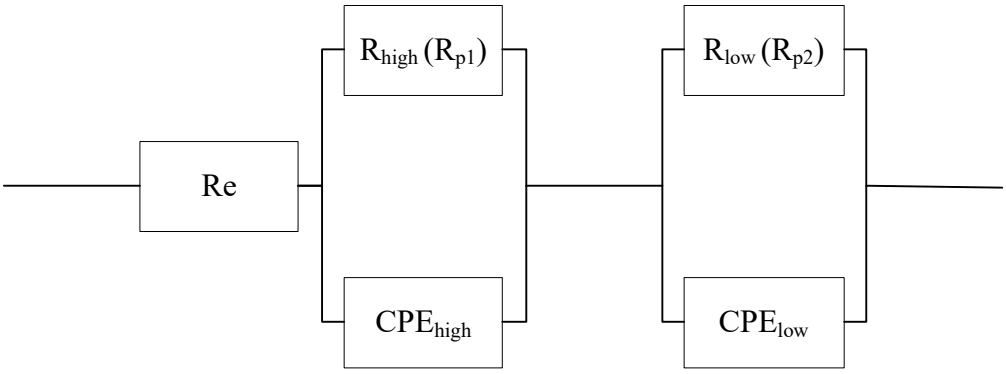


Figure 1 – Equivalent fuel cell circuit: Re, R_{high} and CPE_{high} are associated with the high frequency semi-circle, R_{low} and CPE_{low} with the low frequency semi-circle.

The influence of Hydrogen sulfide on SOFC performance

The main pollutant compound for SOFC operation is widely recognized to be H_2S [3,13–15,36–38]. As reported elsewhere, the H_2S concentration is one of the main trace compounds contained in a biogas mixture [9]. Four separate tests were carried out with three different commercial cells: ASC4, ASC700 and TOFC. The operating temperature was fixed at 750 °C, while the current density was fixed at 0.32 A cm^{-2}. The first test was carried out in order to investigate the impact of H_2S on cell performance, considering a concentration ranging from 0.8 to 6.4 ppm(v), with a mixture that simulates a syngas produced from a wood gasifier. This concentration range has here been named "high concentration", as it is high compared to the limit H_2S concentration value currently fixed for SOFCs, which is around 1 ppm(v) [5,6,39–41]. The second test considered the same H_2S concentration range in order to simulate the partial direct internal reforming (DIR 50%) of a biogas mixture derived from, for example, an anaerobic digestion process. In the next step, the H_2S test was conducted with the goal of testing the H_2S concentration limit and studying its impact on SOFCs in a POx biogas mixture. Finally, a low H_2S range, from 78 to 174 ppb(v), was tested to identify any changes in SOFC performance.

High H_2S concentration test

Figure 2 depicts the Nyquist diagram for the ASC700 cell with a variable H_2S concentration, while figure 3 shows the Nyquist diagram for the ASC4 cell.

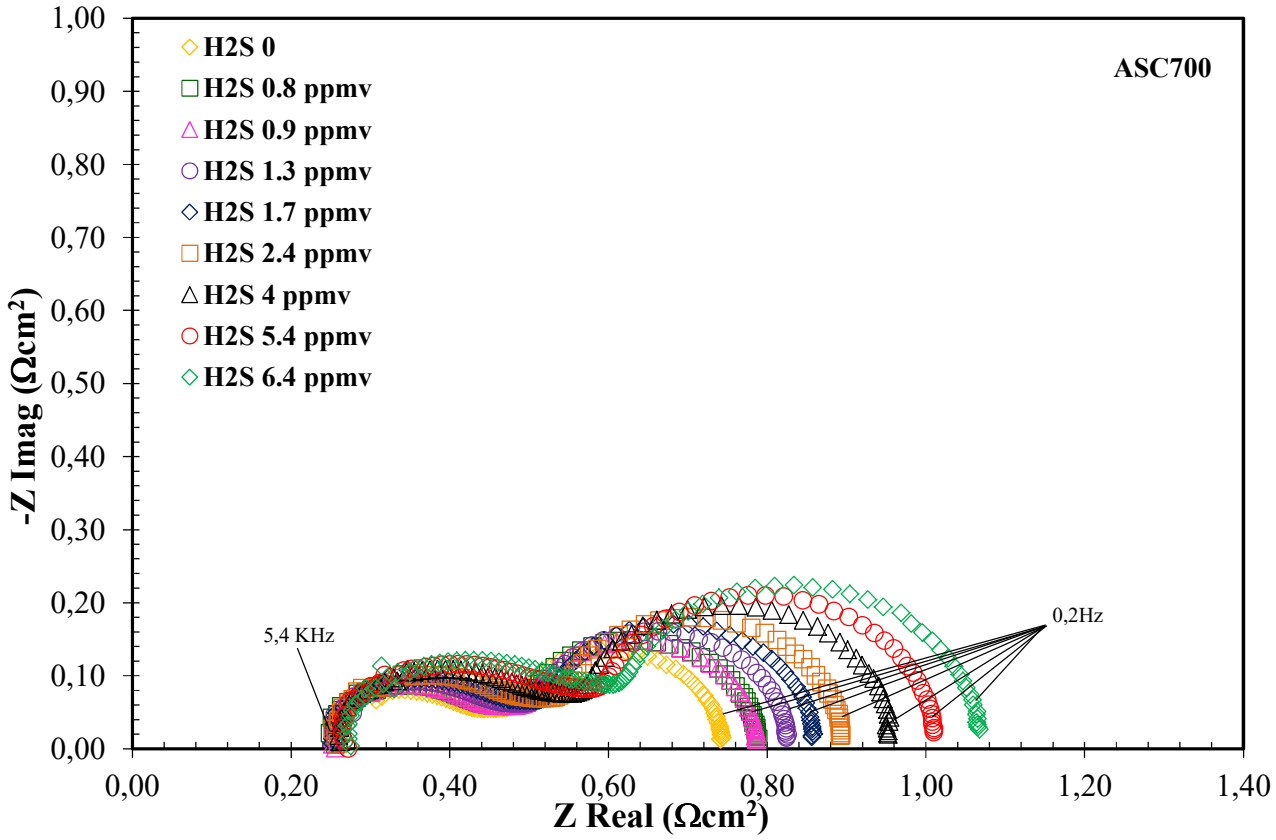


Figure 2 – Nyquist diagram for variations of the H_2S concentration – ASC700.

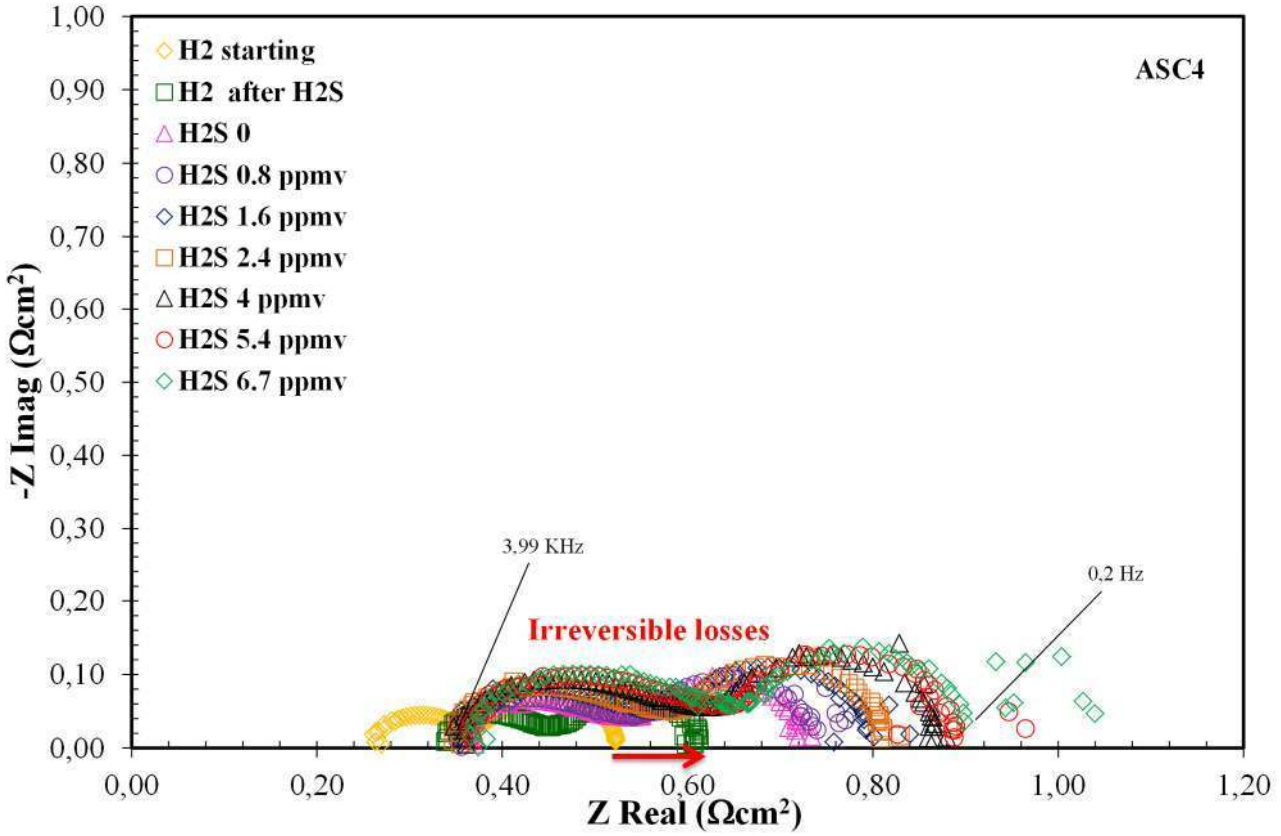
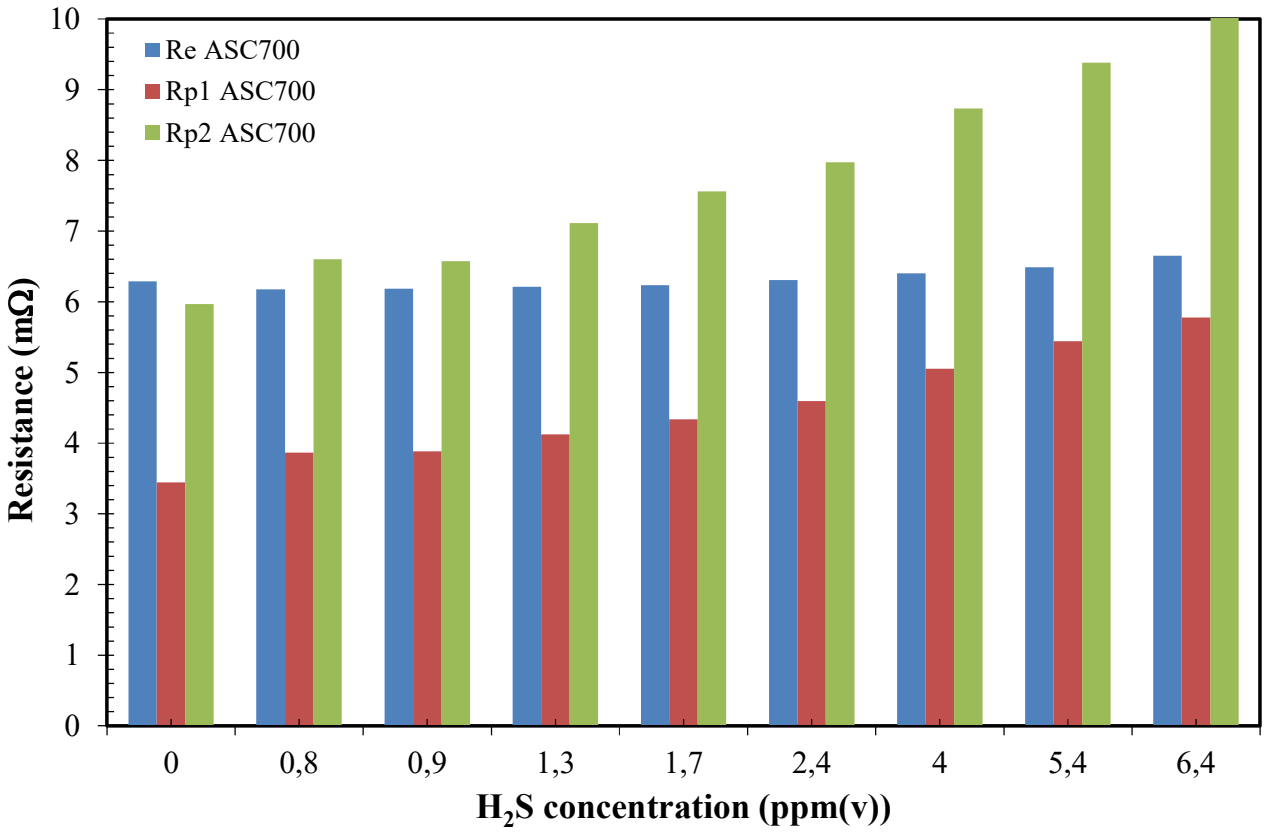


Figure 3 – Nyquist diagram for variations of the H_2S concentration – ASC4.

The ohmic contribution to the ASR value represents the materials and interface resistances due to the transport of ions and electrons through the materials. This value is almost independent of the fuel composition and it is only minimally affected by the H_2S concentration value, as shown in figures 2-3 and 4-5. Comparing the ohmic value of ASC700 and ASC4, it is evident that the latter shows a higher value. This is due to the lower fuel flow compared to the ASC700 case (N_2 content), which causes air backflow. The reason for this air backflow is that the seal-less design could lead to nickel oxidation. The nitrogen content, which on one hand allows nickel oxidation to be avoided, on the other hand, causes a dilution effect of the gas mixture, thereby increasing the total ASR value (see the ASC700 cell results). The H_2S concentration, as reported in figures 2-3 and 4-5, does not cause an important variation of the ohmic resistance value, but instead acts on the R_{high} and R_{low} values. By increasing the H_2S concentration, an increase in the low frequency circle amplitude is obtained, compared to the high frequency circle (see figures 2-3). This result can also be confirmed

202 by observing figures 4-5, where the Rp_2 (R_{low}) trend rises when the H_2S concentration increases.
203 This is due to the mass transport resistance through the electrodes caused by the sulfur blocking
204 sites. An increase in the R_{high} value is also registered when the H_2S concentration rises. This is due
205 to the three phase boundary (TPB) reduction from the nickel active sites which is blocked by the
206 sulfur compound.



207

208 **Figure 4 – Re and Rp values for variations of the H_2S concentration – ASC700.**

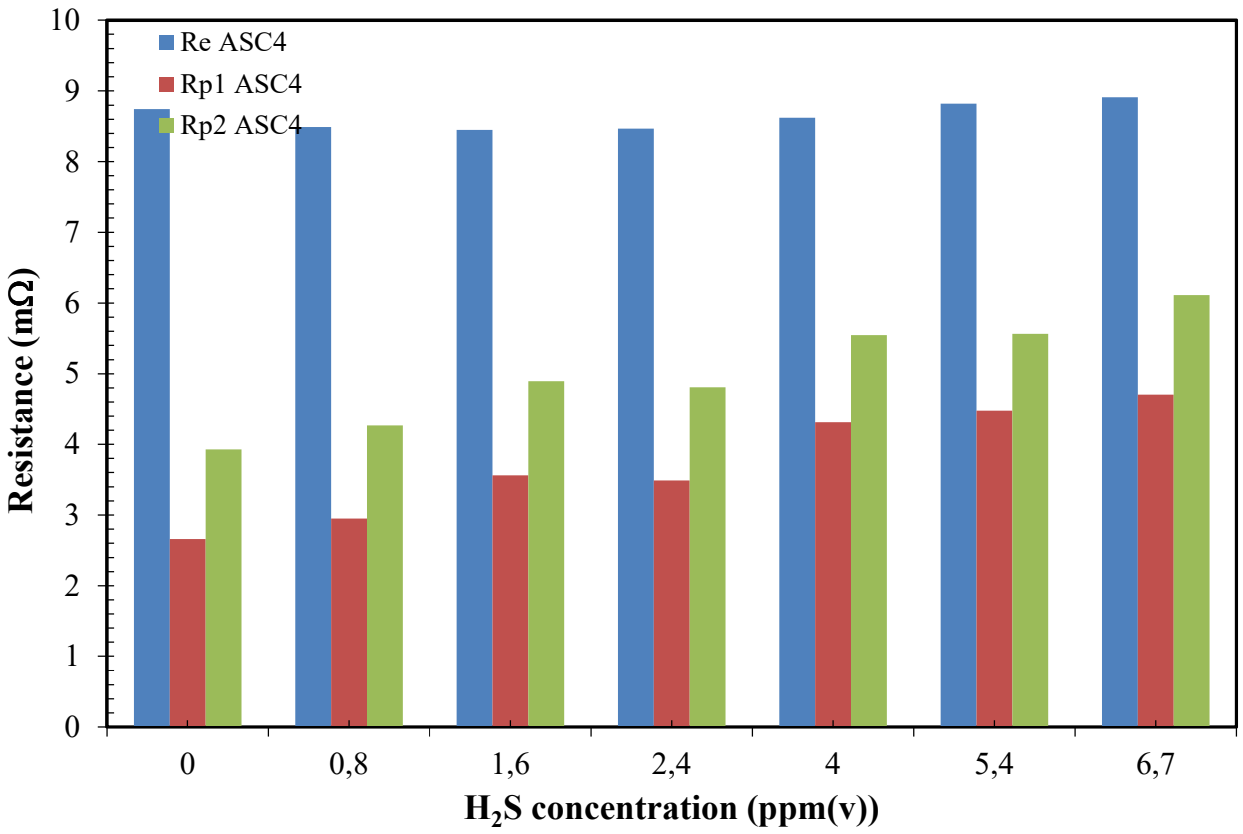


Figure 5 – Re and Rp values for variations of the H_2S concentration – ASC4.

Figure 3 shows that, after the H_2S "high concentration" test, the cell performance is irreversibly affected, as shown by the Nyquist profile for H_2 before and after the H_2S. As reported above, pollutants affect the performance of a SOFC and the voltage potential of a single cell, in terms of electrical power, which is reduced according to the following equation:

$$\Delta P = \Delta R \cdot I^2 \quad \text{(eq.1)}$$

Where ΔP is the power loss due to the variation of the overall resistance of the cell (ΔR), which is obtained from the sum of the ohmic and polarization contributions.

Considering an H_2S concentration in the 0.8 to 6.4 ppm(v) range, the power loss increases by up to 10.7%, compared to the nominal power value. This means that if the exposure time to the pollutants is increased, the electrical power loss will also increase, due to an overall higher ASR value.

<u>H_2S threshold value test</u>

Figure 6 depicts the Nyquist diagram for the POx test, with the threshold concentration value of H_2S fixed at 1 ppm(v) on the basis of results from literature studies. The gas mixture has an important effect on the ohmic value, and a high increase is recorded, compared to the ASC4 case with "high sulfur concentration values". This is due to the amount of air that is added to the reactive fuel sent to the anode side, which may cause combustion and Ni oxidation phenomena. Even at this concentration value, the H_2S concentration influences the polarization losses and, more precisely, the mass transport (R_{low}), and, to a lesser extent, the electrochemical contribution (R_{high}).

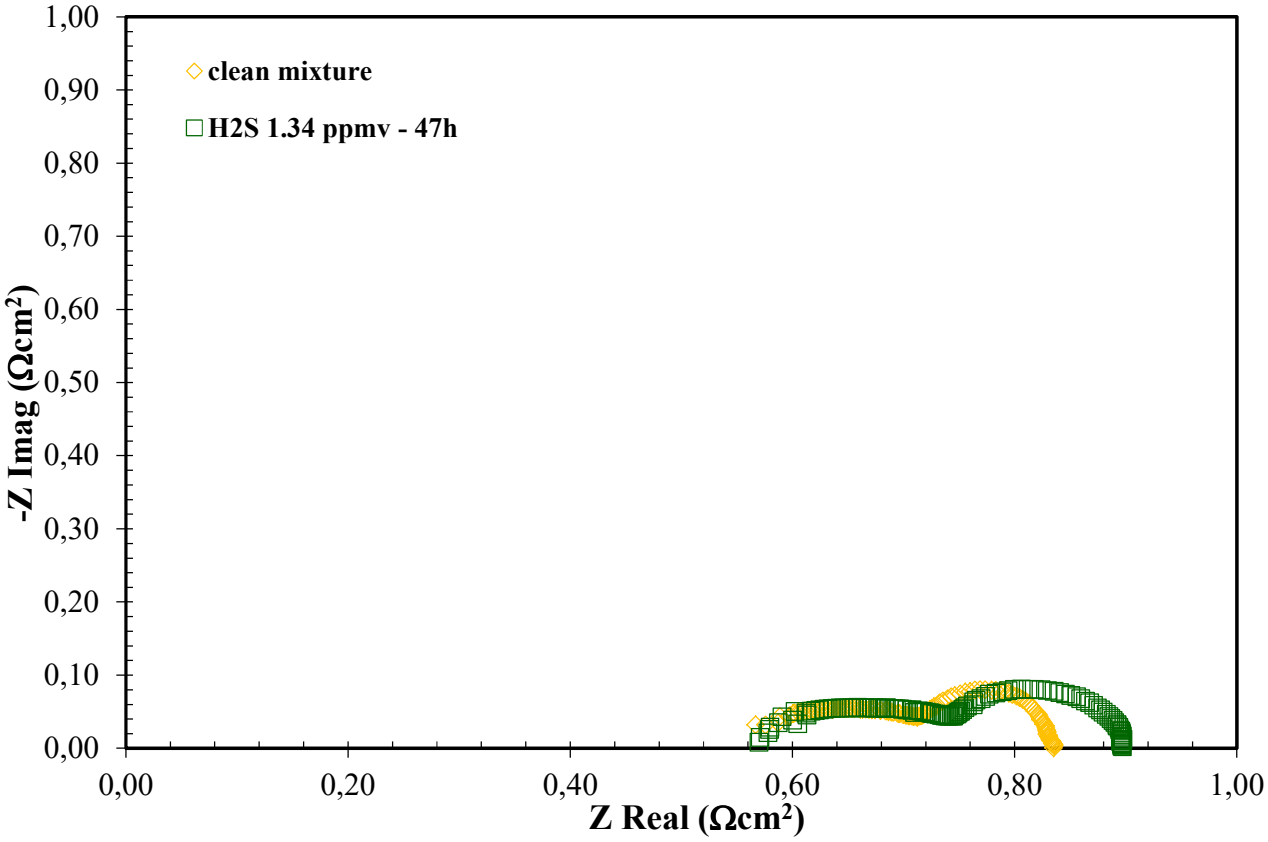
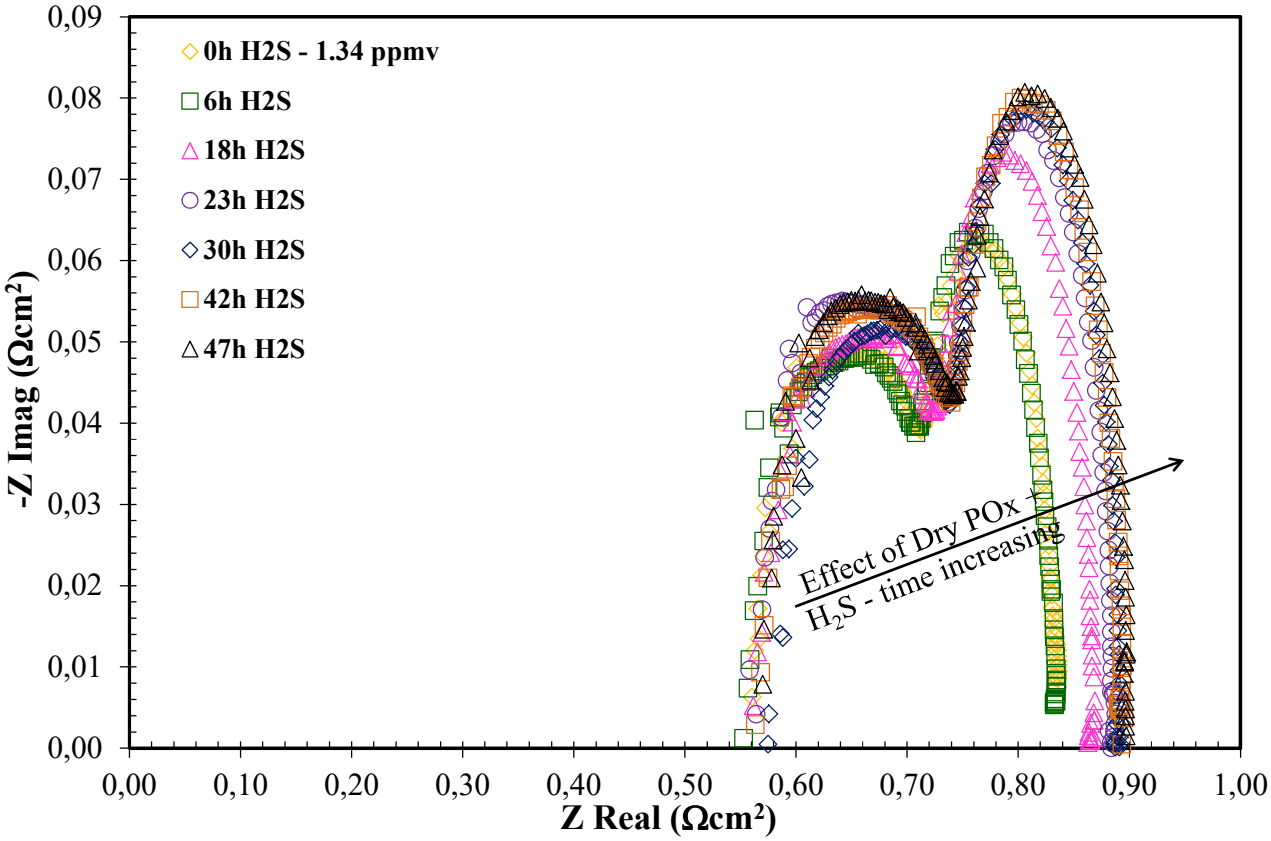


Figure 6 – Nyquist diagram for the H_2S threshold concentration value – ASC700.

It has been found that increasing the exposure time to the H_2S concentration raises the total ASR value. This is mainly due to the mass transport limitation, caused by Sulfur adsorption on active sites, as can be seen by observing the amplitude of the low frequency circle, which increases more than the high frequency circle (see figure 7).

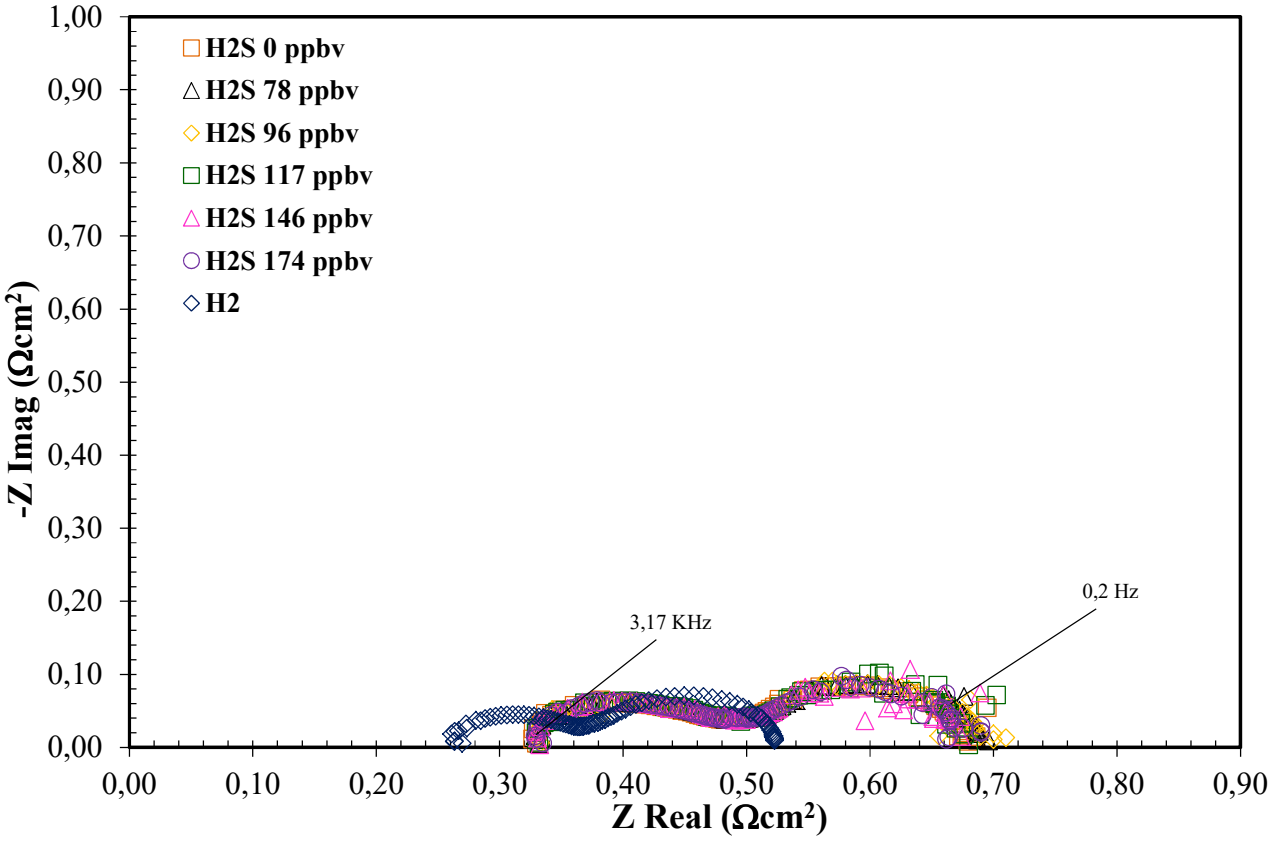


235

236 **Figure 7 – Nyquist diagram for the H_2S threshold concentration value – time variation – ASC700.**

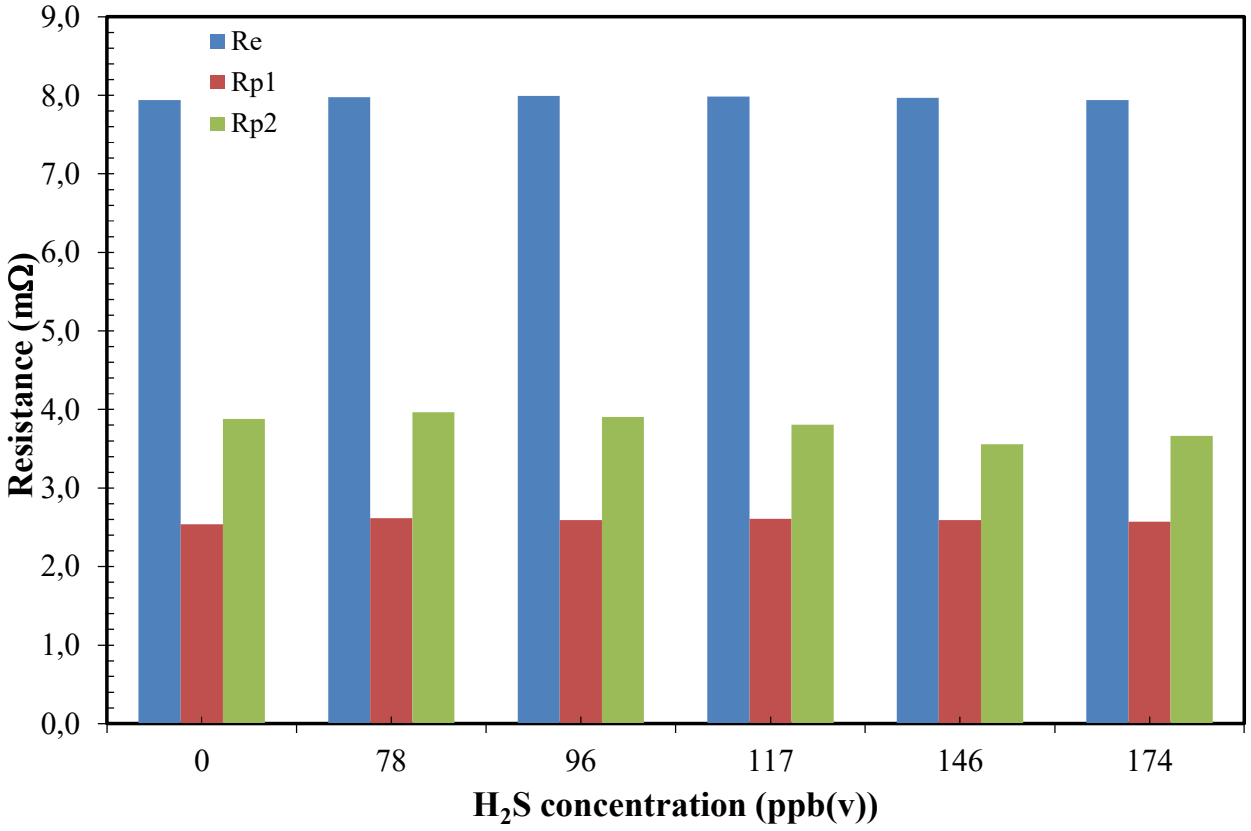
237 Low H_2S concentration test

238 Figure 8 shows the Nyquist diagram for an SOFC cell fed with a gas mixture in which increasing
239 concentrations of H_2S, that is, from 78 ppb(v) to 174 ppb(v), have been added. These H_2S
240 concentration values are below the tolerable threshold value of 1 ppm(v). In fact, Figure 9 shows an
241 almost constant trend for the three different contributions to the ASR value. It appears evident that
242 these H_2S concentrations are well tolerated by the SOFC cell. The ohmic resistance is the main
243 contribution. The ohmic losses account for more than 50% of the total cell resistance, and an
244 enhancement of the performance could be achieved by developing thin layer electrolytes and
245 improved interfaces.



246

247 **Figure 8 – Nyquist diagram for variations of the H_2S "low concentration level" – ASC4.**



248

Figure 9 – Re and Rp values for variations of the H_2S "low concentration level" – ASC4.

Figure 8 shows how the ohmic contribution is low in the H_2 case, compared to the mixture adopted with the pollutants. This is due to the different electrochemical molar flows that are available.

If H_2S concentrations ranging from 78 to 174 ppb(v) are considered, the power loss remains quite stable and ranges from 0.13 – 0.4% of the nominal power value at zero time. This means that if the exposure time to the pollutants is increased, the electrical power loss will remain unchanged.

The influence of Hydrogen chloride on SOFC performance

The dependence of hydrogen chloride on the limiting factors of an anode supported fuel cell has been investigated, considering the addition of a variable concentration of HCl, ranging from 1 ppm(v) to 1000 ppm(v), to the gas reformate mixture. Figure 10 shows the Nyquist diagram with variations in the HCl concentration content in the gas mixture. Increasing the HCl content to 100, 500 or even 1000 ppm(v), does not result in a notable increase in ASR. Figure 11 clearly highlights how, below 20 ppm(v), the HCl concentration does not affect the SOFC performance. The three contributions to the EIS analysis are almost constant. If the HCl concentration is increased from 40 to 1000 ppm(v), the most influential contribution is from R_{high}. The first circle, related to the high frequency, rises and the trace compound concentration therefore increases. This circle is related to the electrochemical processes that occur at the electrodes. In accordance with these results, it has been shown how the Ni catalyst mainly acts by adsorbing HCl. HCl behaves in a similar way to H_2S, but less aggressively; in fact, the tolerable limit appears to be around 20 ppm(v) or more.

These results are in agreement with those of Cayan et al., (2008), where HCl was added to an anode supported fuel cell (NiYSZ/YSZ/LSM) and unstable performance occurred at 40 and 160 ppm(v) [42]. Another study by Aravind et al., (2008) has shown how the impact of 9 ppm(v) of HCl on an NiGDC anode supported fuel cell produced no significant losses [43]. Another study on an NiYSZ cell with HCl + NH_3 (1 ppm(v) + 5000 ppm(v)) has shown no significant performance degradation

[44]. Ammonia, which is often present in coal syngas, does not represent a pollutant for SOFCs, as reported by Cayan et al., (2008) [42]. According to Haga et al., (2008), chlorine compounds react with Ni particles [19]. The formation of $NiCl_2$ may be described by reaction (1):

$$Cl_2(g) + Ni(s) \leftrightarrow NiCl_2(s_o g) \qquad \text{(eq.2)}$$

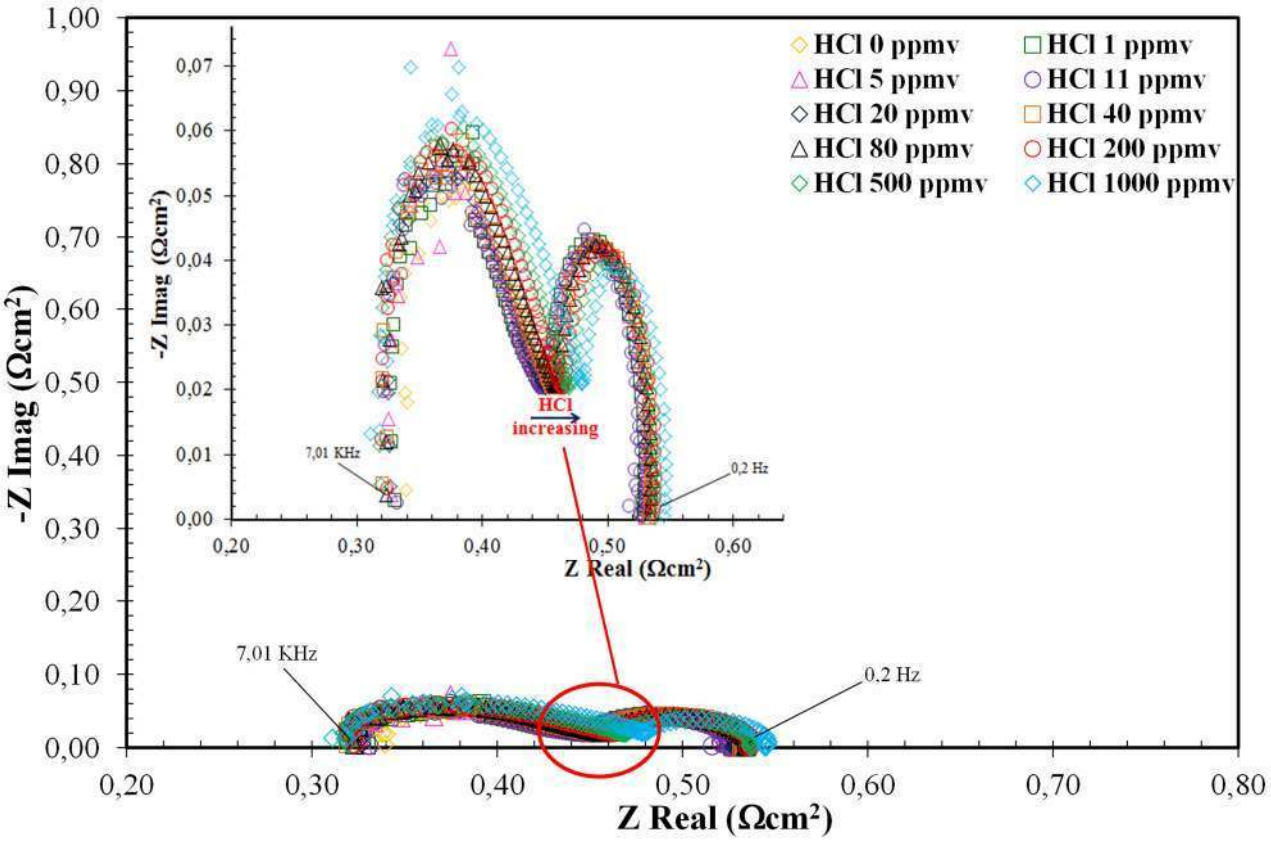


Figure 10 – Nyquist diagram for variations of the HCl concentration – ASC700.

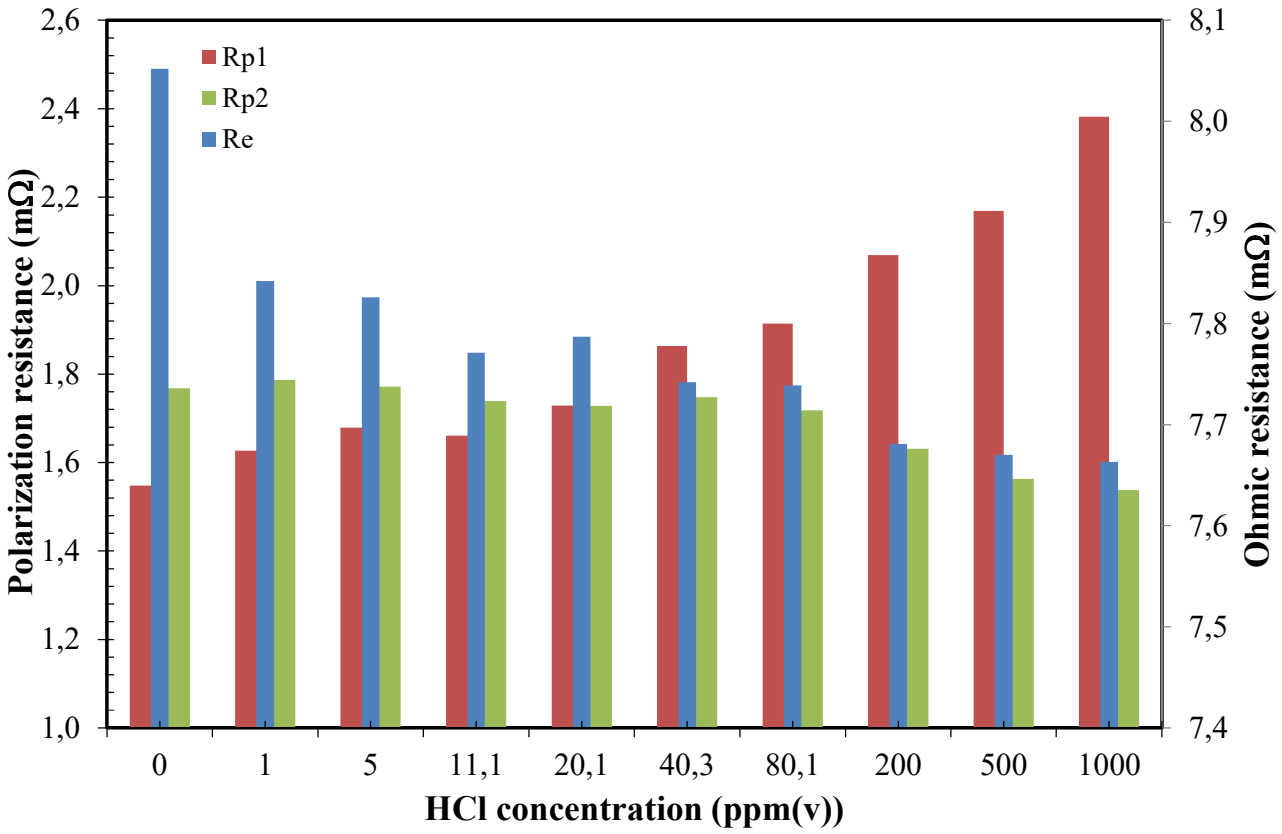


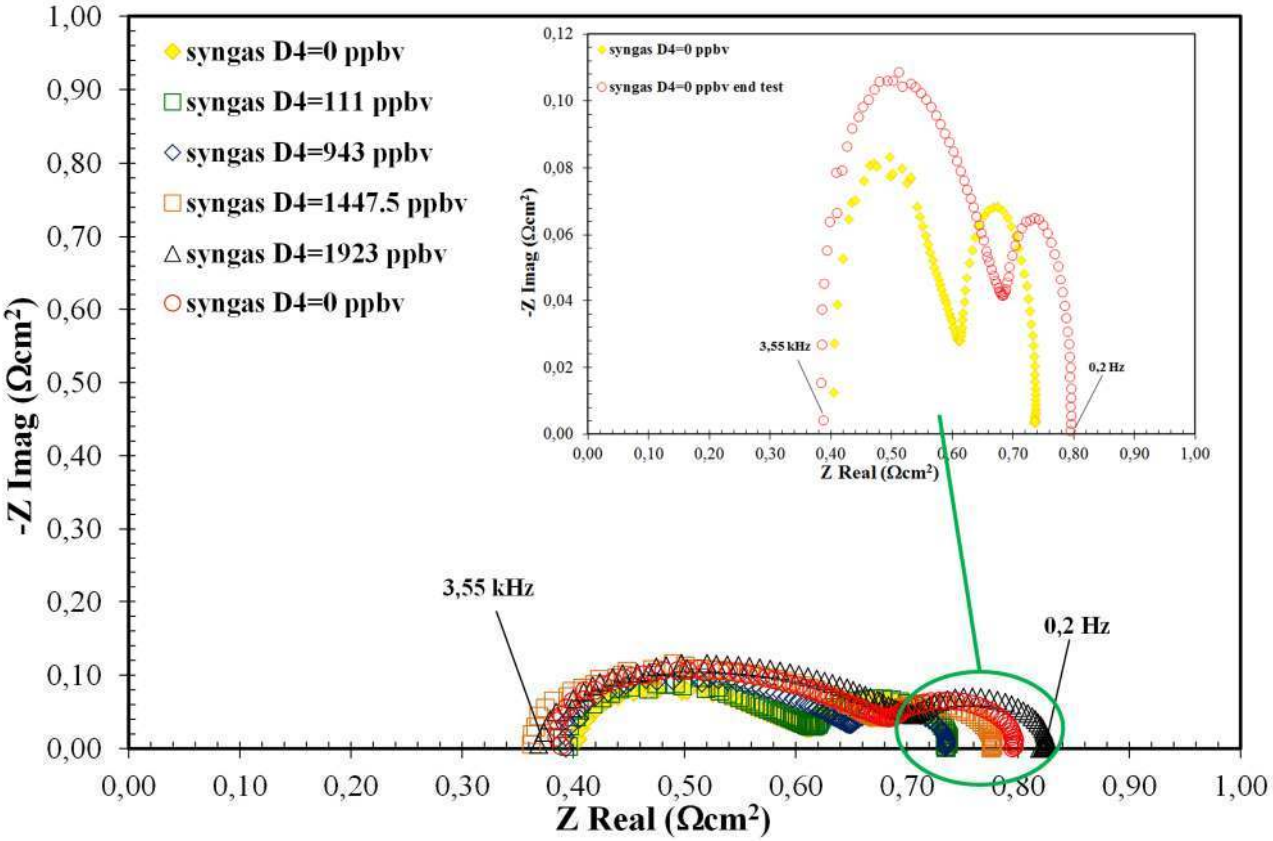
Figure 11 – Re and Rp values for variations of the HCl concentration – ASC700.

If HCl concentrations ranging from 1 to 1000 ppm(v) are considered, the related power losses remain quite stable, and range from 0.17 – 0.3% of the nominal power. This means that if the exposure time to the pollutants is increased, the electrical power loss will remain unchanged. This is due to compensation among the resistance terms, as can be seen in figure 11. The ohmic contribution increases for lower values of the polarization terms at lower HCl concentrations, while the ohmic value decreases and the polarization term increases for higher HCI concentrations.

The influence of Octamethylcyclotetrasiloxane on SOFC performance

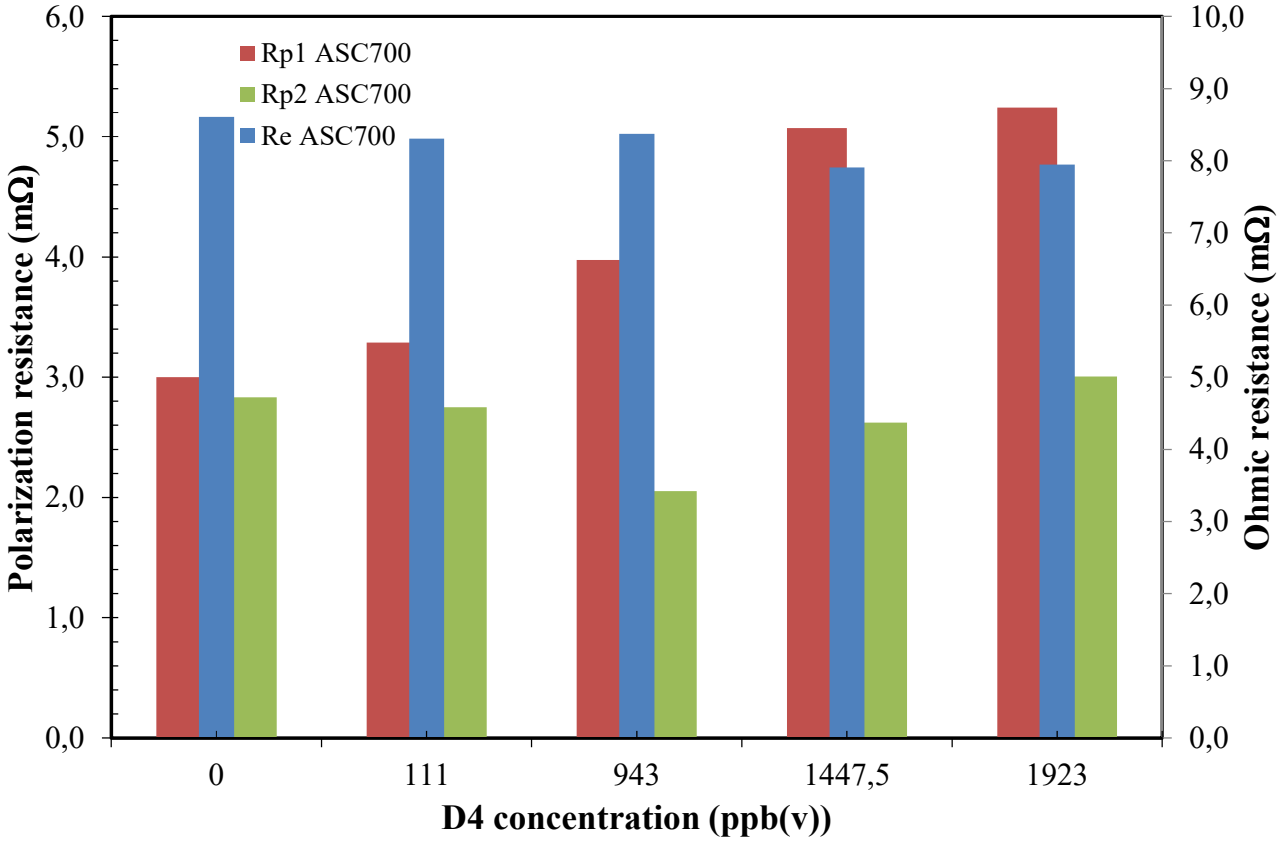
Siloxanes, which are organosilicon compounds, are often contained in the biogas obtained from the anaerobic digestion of sewage sludge and, to a lesser extent, in the biogas of OFMSW. Siloxanes originate from many different industrial processes and consumer products, such as hygiene products, cosmetics and biopharmaceuticals, fuel additives, car waxes, detergents and antifoams [45,46]. The influence of siloxanes on SOFC performance has been studied by a few researchers.

293 Haga et al., (2008) showed that changes in cell voltage occurred when adding 10 ppm(v) of D5 in
294 3%-humidified H_2 at 800 °C, 900 °C, and 1000 °C. The cell voltage decreased gradually in time
295 and, after 30–50 h, resulted in a fatal degradation of the cell performance. This degradation was
296 confirmed from an observation of the formation of SiO_2 (s) in the porous cermet anodes. Madi et al.,
297 (2015) studied the effect of D4 in a single anode based SOFC [20]. The results highlighted an
298 important influence of siloxanes on SOFC performance. In the present study,
299 octamethylcyclotetrasiloxane (D4) was tested with a biogas reformate mixture in a commercial
300 TOFC cell. The concentration ranged from 111 ppb(v) to 1.92 ppm(v). This concentration range
301 was selected to reproduce a possible biogas mixture from a real plant. In fact, data recorded from a
302 real WWTP (SMAT site) showed a D4 concentration that ranged from 0.1 to 0.25 ppm(v) and an
303 L4 concentration that ranged from 0.2 to 0.92 ppm(v). Figure 12 depicts the Nyquist diagram for
304 the TOFC cell fed with a variable D4 concentration. Figure 13 shows the three contributions to the
305 cell losses. As can be seen from the results, if the D4 concentration is increased, the R_{high} value
306 rises, while the other two terms remain constant. The upper right part of Figure 12 shows how the
307 cell performance is irreversibly affected by the D4 test. This is due to silica precipitation, which
308 may cause a decrease in the active triple phase boundary (TPB) areas.



309

310 **Figure 12 – Nyquist diagram for variations of the D4 concentration – TOFC.**



311

Figure 13 – Re and Rp values for variations of the D4 concentration – TOFC.

If D4 concentrations ranging from 111 to 1923 ppb(v) are considered, the power losses increase for D4 values above 1 ppm(v). The power loss ranges from 0.17 – 2.32 % of the nominal power value. This means that if the exposure time to the pollutants is increased, the electrical power loss will also rise, thereby increasing the resistance value, especially as far as the Rp1 term is concerned.

The influence of tars, toluene and naphthalene on SOFC performance

Naphthalene

The direct use of biosyngas may degrade the performance of SOFCs as it contains a number of minor species. Among these trace species, tars have been identified as one of the main concerns in the development of gasifier + SOFC power systems, as they can potentially deactivate the anode catalysts and degrade the performance of the fuel cells through carbon deposition. Aravind et al., (2008) studied the performance of an Ni-GDC anode operation with a naphthalene content of about 110 ppm(v) in an H_2+N_2 matrix. No performance loss was observed and no carbon or other product gas trace constituent contamination of the anodes was found when the SOFC membranes were examined by means of SEM/EDS after the tests [43].

The results reported in this section are in agreement with those of Aravind et al., (2008). An H_2+N_2 mixture with a naphthalene content of 25 ppm(v) does not in fact show any remarkable cell performance decrease (see figure 14). If a syngas mixture is instead considered, the cell performance is influenced to a great extent by the $C_{10}H_8$ content. Figure 14 depicts the Nyquist curves with and without the pollutant concentration. A syngas mixture with 9.3 ppm(v) of $C_{10}H_8$ shows a notable resistance increase.

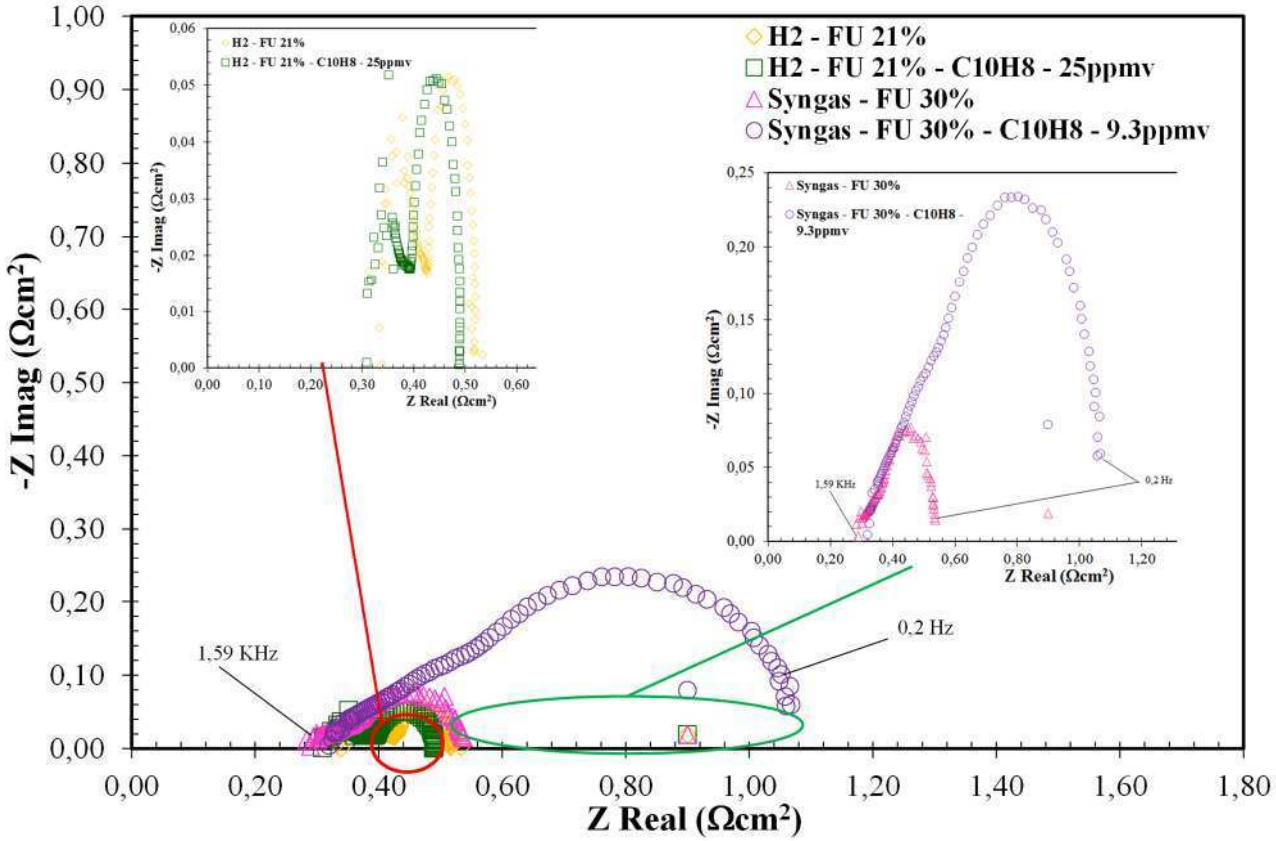
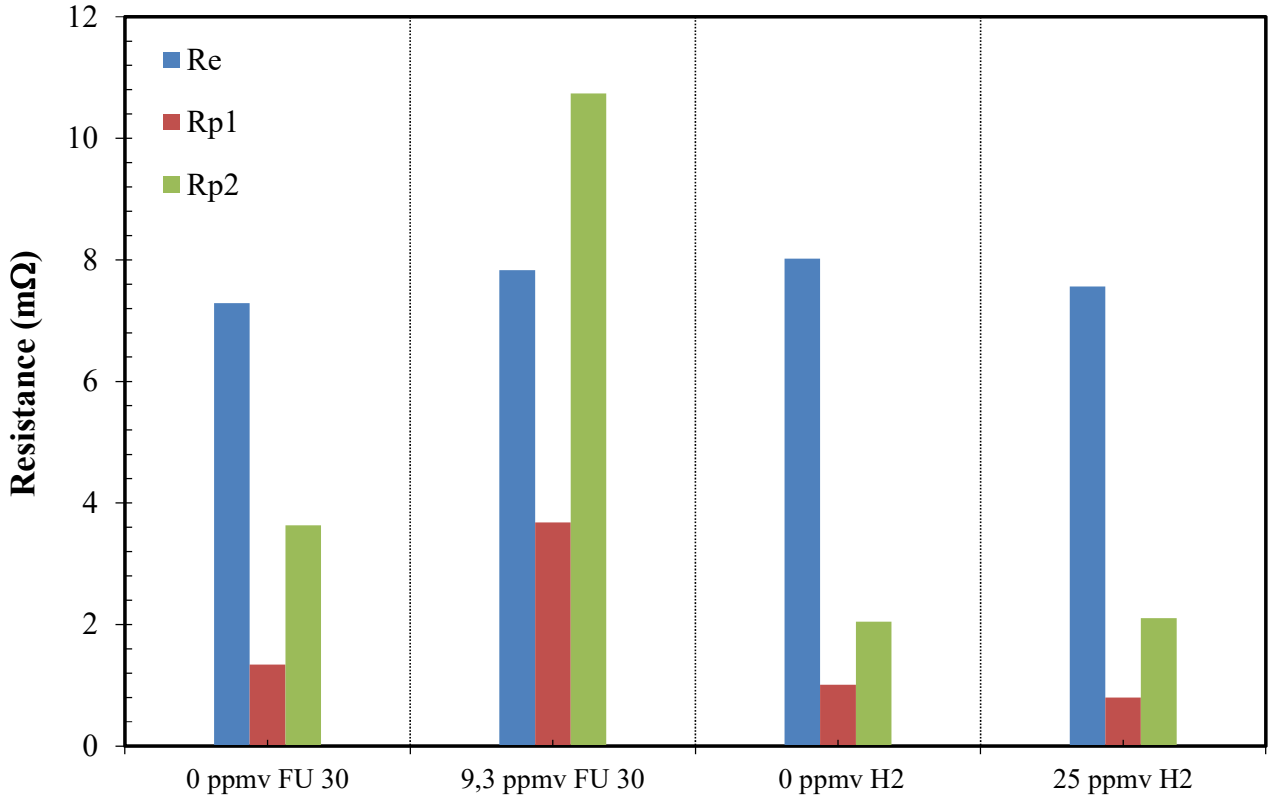


Figure 14 – Nyquist diagram for variations of the $C_{10}H_8$ concentration FU 30% – ASC700.

In figure 15 the three contributions of loss, are showed: at high, medium and low frequency value. For the H_2 case, the ohmic term (Re) and the polarization terms (Rp_1 and Rp_2) remain constant throughout the test. This demonstrates that the $C_{10}H_8$ concentration is not a problem in this condition, as also reported in literature studies [43]. On the contrary, if a syngas mixture and a $C_{10}H_8$ concentration of 9.3 ppm(v) are considered, the polarization losses show a significant increase. The low frequency term (Rp_2), related to the resistance of the mass transport phenomena, shows the largest increase. The high frequency term (Rp_1), related to the electrochemical processes, also increases, but to a lesser extent.



343

344 **Figure 15 – Re and Rp values for variations of the $C_{10}H_8$ concentration – ASC700.**

345 These results show how a low $C_{10}H_8$ concentration could be dangerous, depending on which gas
346 mixture is used to feed the fuel cell. The adsorption and desorption of naphthalene obviously
347 interfere with the reforming of methane and WGS (i.e., CO conversion to H_2) by decreasing the
348 reactive surface of the anodes.

349 If $C_{10}H_8$ concentrations ranging from 0 to 9.3 ppm(v) are considered, the power losses increase to
350 achieve 15.5% of the nominal power value at zero time. This means that, if the exposure time to the
351 pollutants is increased, the electrical power loss will also rise, thereby increasing the resistance
352 value, especially as far as the Rp2 term is concerned.

353 Toluene

354 Toluene is one of the lightest tar compounds and it can be easily detected in biogenous fuels, such
355 as biogas from organic waste [9]. Several studies have investigated the impact of tars on the

performance of SOFCs [18,43,47–49]. Most of these studies have focused on the influence of the tar compound without considering the carbon content in the gas mixture [18,47,48]. Lorente et al., (2012) studied Ni/CGO and Ni/YSZ cells under a tar load of 15 g/Nm^3 (with toluene as the model compound) [18]. In this study, it was found that Ni/CGO shows a better performance (less carbon formation) than Ni/YSZ in the presence of toluene. This result is in agreement with the expected behavior of ceria-based anodes, which have been recognized to be effective in suppressing carbon deposition due to the redox nature of ceria [50]. The amount of carbon deposited on the catalyst was seen to decrease for an increasing steam content in the gas [18]. Toluene, due to the high reactivity of lower weight hydrocarbons, represents the worst case scenario for tar compounds and for this reason it has been selected in the present study. No attempts have been made to study the effects of low toluene concentrations on SOFC performance. The results of tests on low concentrations of toluene, considering a slip over from a gas cleaning section, are presented in this section. The experimental works have demonstrated that if the most dangerous compounds for SOFCs: sulfurs, aromatic, terpenes and carbonyl compounds, are lowered to just a few ppm(v), the performances of SOFCs remain stable [1].

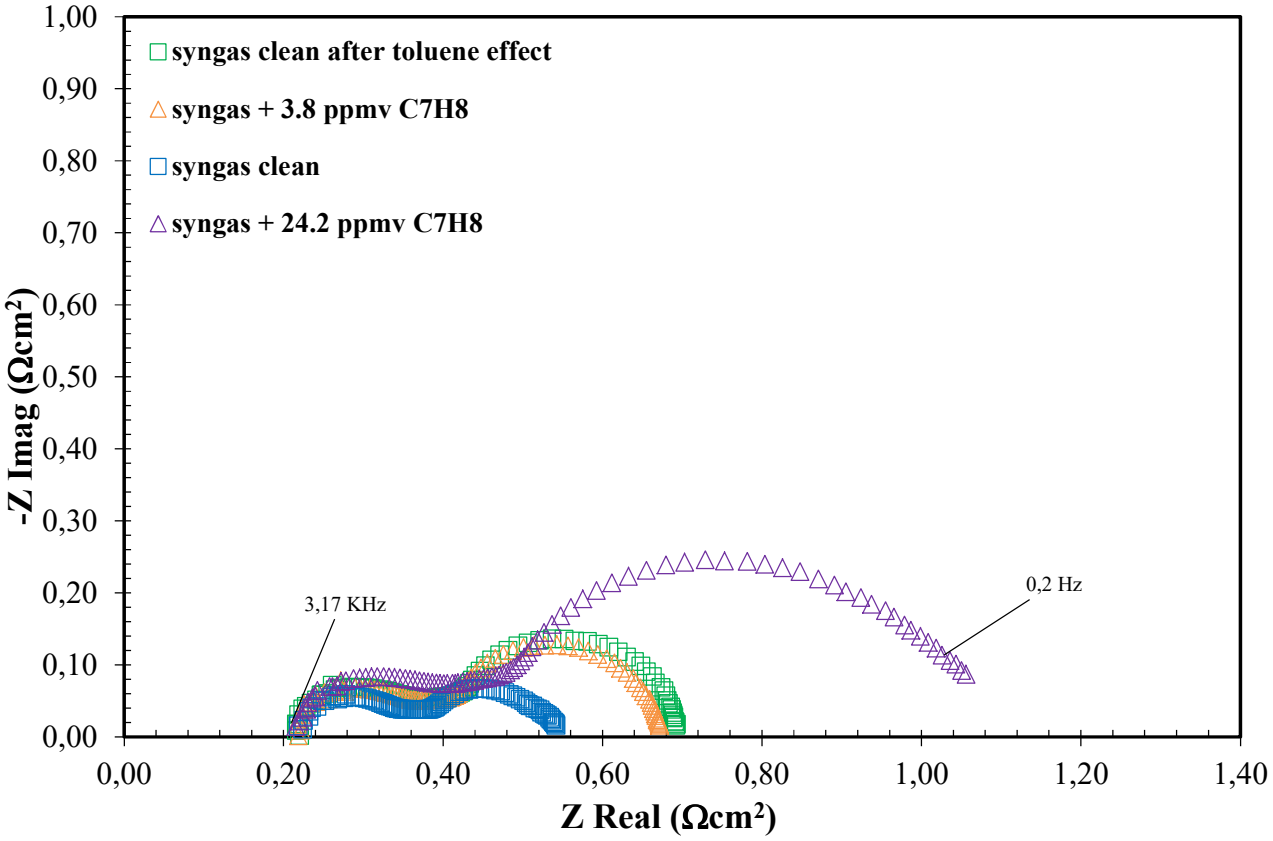


Figure 16 – Nyquist diagram for variations of the C_7H_8 concentration – ASC700.

Figure 16 shows the Nyquist diagram of a SOFC cell being fed with a syngas mixture with variations in the C_7H_8 concentration. As can be seen, already after 3.8 and 24.2 ppm(v) of toluene, the SOFC performances are irreversibly influenced. In fact, if the toluene content is removed, the impedance curve does not recover the starting value. The ohmic contribution remains unchanged, but the polarization losses increase, see figure 17. If the toluene concentration is increased, the polarization losses increase significantly, especially at the low frequency value. This circle is related to the mass transport phenomenon.

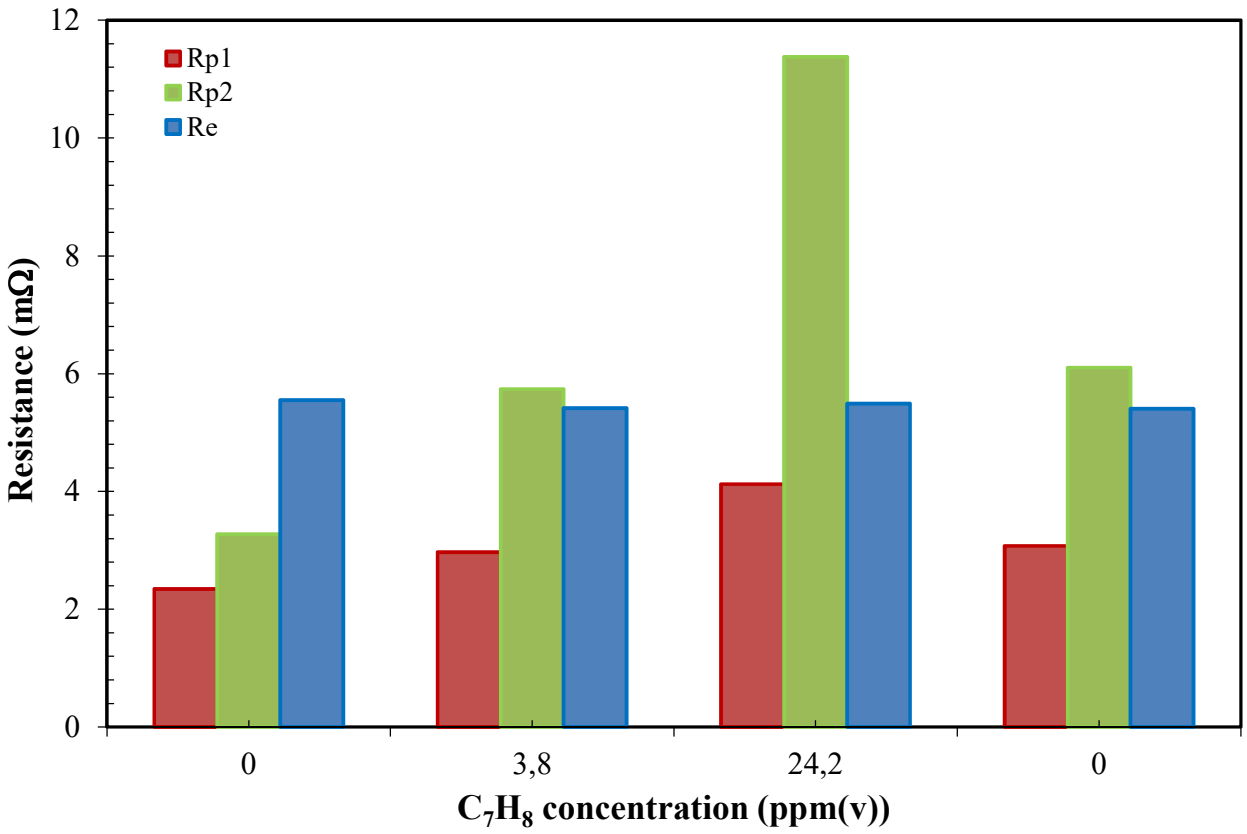


Figure 17 – Re and Rp values for variations of the C_7H_8 concentration – TOFC.

As reported for the naphthalene test, toluene adsorption and desorption obviously interferes with the reforming of methane and WGS (i.e., CO conversion to H_2) by decreasing the reactive surface and SOFC performance.

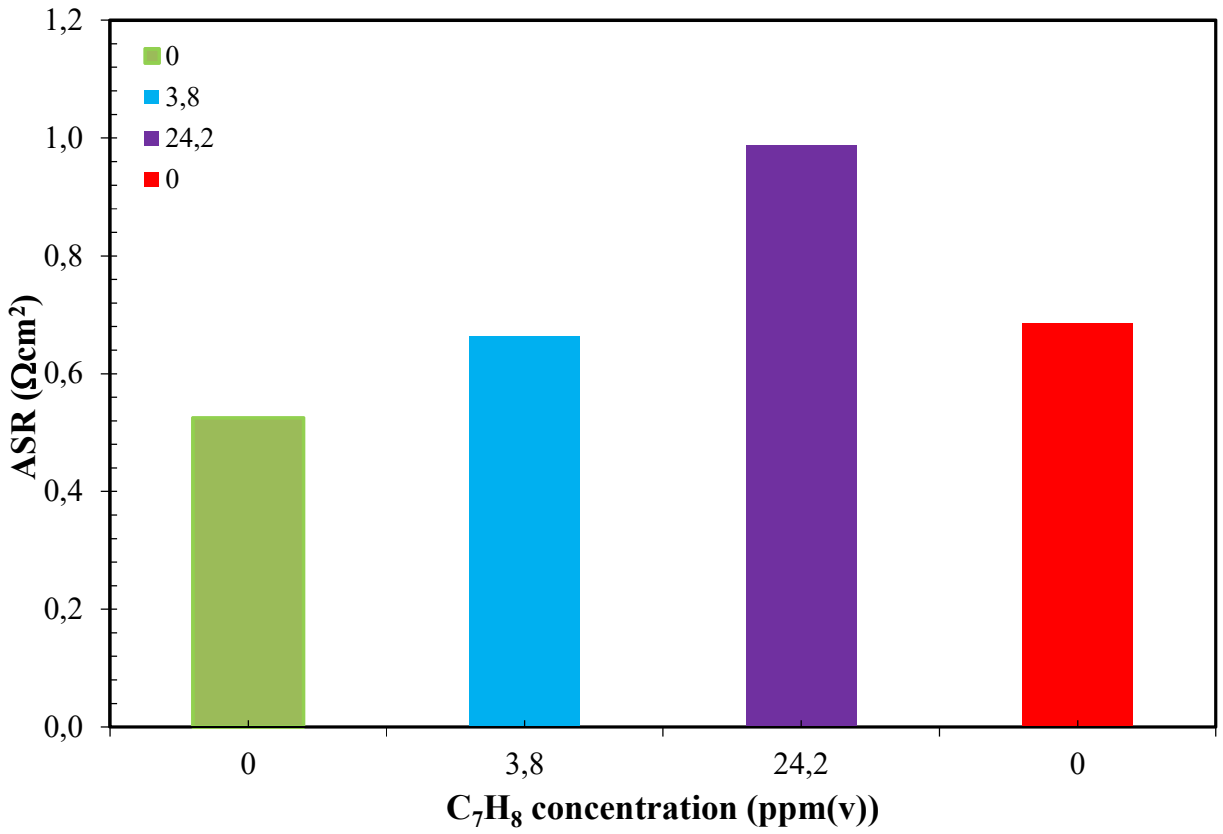


Figure 18 – Area specific resistance diagram for variations of the C_7H_8 concentration – ASC700.

Figure 18 shows the ASR values. A slight increase in the ASR can be observed at 3.8 ppm(v) – which is an almost tolerable limit for SOFC performance – but if the toluene concentration increases to 24.2 ppm(v), the performance decreases to a great extent (+40% losses).

If C_7H_8 concentrations ranging from 0 to 24.2 ppm(v) are considered, the power losses increase to achieve 14.58% of the nominal power value at zero time. This means that if the exposure time to the pollutants is increased, the electrical power loss will also rise, thereby increasing the resistance value, especially as far as the Rp2 term is concerned.

The influence of ethylene Hydrocarbons on SOFC performance

Ethylene is a common hydrocarbon that can be detected in almost all biogenous fuels. Ethylene is a fuel like methane, and like the latter it has to be reformed into hydrogen and carbon monoxide. Ethylene concentrations above a certain level, which mainly depends on the operating temperature,

are difficult to reform. The steam reforming of ethylene is dealt with in this section, considering a concentration value that is representative of a biogas obtained from organic waste digestion. Figure 19 shows the impedance spectra of two gas mixtures containing 0 ppm(v) of ethylene and 371.2 ppm(v) of C_2H_2. By observing the zoom window, it can be seen that ethylene does not influence SOFC performance negatively.

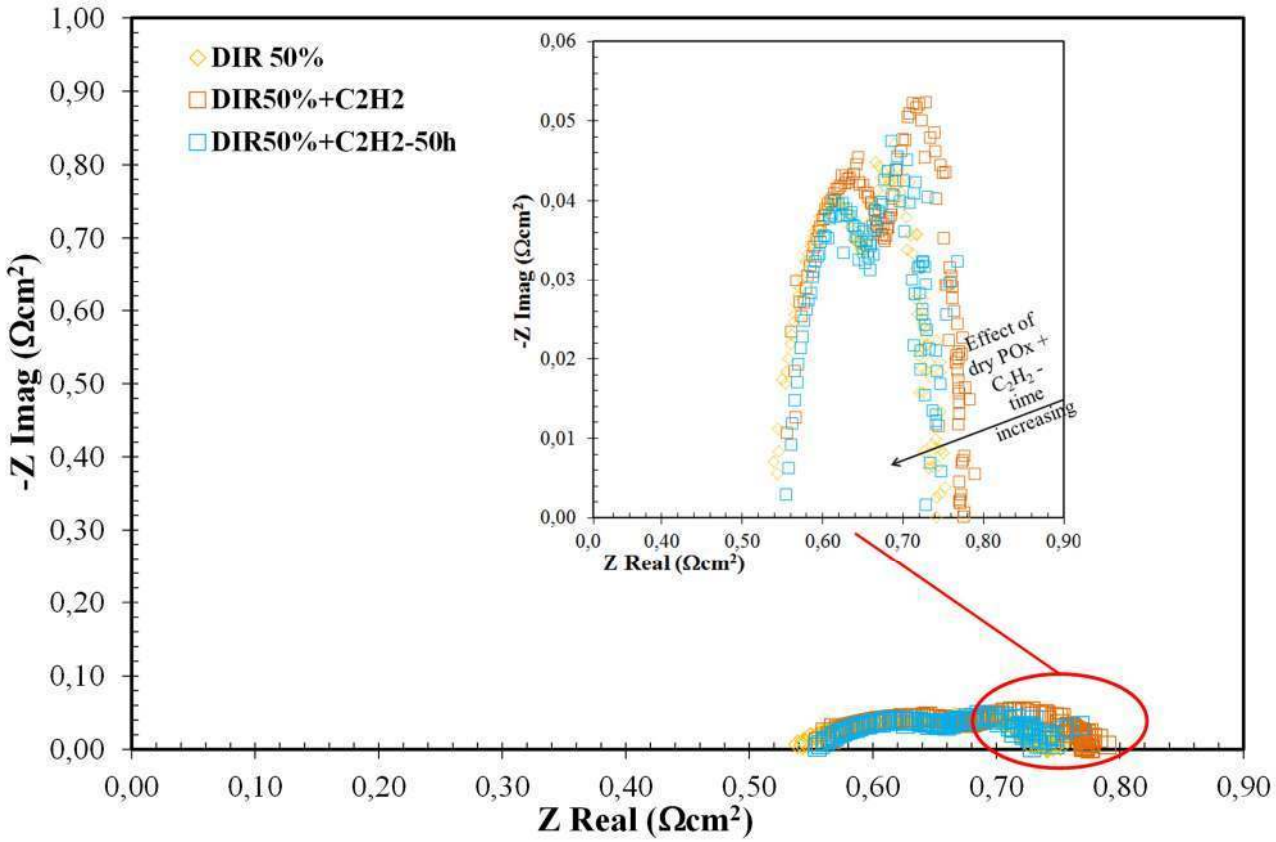
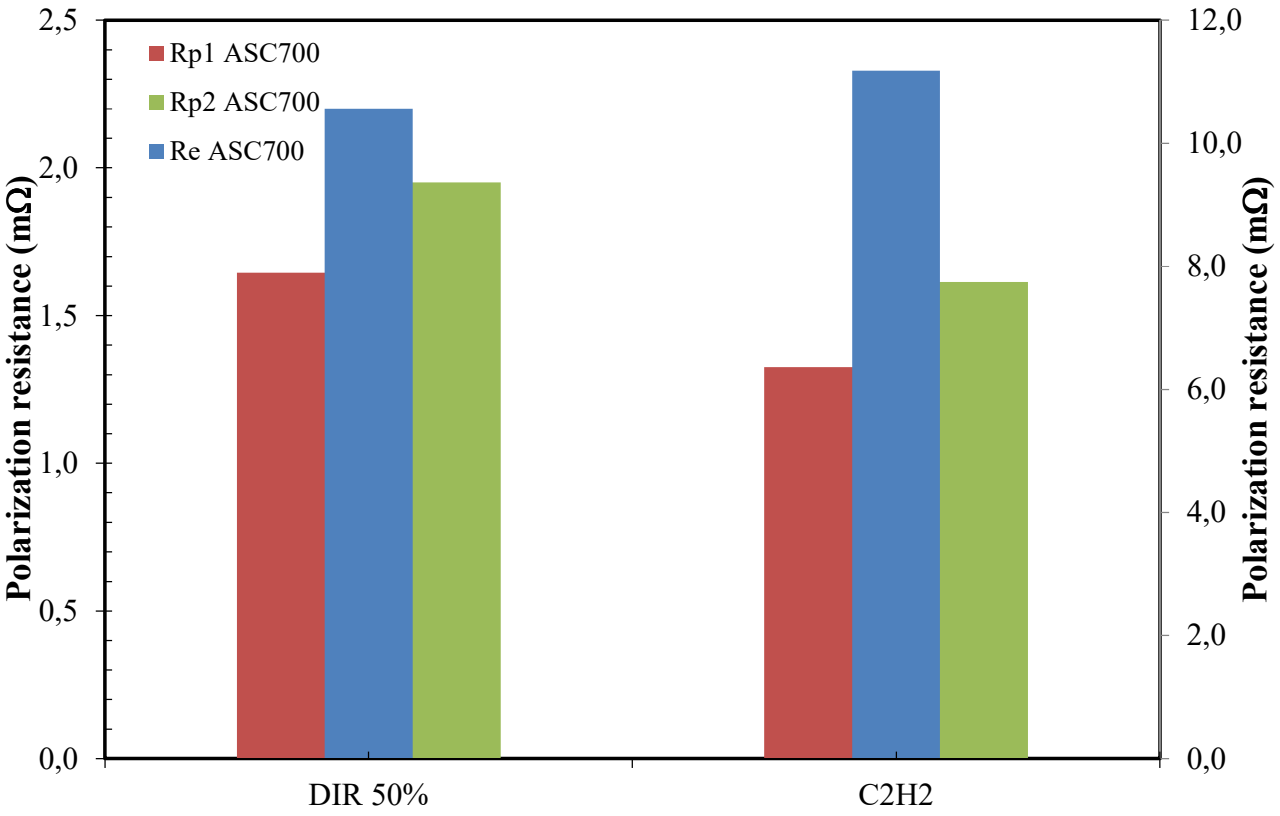


Figure 19 – Nyquist diagram for variations of the C_2H_2 concentration – ASC700.

Figure 20 depicts the contribution of the performance losses. Instead of increasing the polarization losses, ethylene improves SOFC performance. This is due to the increase in the available electrochemical fuel, which is caused by an improvement in the reforming reactions.



408

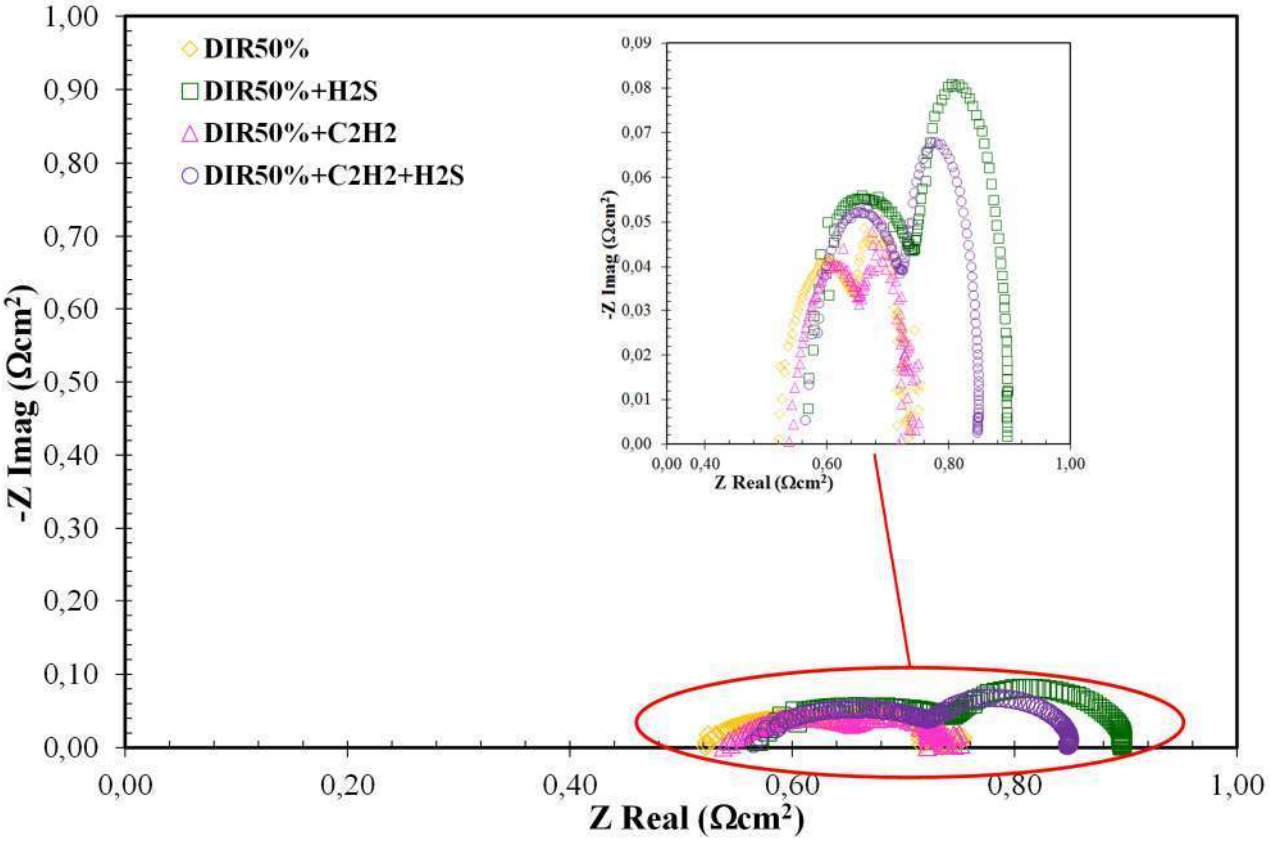
409 **Figure 20 – Re and Rp values for variations of the the C_2H_2 concentration – ASC700.**

410 The influence of Multi concentrations on SOFC performance

411 Since the H_2S concentration has been considered as the most dangerous compound for SOFCs, its
412 contemporary presence with other trace compounds has been studied.

413 $H_2S + C_2H_2$

414 The addition of a hydrogen sulfide content of 1.34 ppm(v) to a gas mixture influences the SOFC
415 performance. An increase in the total ASR value has been registered, see figure 21. The H_2S
416 concentration mainly affects the mass transport phenomena and the electrochemical processes, thus
417 reducing the TPB areas, as reported in figure 22.



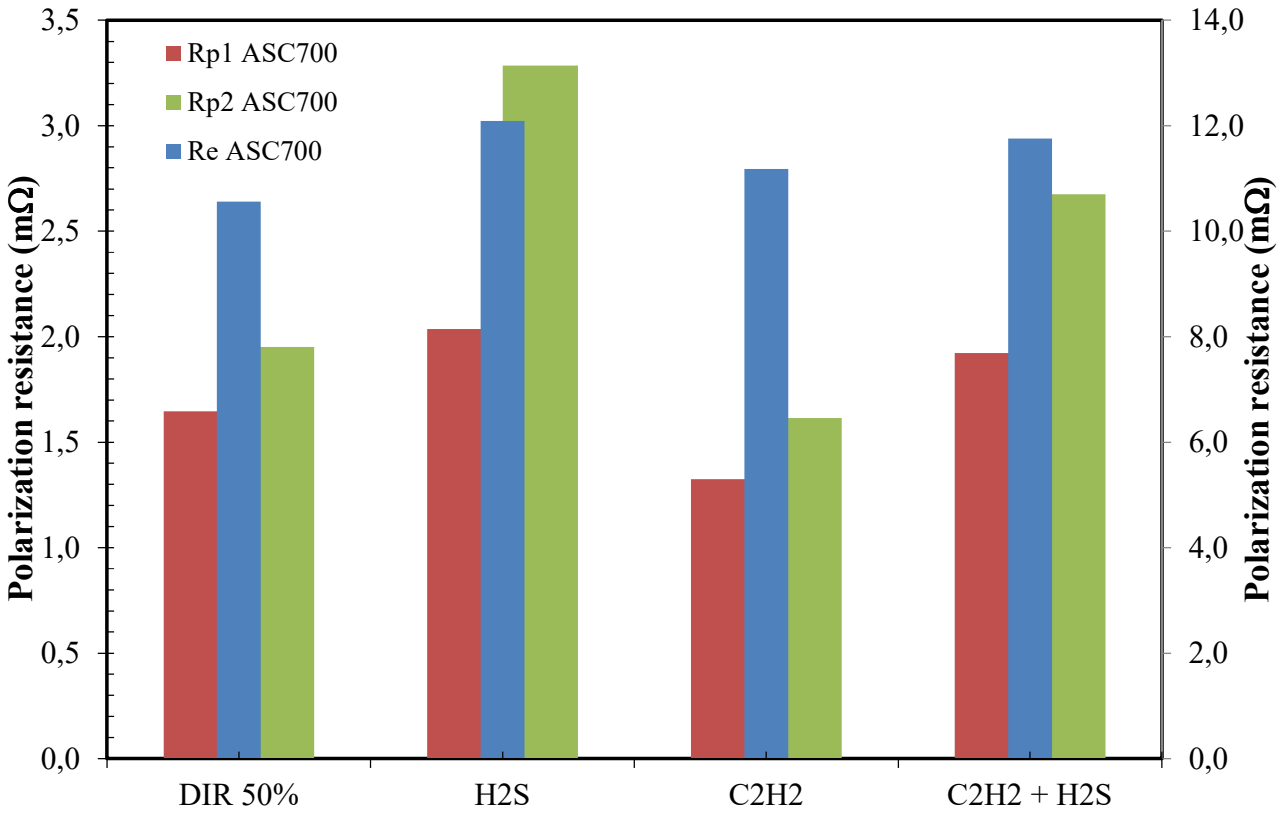
418

419 **Figure 21 – Nyquist diagram for variations of the C_2H_2 and C_2H_2+H_2S concentrations – ASC700.**

420 If a C_2H_2 concentration of 371.2 ppm(v) is added to the H_2S concentration, the total losses decrease,
421 see figure 20. C_2H_2 affects the reduction of the polarization losses and in particular the mass
422 transport resistance, see figures 22 and 23.

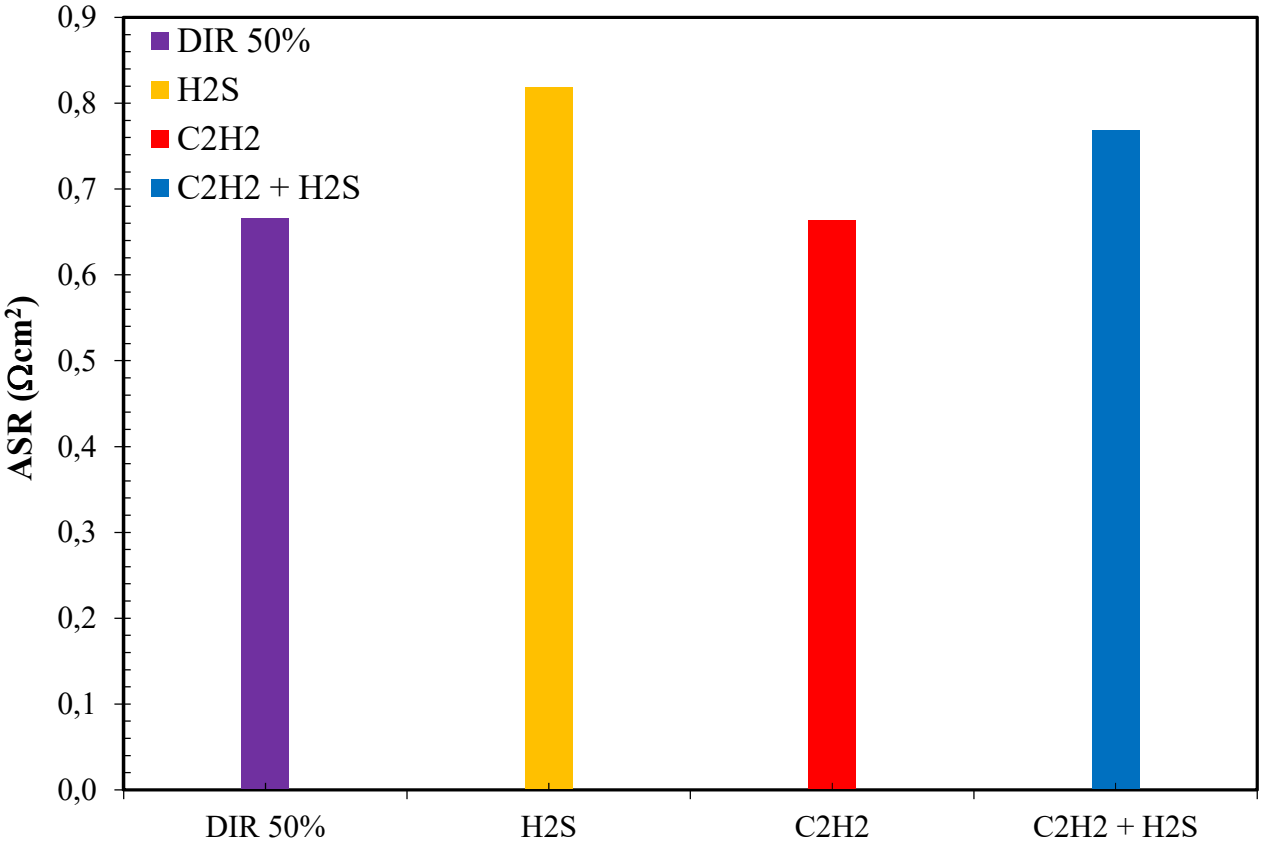
423

424



425

426 **Figure 22 – Re and Rp values for variations of the C_2H_2 and C_2H_2+H_2S concentration – ASC700.**



427

Figure 23 – Area specific resistance diagram for variations of the C_2H_2 and C_2H_2+H_2S concentrations – ASC700.

The ASR values are influenced positively by the C_2H_2 concentration, and a reduction in the double compound case is registered for H_2S.

$H_2S + C_2Cl_4$

As previously mentioned, H_2S is the most detrimental compound, and the addition of chlorine has therefore been studied. Tetrachloroethylene (TCE) is a chloro compound that can be detected in a biogenous fuel, especially from waste water sludges. The possible implications of the inclusion of this compound on SOFC performance have been studied and the results are presented in this section. Concentrations ranging from 0.62 to 1.67 ppm(v) of TCE and 4 to 0 ppm(v) of H_2S have been considered.

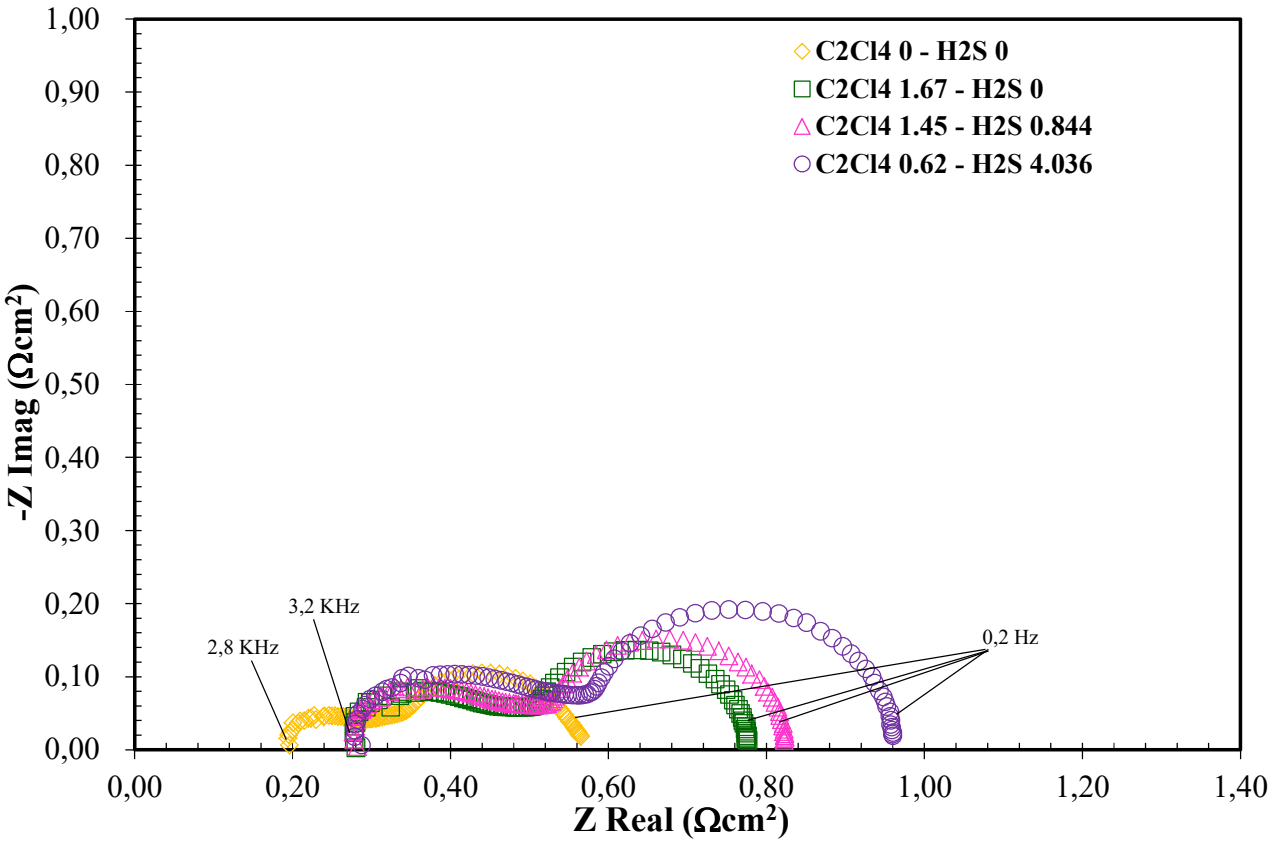


Figure 24 – Nyquist diagram for variations of the C_2Cl_4+H_2S concentration – ASC700.

If the spectra obtained from the clean condition (C_2Cl_4-0 ppm(v) +H_2S-0 ppm(v)) are compared with those of the other gas mixture, it can be seen that the ohmic part rises by the same quantity in all three mixtures. This result is related to the different electrochemical molar fuel contents. As reported in figure 25, the ohmic contribution remains constant in the double contaminant case. The polarization losses increase the most for the highest H_2S concentration case. This shows how the sulfur compound is a heavier contaminant than chlorine. C_2Cl_4 acts mainly on the high frequency polarization term, that is, on the electrochemical processes caused by the adsorption/desorption behavior of chlorine. The term related to the transport phenomena is instead influenced more by the sulfur compound.

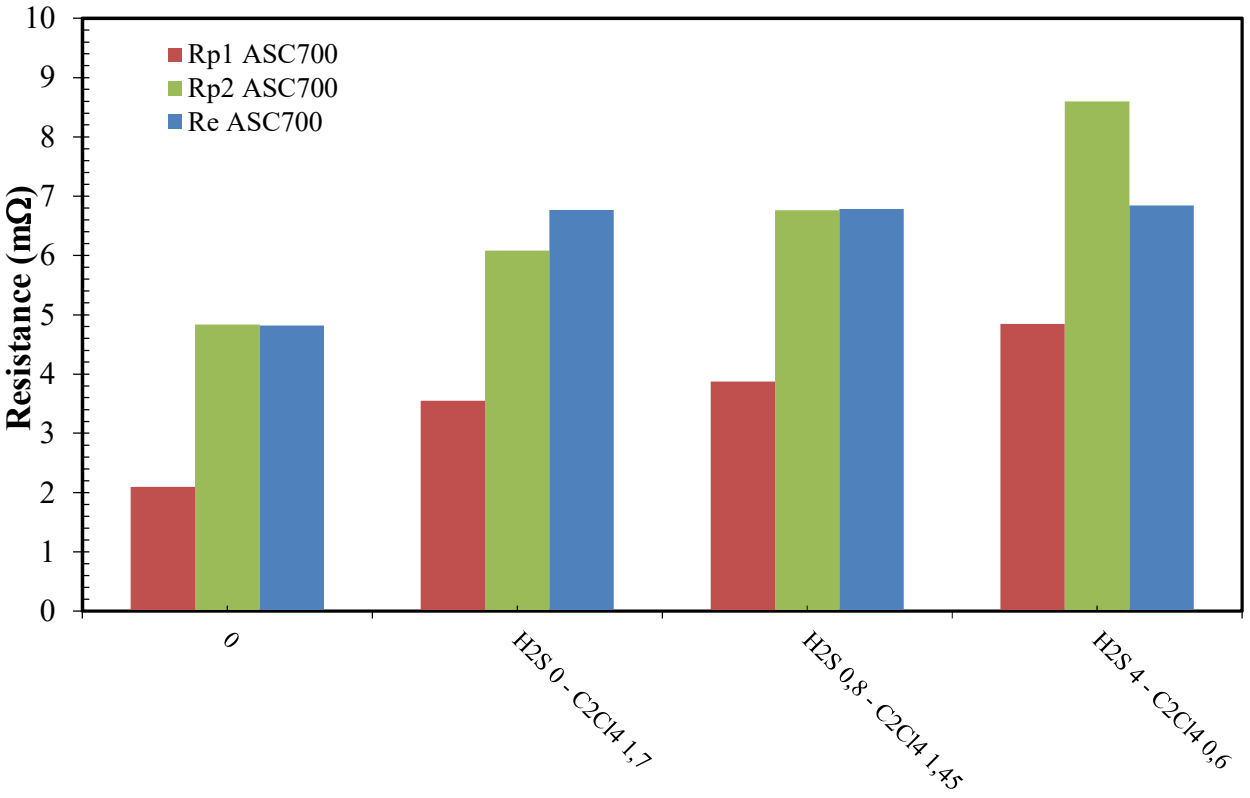


Figure 25 – Re and Rp values for variations of the C_2Cl_4+H_2S concentration – ASC700.

The worst case scenario for the SOFC performance is related to the sulfur compound content, as reported in figure 25, where the highest ASR value is achieved. If the H_2S 4 ppm(v) + C_2Cl_4 0.6

ppm(v) case is compared with the H_2S 4 ppm(v) case, it can be seen that chlorine does not cause a deterioration of the cell performance.

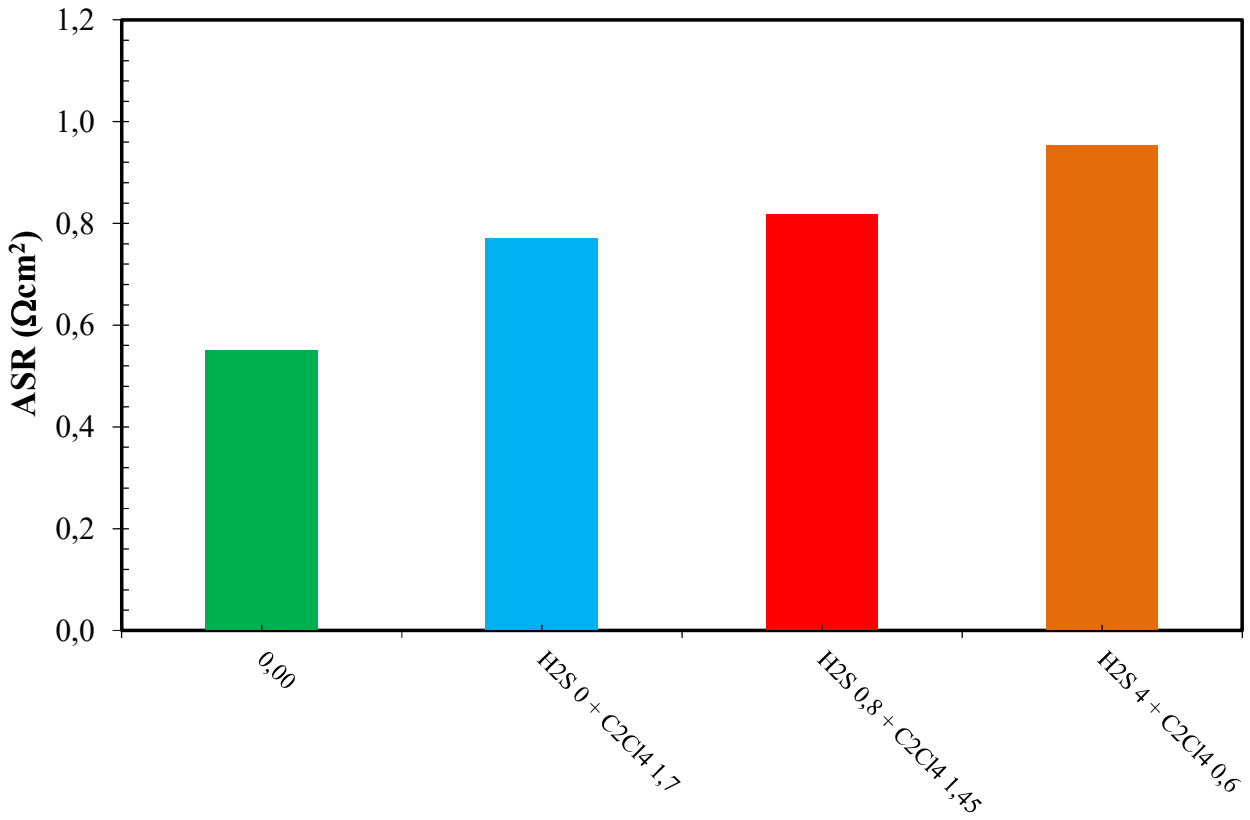


Figure 26 – Area specific resistance diagram for variations of the C_2Cl_4+H_2S concentration – ASC700.

The power loss increases directly as H_2S concentration increases until it reaches 12.86% of the nominal power value at zero time. This means that if the exposure time to the pollutants is increased, the electrical power loss will also rise, thereby increasing the resistance value, especially as far as the Rp2 term is concerned. The contemporary presence of C_2Cl_4 and H_2S causes a two-fold power loss compared to the single pollutant case.

$\underline{H_2S + C_7H_8}$

Figure 27 depicts the Nyquist diagram for the case of the contemporary presence of H_2S and C_7H_8. The concentration of H_2S was fixed at 4 ppm(v), while C_7H_8 was fixed at 3.7 ppm(v). The test was conducted by adding or not adding the toluene concentration at three different temperatures. It has

been observed that the toluene concentration affects the SOFC performance to a lesser extent than the temperature. Figures 27, 28 and 29 show that when the operating temperature is decreased, an increase in the cell resistance is registered. This is caused by a decrease in the electronic conductivity of the electrodes and in the ionic conductivity of the cell layer. This is especially true for the electrolyte layer, but also for the composite electrodes.

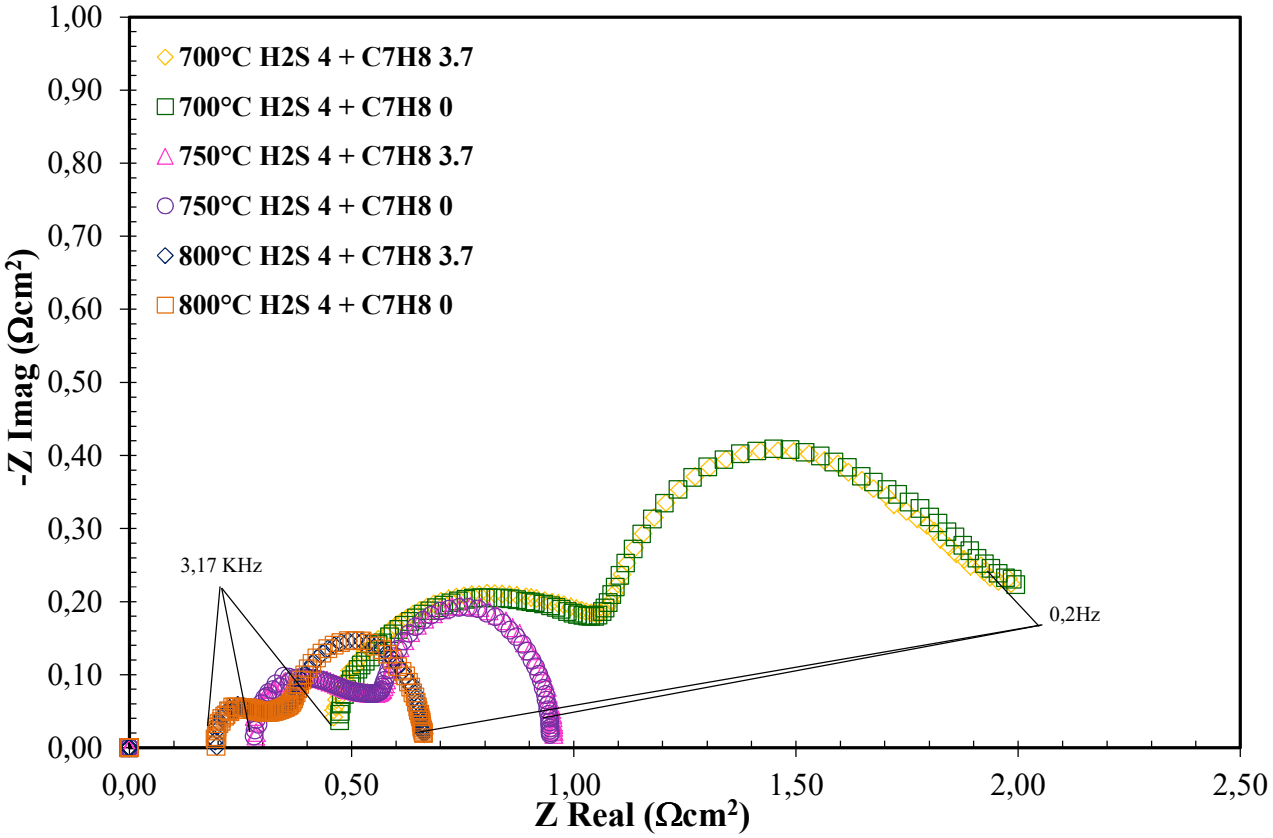


Figure 27 – Nyquist diagram for variations of the H_2S + C_7H_8 concentration – ASC700.

Figure 28 shows the three term losses considered singularly; R_{high} is the only contribution that seems to be affected by the addition of toluene to the gas mixture in which H_2S is already present. This percentage increases as the operating temperature decreases. Moreover, the electrochemical reaction kinetics is slowed down, and this leads to an increase in the activation polarization resistance. Finally, the diffusion capability of the chemical species is reduced both on the bulk flow in the channels and on the porous electrodes.

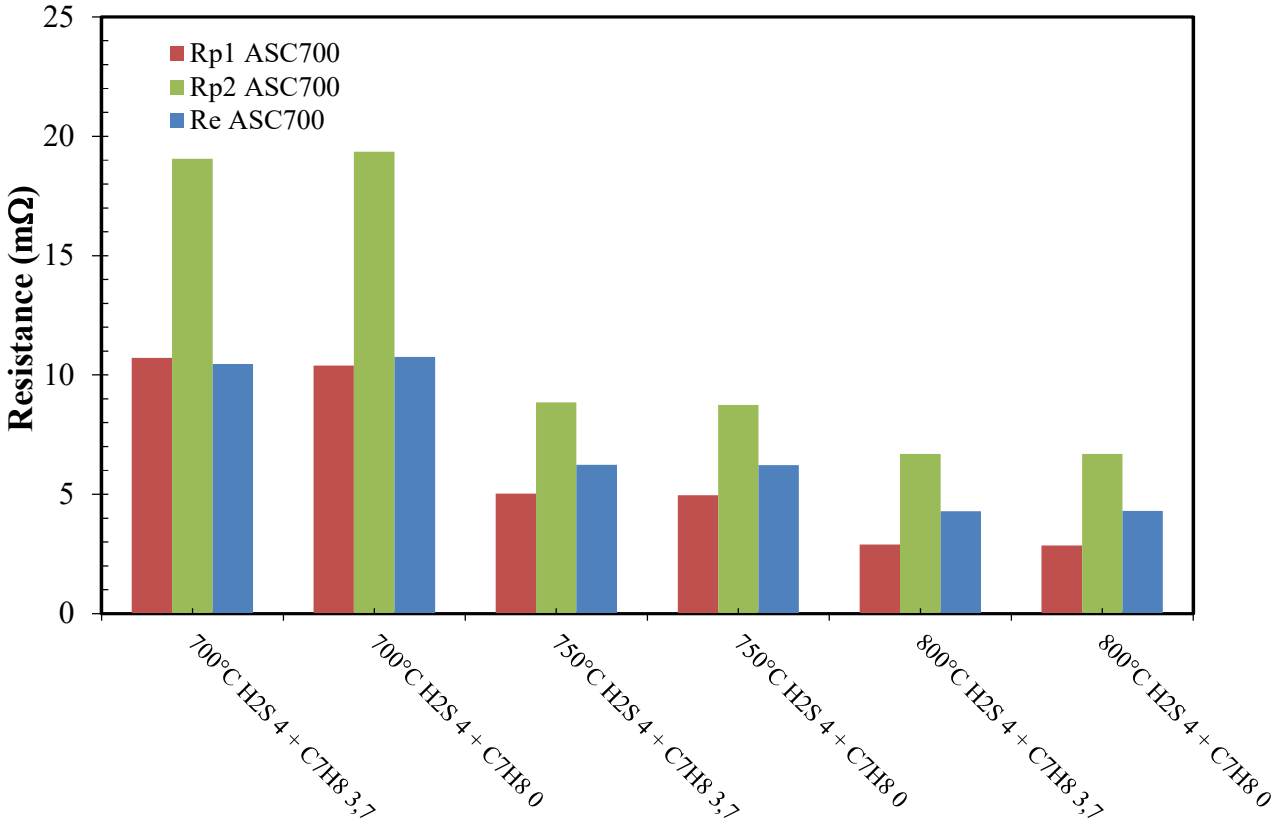


Figure 28 – Re and Rp values for variations of the H_2S + C_7H_8 concentration – ASC700.

The ASR value is affected more by the temperature variation than by the contemporary presence of toluene and hydrogen sulfide. Even in this case, the sulfur concentration weighs more than the toluene concentration at the same operating temperature. The toluene concentration needs to be increased before significant effects on the SOFC performance can be observed, but this condition is not realistic of a real clean up gas condition used to feed a SOFC system.

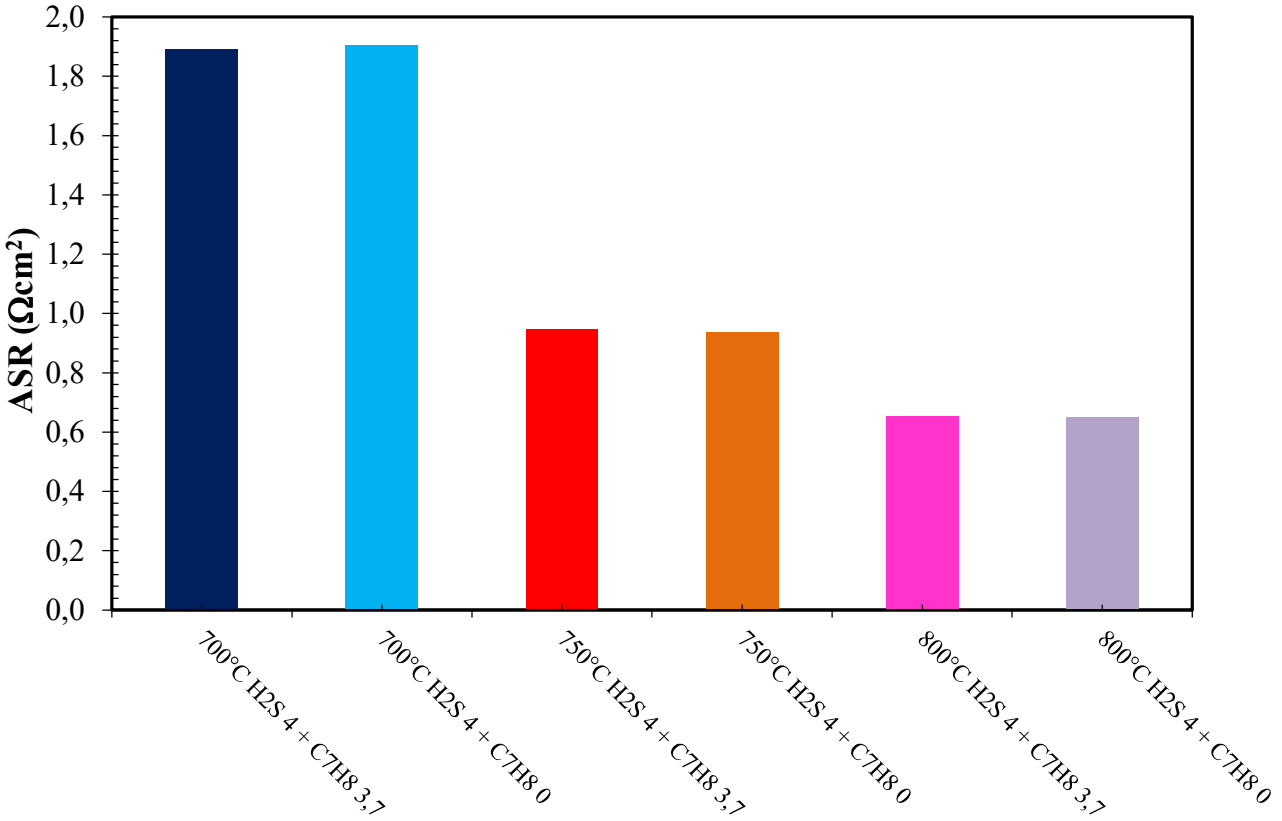


Figure 29 – Area specific resistance diagram for variations of the H_2S + C_7H_8 concentration – ASC700.

Conclusions

This paper has investigated the performance of an anode supported solid oxide fuel cell considering a wide range of trace compounds. These compounds are found in biogenous fuels, such as biogas from OFMSW or from sewage sludge: H_2S, HCl, D4, $C_{10}H_8$, C_7H_8, C_2H_2, C_2Cl_4. Various concentrations of Hydrogen sulfide have been studied in three tests. The first two tests considered high and low concentration ranges, thus simulating an early breakthrough slip from the clean-up section under operation with digester biogas. The third test considered the literature threshold limit for SOFCs (≈1 ppm(v)). The effect of Chlorine has been tested for variable concentrations of HC1, ranging from 1 to 1000 ppm(v). The effect of Siloxanes on SOFC performance has been studied considering concentrations ranging from 111 ppb(v) to 1.9 ppm(v), in order to simulate a clean-up section slip. In the same way, $C_{10}H_8$ and C_7H_8 have been tested on SOFC performance and in a

499 double compound condition test (C_2H_2+H_2S, C_2Cl_4+H_2S and C_7H_8+H_2S). All these tests have been
500 conducted to simulate possible biogas conditions that could arise from biological matter.

501 Electrochemical impedance spectroscopy has been used to study an SOFC cell in order to identify
502 the main contribution to the cell losses from trace compound contaminations. This was done with an
503 electrical equivalent circuit constituted by an ohmic resistance, Re, and two parallel combinations
504 of a resistance and a constant phase element, CPE. The polarization resistance, Rp, related to the
505 concentration and activation polarizations, has been obtained from the sum of the low and high
506 frequency resistances. The different sources of performance limitation have been obtained from fuel
507 cell impedance considering the action of different trace compounds.

508 In particular it has been found that:

509 ▪ The ohmic contribution is almost independent of the fuel composition and it is only affected
510 minimally by the H_2S concentration. However, this contribution is influenced by the
511 modification of the nickel grain caused by cell operation with an H_2S concentration, as also
512 reported by Ivey et al., (2010) [51]. The electrochemical fuel content of hydrocarbons can
513 influence this term: lower values are achieved in an H_2 condition, compared to the same
514 electrochemical molar value in a CH_4 + CO condition.
515 ▪ The H_2S concentration mainly affects the polarization losses, especially the mass transport
516 resistance through the electrodes caused by the sulfur blocking sites. The three-phase boundary
517 decreases as a consequence of the sulfur action on nickel active sites.
518 ▪ Ultra low concentrations of sulfur, around 100 – 200 ppb(v), do not cause any changes in the
519 loss terms.
520 ▪ The influence of HCl on SOFC performance is mainly due to the increase in $R_{high,}$ related to the
521 electrochemical processes that occur at the electrodes. Below 40 ppm(v), HCl concentrations
522 only have a slight influence on the SOFC performance.

- D4, a model compound for siloxanes, already acts on SOFC performance at ppb(v) levels. The term that is influenced most is $R_{high,}$ thus highlighting the action of siloxanes on SOFC performance. In fact, these compounds, together with the formation of silica oxide in the anode cermet, reduce the porosity and the flow of the fuel toward the active sites, and thus limit the energy generation of a SOFC.
- Naphthalene and toluene have been considered as model compounds for tars. No performance losses have been observed in an H_2 mixture. When a syngas mixture was considered, it was observed that even 9.3 ppm(v) of $C_{10}H_8$ can reduce SOFC performance. The polarization losses are those that are influenced the most, and the largest increase has been recorded for the low frequency term Rp_2, related to mass transport resistance. The same behavior has been observed for the toluene case.
- The tested concentrations of ethylene have been shown to positively influence SOFC performance and, at the same time, to limit the action of H_2S in a case in which two contaminants were considered together.
- H_2S, introduced with other contaminants (C_2Cl_4), has led to an increased instantaneous deterioration, and the more types of contaminants included, the larger the initial deterioration.
- H_2S, introduced with another contaminant (C_7H_8), has shown how the operating temperature has more influence than 3.7 ppm(v) of toluene.

The worst case scenario is represented by the presence of higher H_2S concentrations than 1 ppm(v) and by the presence of D4 already at the ppb(v) level. The contemporary presence of these compounds has led to an increase in the detrimental effects on SOFC performance, and even to fatal cell degradation.

Acknowledgments

This work has been partly funded by the European Union under the SOFCOM project (www.sofcom.eu, contract number 278798). In addition, this research has been conducted as a part of the BioWaste for SOFCs (BWS) project carried out together with Fondazione Edmund Mach and SOLIDpower SpA. The project has been funded with the contribution of Fondazione Caritro (TN).

References

[1] D. Papurello, A. Lanzini, L. Tognana, S. Silvestri, M. Santarelli, Waste to energy: Exploitation of biogas from organic waste in a 500 Wel solid oxide fuel cell (SOFC) stack, Energy. 85 (2015) 145–158. doi:10.1016/j.energy.2015.03.093.

[2] A.J. Appleby, Fuel cell technology: Status and future prospects, Energy. 21 (1996) 521–653. doi:10.1016/0360-5442(96)00030-8.

[3] D.D. Papadias, S. Ahmed, R. Kumar, Fuel quality issues with biogas energy - An economic analysis for a stationary fuel cell system, Energy. 44 (2012) 257–277. doi:10.1016/j.energy.2012.06.031.

[4] S.W. (Volume E. Narottam P. Bansal (Editor), Mihails Kusnezoff (Editor), Soshu Kirihara (Volume Editor), Advances in Solid Oxide Fuel Cells IV: Ceramic Engineering and Science Proceedings, 2013.

[5] K. Sasaki, K. Haga, T. Yoshizumi, D. Minematsu, E. Yuki, R. Liu, et al., Chemical durability of Solid Oxide Fuel Cells: Influence of impurities on long-term performance, J. Power Sources. 196 (2011) 9130–9140. doi:10.1016/j.jpowsour.2010.09.122.

[6] D. Papurello, A. Lanzini, P. Leone, M. Santarelli, S. Silvestri, Biogas from the organic fraction of municipal solid waste: Dealing with contaminants for a solid oxide fuel cell energy generator, Waste Manag. (2014).

[7] E. Bocci, A. Di Carlo, S.J. McPhail, K. Gallucci, P.U. Foscolo, M. Moneti, et al., Biomass to fuel cells state of the art: A review of the most innovative technology solutions, Int. J. Hydrogen Energy. 39 (2014) 21876–21895. doi:10.1016/j.ijhydene.2014.09.022.

[8] D. Thimsen, Gas Fueled Power Generation, 3 (2006).

[9] D. Papurello, C. Soukoulis, E. Schuhfried, L. Cappellin, F. Gasperi, S. Silvestri, et al., Monitoring of volatile compound emissions during dry anaerobic digestion of the Organic Fraction of Municipal Solid Waste by Proton Transfer Reaction Time-of-Flight Mass Spectrometry, in: Bioresour. Technol., 2012: pp. 254–265.

[10] D. Papurello, E. Schuhfried, A. Lanzini, A. Romano, L. Cappellin, T.D. Märk, et al., Influence of co-vapors on biogas filtration for fuel cells monitored with PTR-MS (Proton Transfer Reaction-Mass Spectrometry), Fuel Process. Technol. 118 (2014) 133–140.

[11] D. Papurello, L. Tognana, A. Lanzini, F. Smeacetto, M. Santarelli, I. Belcari, et al., Proton transfer reaction mass spectrometry technique for the monitoring of volatile sulfur compounds in a fuel cell quality clean-up system, Fuel Process. Technol. 130 (2015) 136–146. doi:10.1016/j.fuproc.2014.09.041.

[12] L. Sigot, G. Ducom, B. Benadda, C. Labouré, Comparison of adsorbents for H_2S and D4 removal for biogas conversion in a solid oxide fuel cell, Environ. Technol. 3330 (2015) 1–10. doi:10.1080/09593330.2015.1063707.

[13] A. Weber, S. Dierickx, A. Kromp, E. Ivers-Tiffée, Sulfur poisoning of anode-supported SOFCs under reformate operation, Fuel Cells. 13 (2013) 487–493. doi:10.1002/fuce.201200180.

[14] A. Hauch, A. Hagen, J. Hjelm, T. Ramos, Sulfur Poisoning of SOFC Anodes: Effect of Overpotential on Long-Term Degradation, J. Electrochem. Soc. 161 (2014) F734–F743. doi:10.1149/2.080406jes.

[15] D. Papurello, A. Lanzini, S. Fiorilli, F. Smeacetto, R. Singh, M. Santarelli, Sulfur poisoning in Ni-anode solid oxide fuel cells (SOFCs): Deactivation in single cells and a stack, Chem. Eng. J. 283 (2016) 1224–1233. doi:10.1016/j.cej.2015.08.091.

[16] A.L. da Silva, N.C. Heck, Thermodynamics of sulfur poisoning in solid oxide fuel cells revisited: The effect of H2S concentration, temperature, current density and fuel utilization, J. Power Sources. 296 (2015) 92–101. doi:10.1016/j.jpowsour.2015.07.046.

[17] M. Błesznowski, J. Jewulski, A. Zieleniak, Determination of H2S and HCl concentration limits in the fuel for anode supported SOFC operation, Cent. Eur. J. Chem. 11 (2013) 960–967. doi:10.2478/s11532-013-0228-1.

[18] E. Lorente, M. Millan, N.P. Brandon, Use of gasification syngas in SOFC: Impact of real tar on anode materials, Int. J. Hydrogen Energy. 37 (2012) 7271–7278. doi:10.1016/j.ijhydene.2011.11.047.

[19] K. Haga, S. Adachi, Y. Shiratori, K. Itoh, K. Sasaki, Poisoning of SOFC anodes by various fuel impurities, Solid State Ionics. 179 (2008) 1427–1431. doi:10.1016/j.ssi.2008.02.062.

[20] H. Madi, A. Lanzini, S. Diethelm, D. Papurello, J. Van herle, M. Lualdi, et al., Solid oxide fuel cell anode degradation by the effect of siloxanes, J. Power Sources. 279 (2015) 460–471. doi:10.1016/j.jpowsour.2015.01.053.

[21] M.J. Jørgensen, S. Primdahl, M. Mogensen, Characterisation of composite SOFC cathodes using electrochemical impedance spectroscopy, Electrochim. Acta. 44 (1999) 4195–4201. doi:10.1016/S0013-4686(99)00134-6.

[22] N. Wagner, K. a. Friedrich, Application of electrochemical impedance spectroscopy for fuel cell characterization: PEFC and oxygen reduction reaction in alkaline solution, Fuel Cells. 9 (2009) 237–246. doi:10.1002/fuce.200800071.

[23] H. Schichlein, H. Schichlein, E. Ivers-tiffe, E. Ivers-tiffe, Deconvolution of electrochemical impedance spectra for the identification of electrode reaction mechanisms in solid oxide fuel cells, J. Appl. Electrochem. 32 (2002) 875–882. doi:10.1023/A:1020599525160.

[24] P. V. Aravind, J.P. Ouweltjes, J. Schoonman, Diffusion Impedance on Nickel/Gadolinia-Doped Ceria Anodes for Solid Oxide Fuel Cells, J. Electrochem. Soc. 156 (2009) B1417. doi:10.1149/1.3231490.

[25] Q.A. Huang, R. Hui, B. Wang, J. Zhang, A review of AC impedance modeling and validation in SOFC diagnosis, Electrochim. Acta. 52 (2007) 8144–8164. doi:10.1016/j.electacta.2007.05.071.

[26] E. Brightman, D.G. Ivey, D.J.L. Brett, N.P. Brandon, The effect of current density on H2S-poisoning of nickel-based solid oxide fuel cell anodes, J. Power Sources. 196 (2011) 7182–7187. doi:10.1016/j.jpowsour.2010.09.089.

[27] P. Leone, T. Matencio, M.E. Garciä, Z.R. Domigues, A. Lanzini, M. Santarelli, Limiting Factors for a Planar Solid Oxide Fuel Cell Under Different Flow and Temperature Conditions, Fuel Cells. (2013) n/a–n/a. doi:10.1002/fuce.201200154.

[28] S.H. Jensen, A. Hauch, P.V. Hendriksen, M. Mogensen, N. Bonanos, T. Jacobsen, A Method to Separate Process Contributions in Impedance Spectra by Variation of Test Conditions, J. Electrochem. Soc. 154 (2007) B1325. doi:10.1149/1.2790791.

[29] A. Leonide, V. Sonn, A. Weber, E. Ivers-Tiffée, Evaluation and Modeling of the Cell Resistance in Anode-Supported Solid Oxide Fuel Cells, J. Electrochem. Soc. 155 (2008) B36. doi:10.1149/1.2801372.

[30] W.G. Bessler, S. Gewies, Gas Concentration Impedance of Solid Oxide Fuel Cell Anodes, J. Electrochem. Soc. 154 (2007) B548. doi:10.1149/1.2720639.

[31] M. Lang, C. Auer, A. Eismann, P. Szabo, N. Wagner, Investigation of solid oxide fuel cell short stacks for mobile applications by electrochemical impedance spectroscopy, Electrochim. Acta. 53 (2008) 7509–7513. doi:10.1016/j.electacta.2008.04.047.

[32] L.R.F. Allen J. Bard, Electrochemical methods: Fundamentals and Applications, New York, 2000. doi:10.1146/annurev.matsci.30.1.117.

[33] S. S, High-Temperature Solid Oxide Fuel Cells: Fundamentals, Design and Applications, Elsevier science, Amsterdam The Netherlands, 2003.

[34] F.T. and E.I.-T. Cornelia Endler, André Leonide, André Weber, Cells, Long-Term Study of MIEC Cathodes for Intermediate Temperature Solid Oxide Fuel Cells, ECS Trans. 25 (2009) 2381–2390. doi:doi: 10.1149/1.3205791.

[35] L.P. Hendriksen PV, Koch S, Mogensen M, Liu YL, Solid Oxide Fuel Cells VIII, (Eds. S. C. Singhal, M. Dokiya), in: Electrochem. Soc. Proc. Ser., Pennington, NJ, USA, 2003.

[36] Z. Cheng, S. Zha, M. Liu, Influence of cell voltage and current on sulfur poisoning behavior of solid oxide fuel cells, J. Power Sources. 172 (2007) 688–693. doi:10.1016/j.jpowsour.2007.07.052.

[37] Y. Zhang, Z. Lu, Z. Yang, T. Woo, Short communication the mechanism of sulfur poisoning on the nickel/yttrium-stabilized zirconia anode of solid oxide fuel cells: The role of the oxygen vacancy, J. Power Sources. 237 (2013) 128–131. doi:10.1016/j.jpowsour.2013.03.030.

[38] Z. Cheng, J.-H. Wang, Y. Choi, L. Yang, M.C. Lin, M. Liu, From Ni-YSZ to sulfur-tolerant anode materials for SOFCs: electrochemical behavior, in situ characterization, modeling, and future perspectives, Energy Environ. Sci. 4 (2011) 4380. doi:10.1039/c1ee01758f.

[39] A. Hagen, J.F.B. Rasmussen, K. Thydén, Durability of solid oxide fuel cells using sulfur containing fuels, J. Power Sources. 196 (2011) 7271–7276. doi:10.1016/j.jpowsour.2011.02.053.

[40] J.F.B. Rasmussen, A. Hagen, The Effect of H 2 S on the Performance of SOFCs using Methane Containing Fuel, (2010) 1135–1142. doi:10.1002/fuce.201000012.

[41] D. Papurello, R. Borchiellini, P. Bareschino, V. Chiodo, S. Freni, A. Lanzini, et al., Performance of a Solid Oxide Fuel Cell short-stack with biogas feeding, Appl. Energy. 125 (2014) 254–263.

[42] F.N. Cayan, M. Zhi, S.R. Pakalapati, I. Celik, N. Wu, R. Gemmen, Effects of coal syngas impurities on anodes of solid oxide fuel cells, J. Power Sources. 185 (2008) 595–602. doi:10.1016/j.jpowsour.2008.06.058.

[43] P. V. Aravind, J.P. Ouweltjes, N. Woudstra, G. Rietveld, Impact of Biomass-Derived Contaminants on SOFCs with Ni/Gadolinia-Doped Ceria Anodes, Electrochem. Solid-State Lett. 11 (2008) B24. doi:10.1149/1.2820452.

[44] Veyo, EVALUATION OF FUEL IMPURITY EFFECTS ON SOLID OXIDE FUEL CELL PERFORMANCE Final Technical Report, 1998.

[45] M. Arnold, T. Kajolinna, Development of on-line measurement techniques for siloxanes and

738 other trace compounds in biogas, Waste Manag. 30 (2010) 1011–1017.
739 doi:10.1016/j.wasman.2009.11.030.
740
741 [46] M. Arnold, Reduction and monitoring of biogas trace compounds, 2009.
742
743 [47] T. Namioka, T. Naruse, R. Yamane, Behavior and mechanisms of Ni/ScSZ cermet anode
744 deterioration by trace tar in wood gas in a solid oxide fuel cell, Int. J. Hydrogen Energy. 36
745 (2011) 5581–5588. doi:10.1016/j.ijhydene.2011.01.165.
746
747 [48] T. Namioka, Y. Nagai, K. Yoshikawa, T. Min, A tolerance criterion for tar concentration in a
748 model wood gas for a nickel/scandia-stabilized zirconia cermet anode in a solid oxide fuel
749 cell, Int. J. Hydrogen Energy. 37 (2012) 17245–17252. doi:10.1016/j.ijhydene.2012.09.005.
750
751 [49] R. Coll, J. Salvadó, X. Farriol, D. Montané, Steam reforming model compounds of biomass
752 gasification tars: Conversion at different operating conditions and tendency towards coke
753 formation, Fuel Process. Technol. 74 (2001) 19–31. doi:10.1016/S0378-3820(01)00214-4.
754
755 [50] W.Z. Zhu, S.C. Deevi, A review on the status of anode materials for solid oxide fuel cells,
756 Mater. Sci. Eng. A. 362 (2003) 228–239. doi:10.1016/S0921-5093(03)00620-8.
757
758 [51] D.G. Ivey, E. Brightman, N. Brandon, Structural modifications to nickel cermet anodes in
759 fuel cell environments, J. Power Sources. 195 (2010) 6301–6311.
760 doi:10.1016/j.jpowsour.2010.04.059.
761

Table captions

Table 1 – Test conditions.

20 **Table 1**

Pollutant test	Conc. Range (ppm(v))	Cell adopted	H_2 (ml min^{-1})	CO (ml min^{-1})	CO_2 (ml min^{-1})	CH_4 (ml min^{-1})	N_2 (ml min^{-1})	H_2O (ml min^{-1})	H_2O (g h^{-1})	T (°C)	FU	Fuel condition
H_2S high conc.	0,84-6,4	ASC700	151,5	136,4	68,2	15,2	386,4	60,2	2,9	750	30,0	syngas
H_2S high conc.	0,8-6,7	ASC4	250	0	41,7	62,5	0	124,5	6	750	20,9	DIR 50% biogas
H_2S low conc.	0,078-0,174	ASC4	250	0	41,7	62,5	0	124,5	6	750	20,9	DIR 50% biogas
HCl	1-1000	ASC700	348	133,7	62,1	5		136,5	6,58	750	29,9	biogas reformate
D4	0,11-1,92	TOFC	348	133,7	62,1	5		136,5	6,58	750	20,8	biogas reformate
C_7H_8	3,8-24,2	ASC700	151,5	136,4	68,2	15,2	386,4	269,8	13	750	30,0	syngas
$C_{10}H_8$	0-9,3	ASC700	151,5	136,4	68,2	15,2	386,4	269,8	13	750	30,0	syngas
C_2H_2	371,2	ASC700	250	0	42	63	0	0,0	0	750	20,8	POx 50% biogas
H_2S	1,34	ASC700	250	0	42	63	0	0,0	0	750	20,8	POx 50% biogas
H_2S +C_2Cl_4	0-4/1,7-0	ASC700	151,5	136,4	68,2	15,2	386,4	269,8	13	750	30,0	syngas
H_2S +C_2H_2	1,34/371,2	ASC700	250	0	42	63	0	0,0	0	750	20,8	POx 50% biogas
H_2S + C_7H_8	4/3,7	ASC700	151,5	136,4	68,2	15,2	386,4	269,8	13	750	30,0	syngas

21

Figure captions

Figure 1 – Equivalent fuel cell circuit: Re, R_{high} and CPE_{high} are associated with the high frequency semi-circle, R_{low} and CPE_{low} with the low frequency semi-circle.

Figure 2 – Nyquist diagram for variations of the H_2S concentration – ASC700.

Figure 3 – Nyquist diagram for variations of the H_2S concentration – ASC4.

Figure 4 – Re and Rp values for variations of the H_2S concentration – ASC700.

Figure 5 – Re and Rp values for variations of the H_2S concentration – ASC4.

Figure 6 – Nyquist diagram for the H_2S threshold concentration value – ASC700.

Figure 7 – Nyquist diagram for the H_2S threshold concentration value – time variation – ASC700.

Figure 8 – Nyquist diagram for variations of the H_2S "low concentration level" – ASC4.

Figure 9 – Re and Rp values for variations of the H_2S "low concentration level" – ASC4.

Figure 10 – Nyquist diagram for variations of the HCl concentration – ASC700.

Figure 11 – Re and Rp values for variations of the HCl concentration – ASC700.

Figure 12 – Nyquist diagram for variations of the D4 concentration – TOFC.

Figure 13 – Re and Rp values for variations of the D4 concentration – TOFC.

Figure 14 – Nyquist diagram for variations of the $C_{10}H_8$ concentration FU 30% – ASC700.

Figure 15 – Re and Rp values for variations of the $C_{10}H_8$ concentration – ASC700.

Figure 16 – Nyquist diagram for variations of the C_7H_8 concentration – ASC700.

Figure 17 – Re and Rp values for variations of the C_7H_8 concentration – TOFC.

Figure 18 – Area specific resistance diagram for variations of the C_7H_8 concentration – ASC700.

Figure 19 – Nyquist diagram for variations of the C_2H_2 concentration – ASC700.

Figure 20 – Re and Rp values for variations of the the C_2H_2 concentration – ASC700.

Figure 21 – Nyquist diagram for variations of the C_2H_2 and C_2H_2+H_2S concentrations – ASC700.

Figure 22 – Re and Rp values for variations of the C_2H_2 and C_2H_2+H_2S concentration – ASC700.

Figure 23 – Area specific resistance diagram for variations of the C_2H_2 and C_2H_2+H_2S concentrations – ASC700.

Figure 24 – Nyquist diagram for variations of the C_2Cl_4+H_2S concentration – ASC700.

Figure 25 – Re and Rp values for variations of the C_2Cl_4+H_2S concentration – ASC700.

Figure 26 – Area specific resistance diagram for variations of the C_2Cl_4+H_2S concentration – ASC700.

Figure 27 – Nyquist diagram for variations of the H_2S + C_7H_8 concentration – ASC700.

Figure 28 – Re and Rp values for variations of the H_2S + C_7H_8 concentration – ASC700.

Figure 29 – Area specific resistance diagram for variations of the H_2S + C_7H_8 concentration – ASC700.

Figure 1

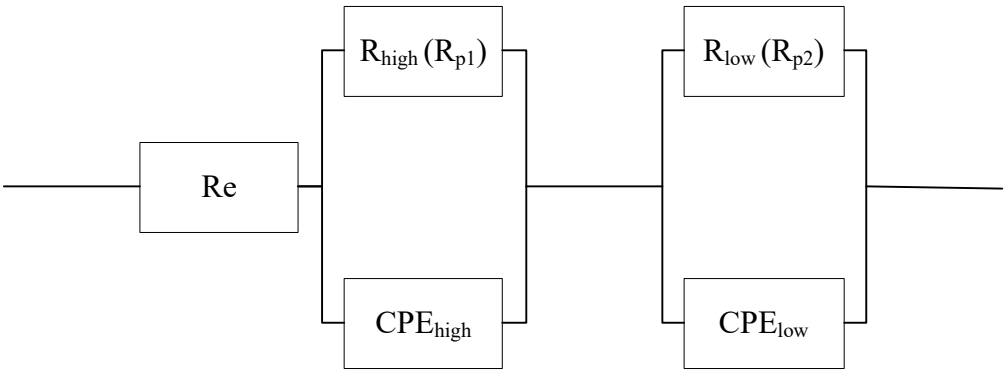
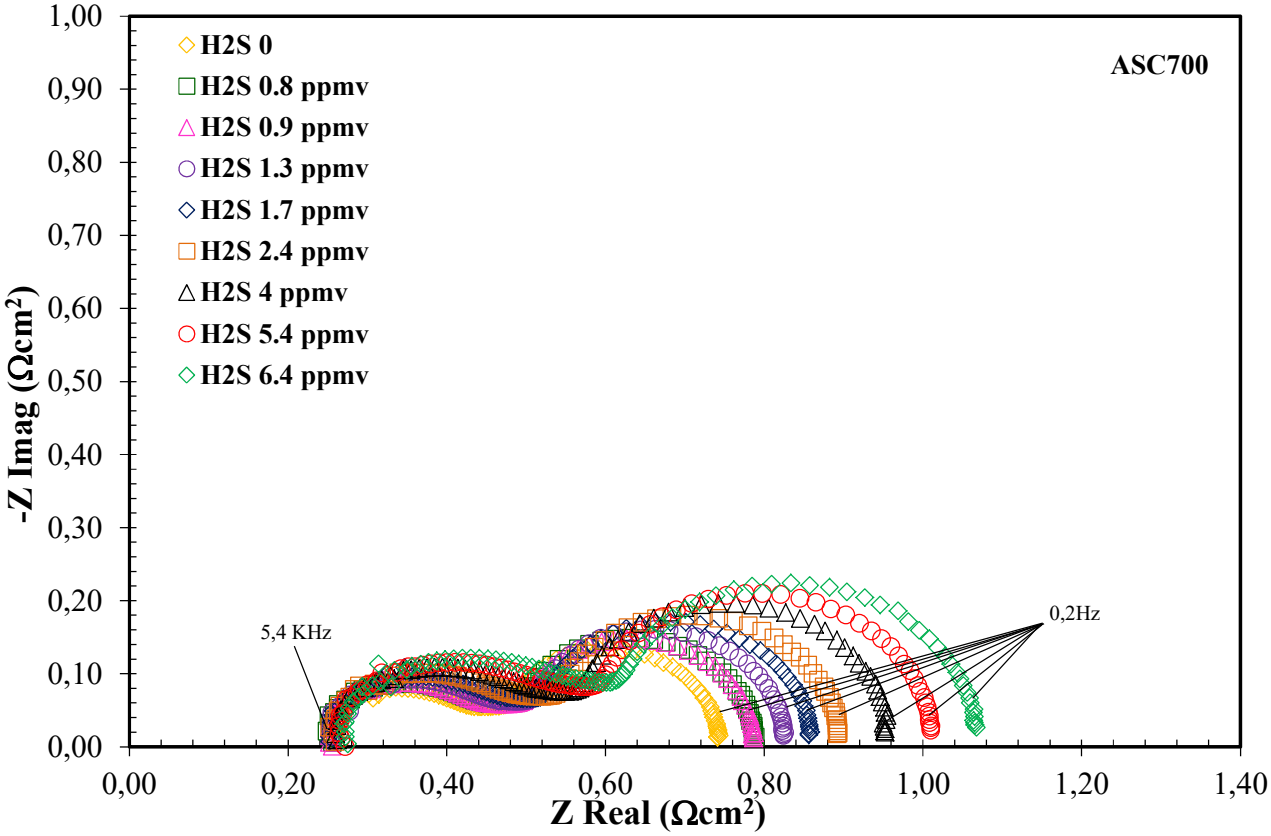
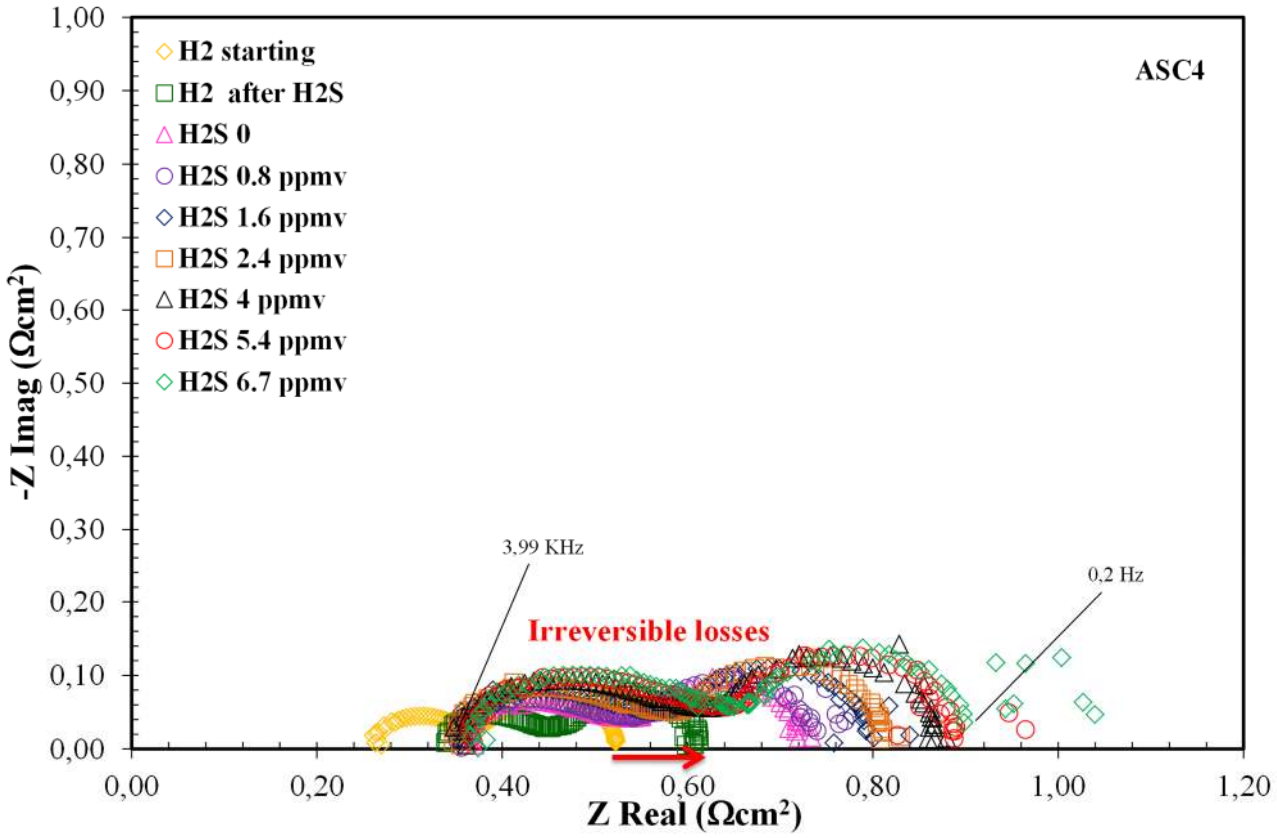


Figure 2


H2S 0
H2S 0.8 ppmv
H2S 0.9 ppmv
H2S 1.3 ppmv
H2S 1.7 ppmv
H2S 2.4 ppmv
H2S 4 ppmv
H2S 5.4 ppmv
H2S 6.4 ppmv
ASC700
5,4 KHz
0,2Hz
-Z Imag (Ωcm²)
Z Real (Ωcm²)
1,00
0,90
0,80
0,70
0,60
0,50
0,40
0,30
0,20
0,10
0,00
0,00
0,20
0,40
0,60
0,80
1,00
1,20
1,40

78 **Figure 3**



79

80

81

82

83

84

85

86

87

88

Figure 4

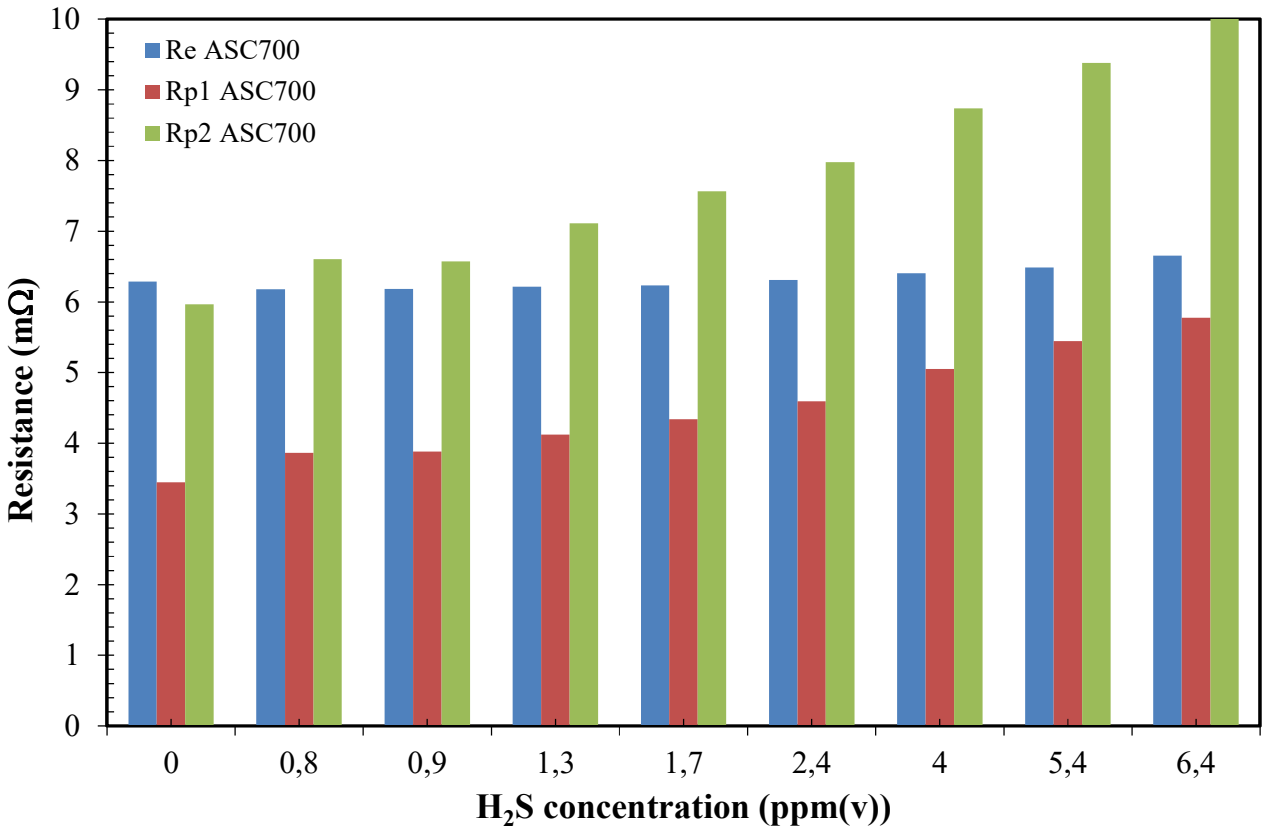

Re ASC700
Rp1 ASC700
Rp2 ASC700
Resistance (mΩ)
0
1
2
3
4
5
6
7
8
9
10
0
0,8
0,9
1,3
1,7
2,4
4
5,4
6,4
H2S concentration (ppm(v))

Figure 5

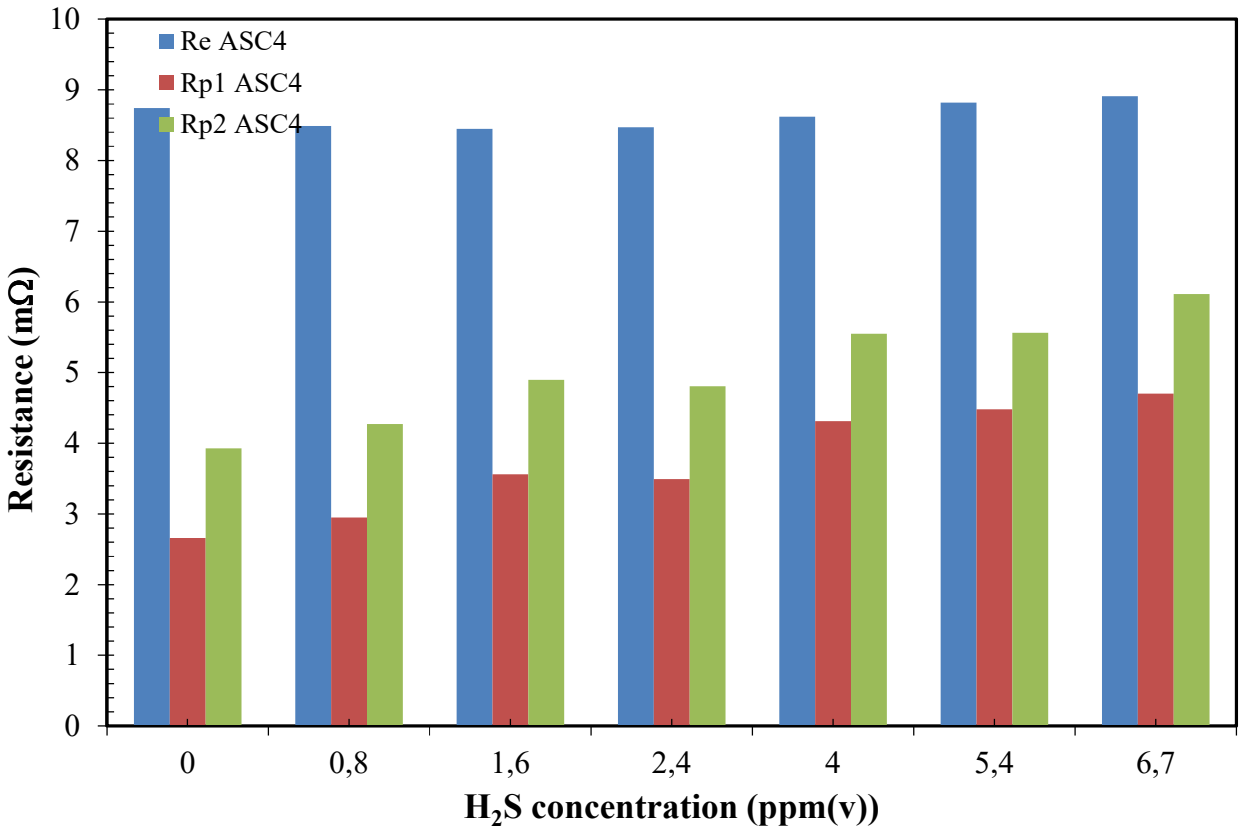

Re ASC4
Rp1 ASC4
Rp2 ASC4
Resistance (mΩ)
0
1
2
3
4
5
6
7
8
9
10
0
0,8
1,6
2,4
4
5,4
6,7
H2S concentration (ppm(v))

Figure 6

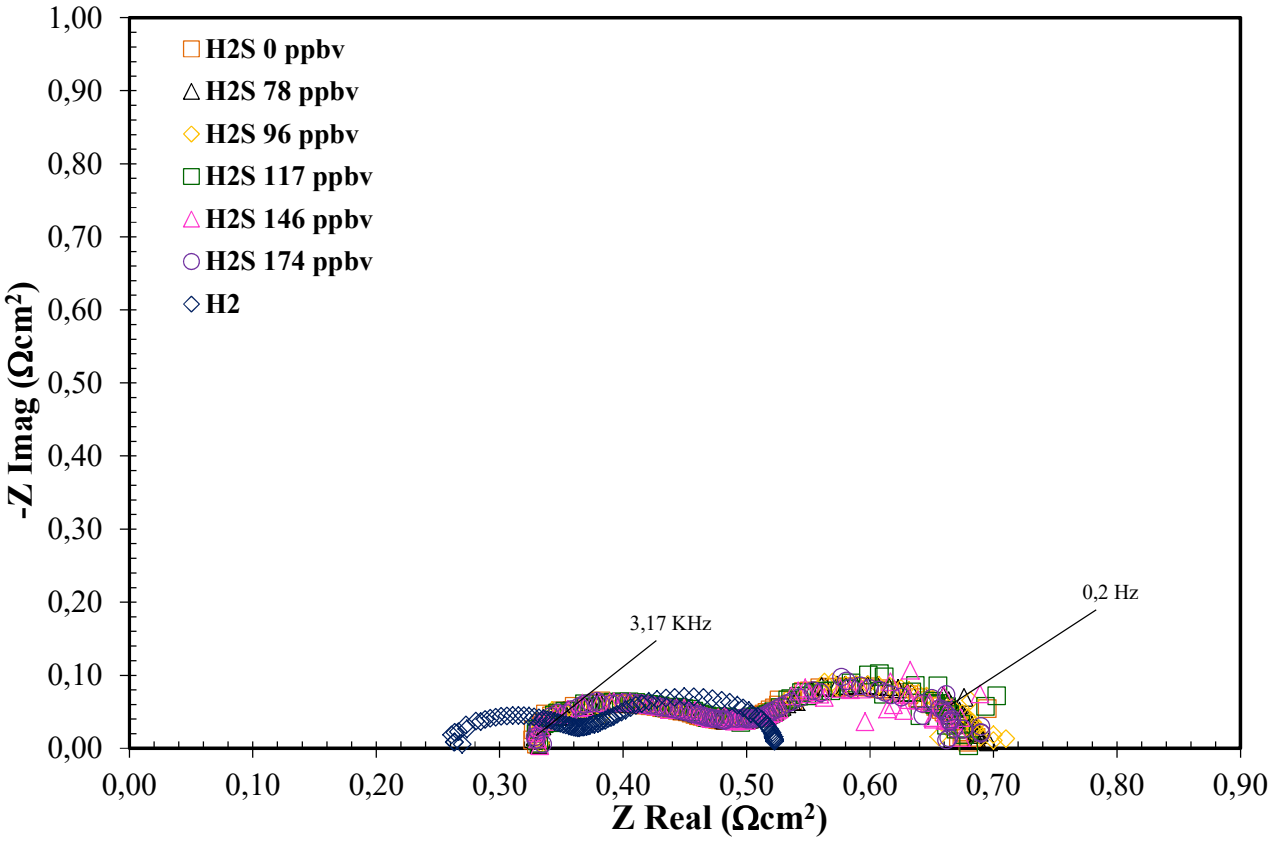

H2S 0 ppbv
H2S 78 ppbv
H2S 96 ppbv
H2S 117 ppbv
H2S 146 ppbv
H2S 174 ppbv
H2
-Z Imag (Ωcm²)
Z Real (Ωcm²)
3,17 KHz
0,2 Hz
1,00
0,90
0,80
0,70
0,60
0,50
0,40
0,30
0,20
0,10
0,00
0,00
0,10
0,20
0,30
0,40
0,50
0,60
0,70
0,80
0,90

Figure 7

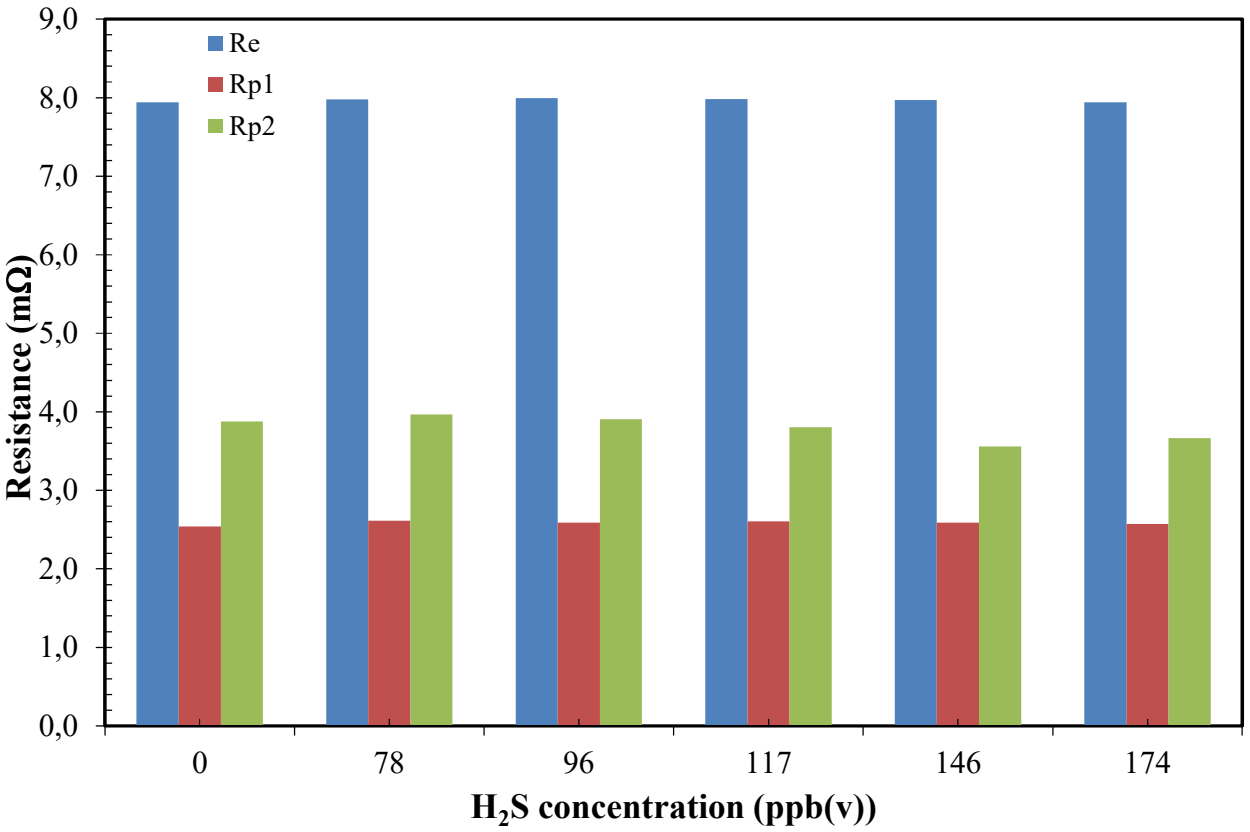
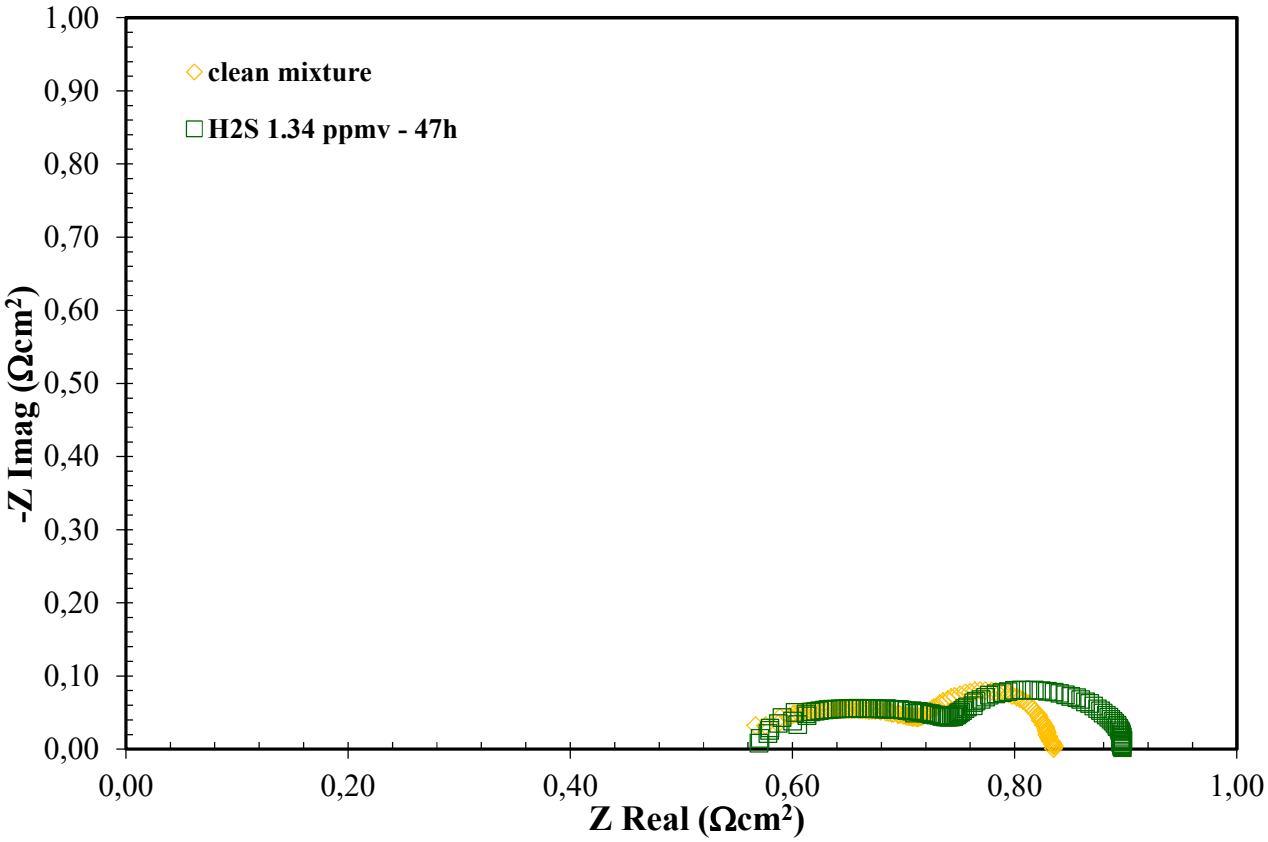
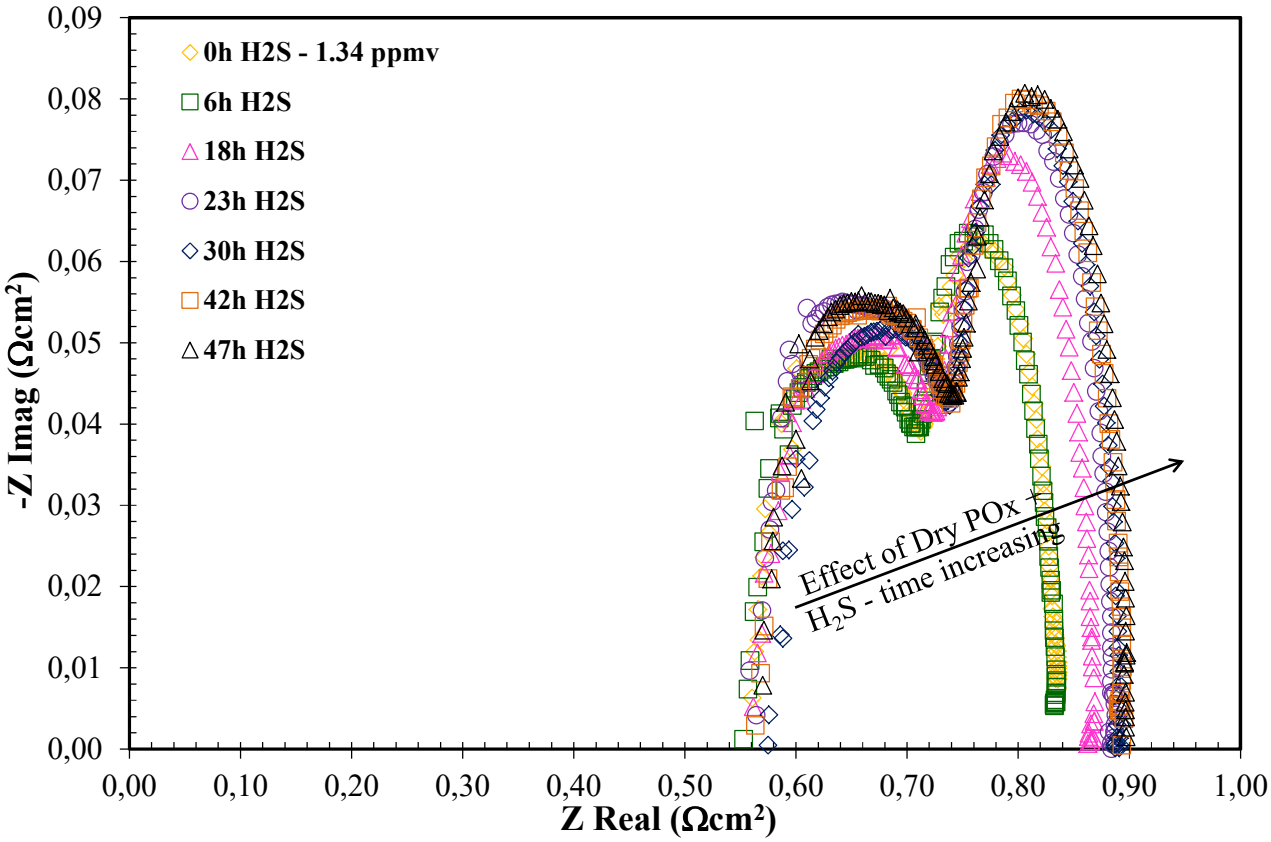

Re
Rp1
Rp2
Resistance (mΩ)
9,0
8,0
7,0
6,0
5,0
4,0
3,0
2,0
1,0
0,0
0
78
96
117
146
174
H2S concentration (ppb(v))

Figure 8


clean mixture
H2S 1.34 ppmv - 47h
-Z Imag (Ωcm²)
Z Real (Ωcm²)
1,00
0,90
0,80
0,70
0,60
0,50
0,40
0,30
0,20
0,10
0,00
0,00
0,20
0,40
0,60
0,80
1,00

144 **Figure 9**



145

146

147

148

149

150

151

152

153

154

Figure 10

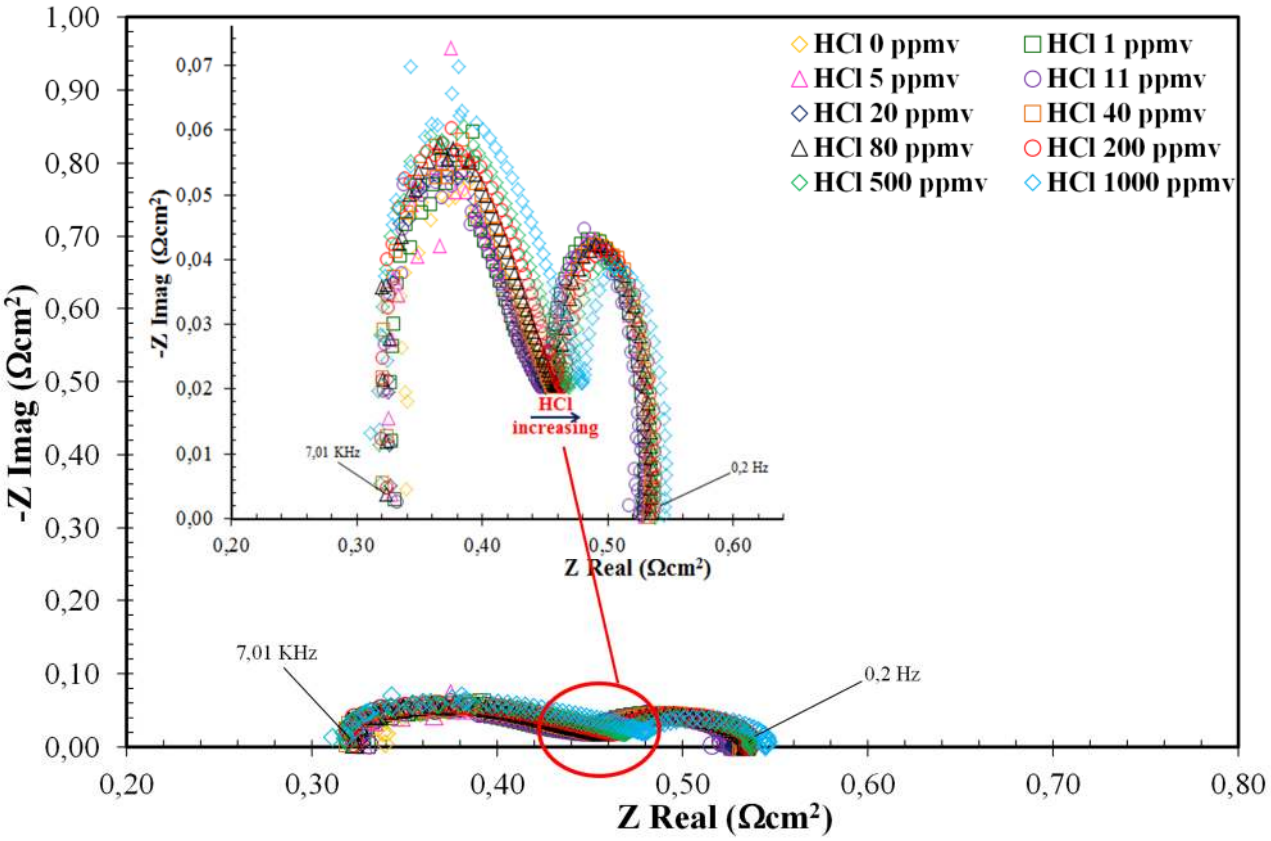
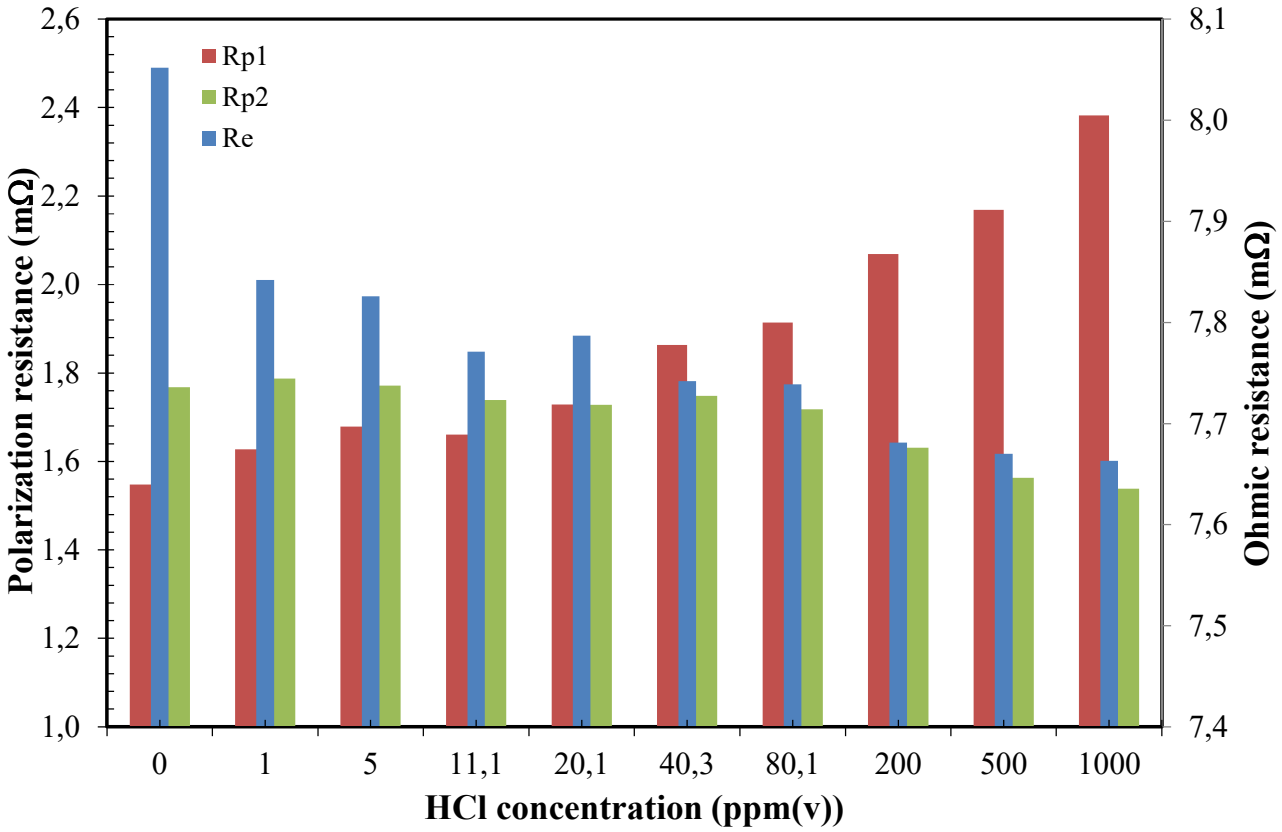
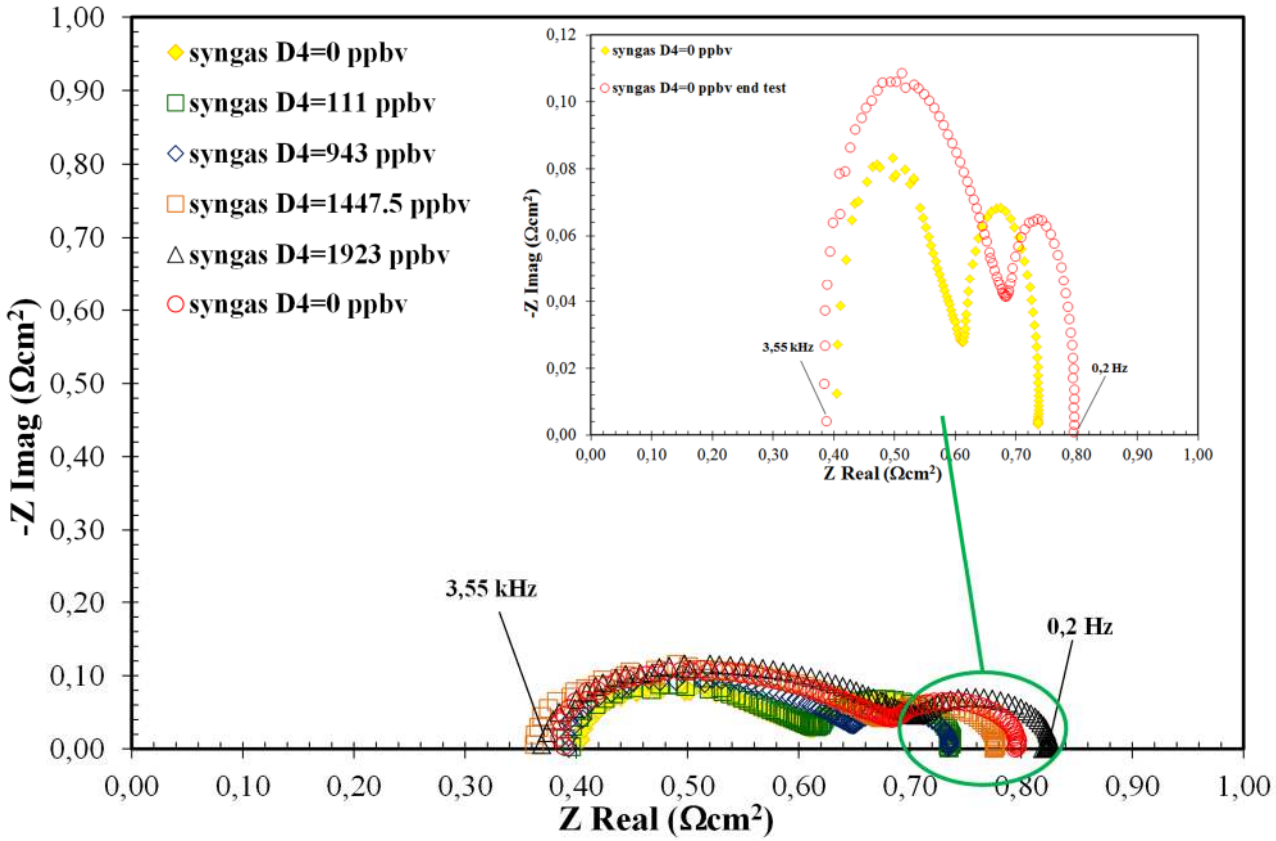

HCl 0 ppmv
HCl 1 ppmv
HCl 5 ppmv
HCl 11 ppmv
HCl 20 ppmv
HCl 40 ppmv
HCl 80 ppmv
HCl 200 ppmv
HCl 500 ppmv
HCl 1000 ppmv
-Z Imag (Ωcm²)
Z Real (Ωcm²)
HCl increasing
7,01 KHz
0,2 Hz

Figure 11


Rp1
Rp2
Re
Polarization resistance (mΩ)
Ohmic resistance (mΩ)
HCl concentration (ppm(v))
2,6
2,4
2,2
2,0
1,8
1,6
1,4
1,2
1,0
8,1
8,0
7,9
7,8
7,7
7,6
7,5
7,4
0
1
5
11,1
20,1
40,3
80,1
200
500
1000

177 **Figure 12**



178

179

180

181

182

183

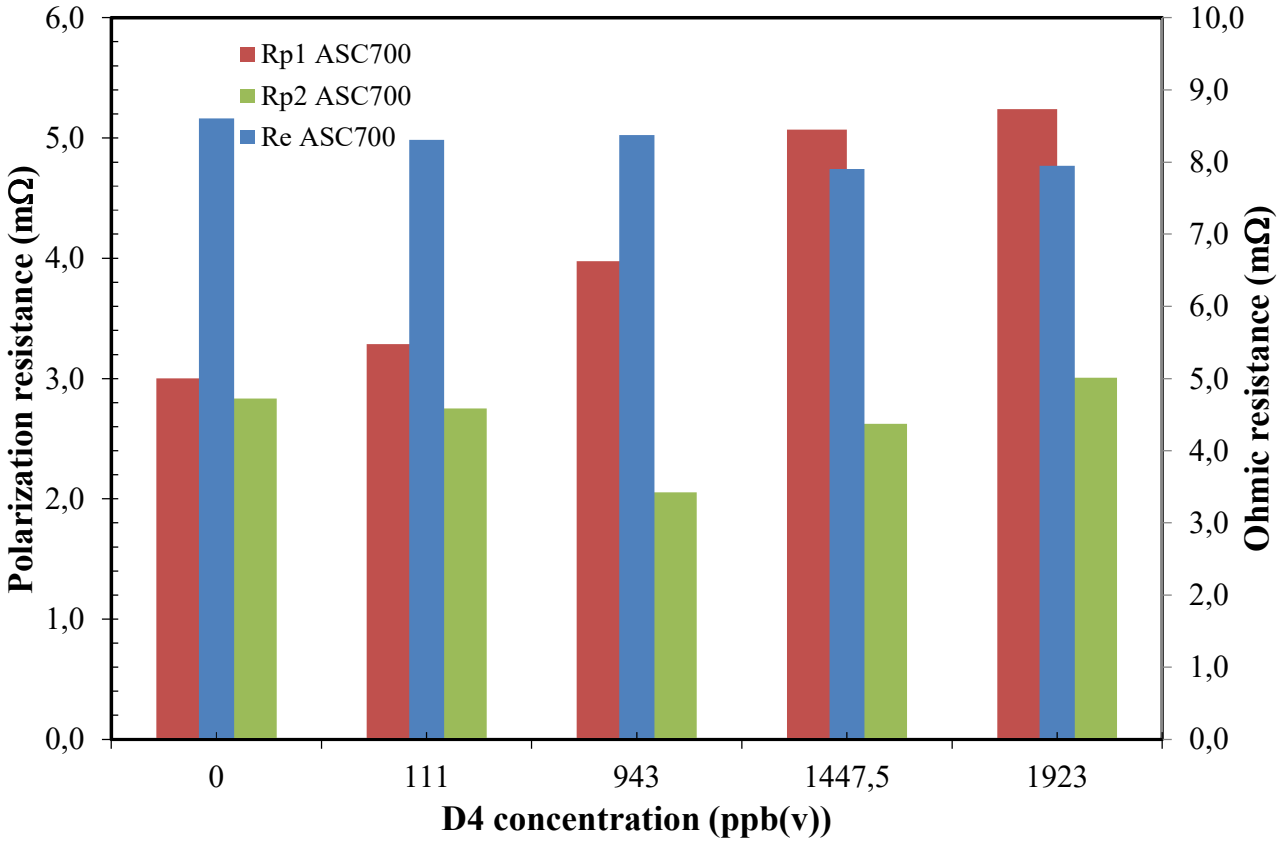
184

185

186

187

188 **Figure 13**



189

190

191

192

193

194

195

196

197

198

Figure 14

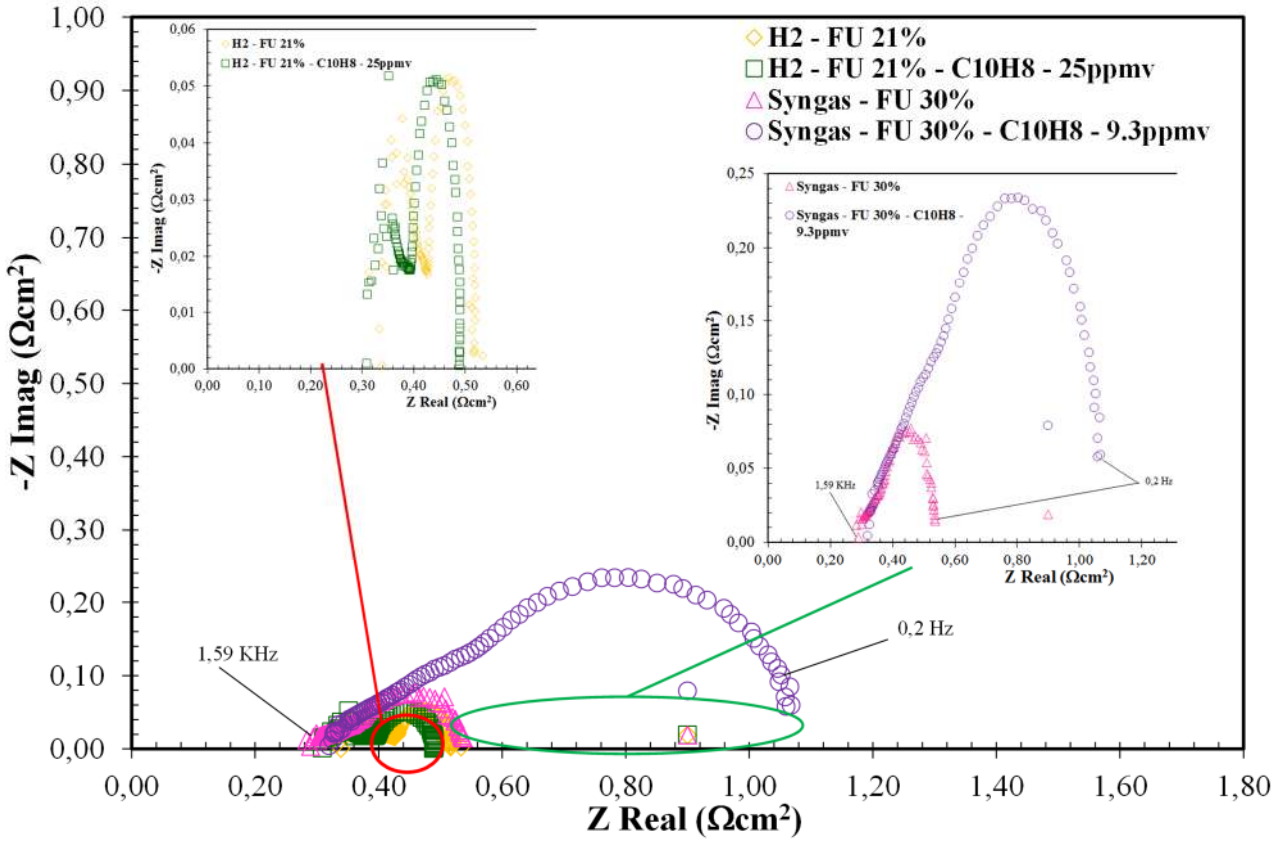

H2 - FU 21%
H2 - FU 21% - C10H8 - 25ppmv
Syngas - FU 30%
Syngas - FU 30% - C10H8 - 9.3ppmv
1,59 KHz
0,2 Hz
-Z Imag (Ωcm²)
Z Real (Ωcm²)

Figure 15

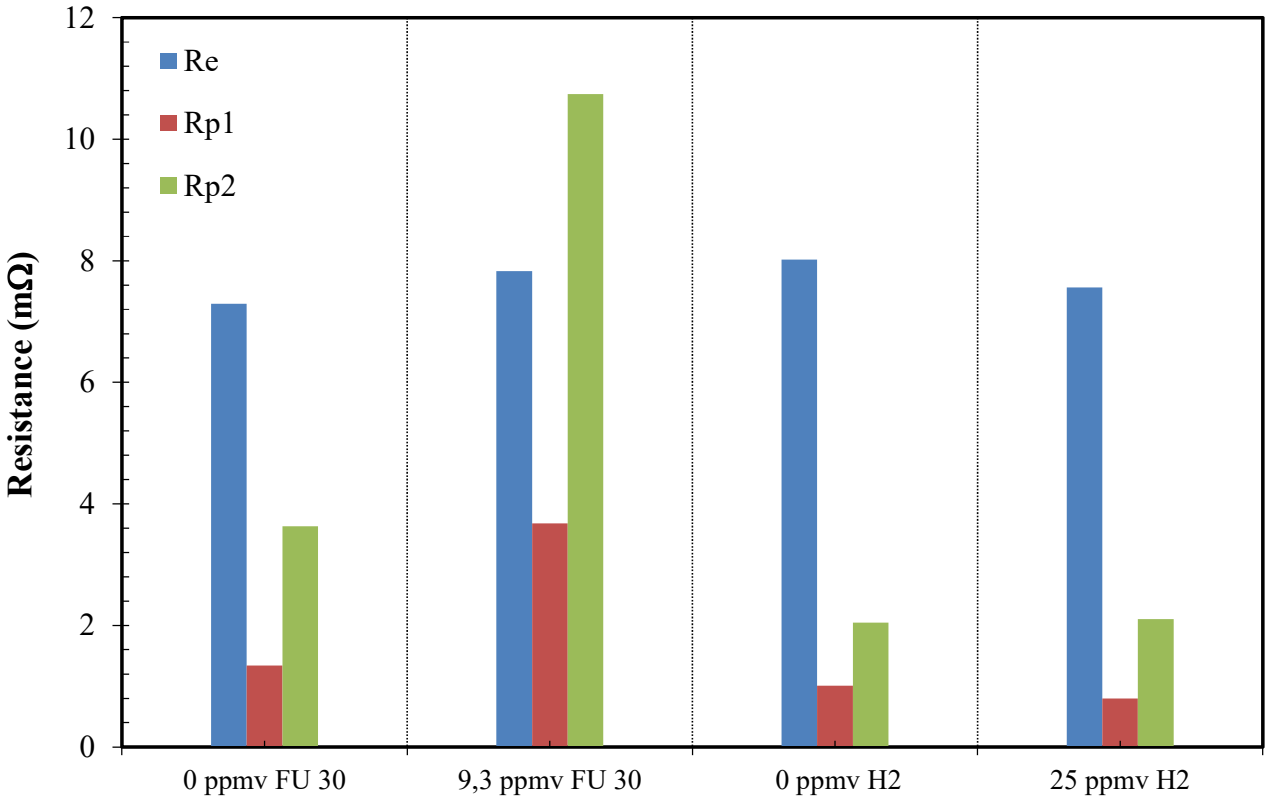

Re
Rp1
Rp2
Resistance (mΩ)
12
10
8
6
4
2
0
0 ppmv FU 30
9,3 ppmv FU 30
0 ppmv H2
25 ppmv H2

Figure 16

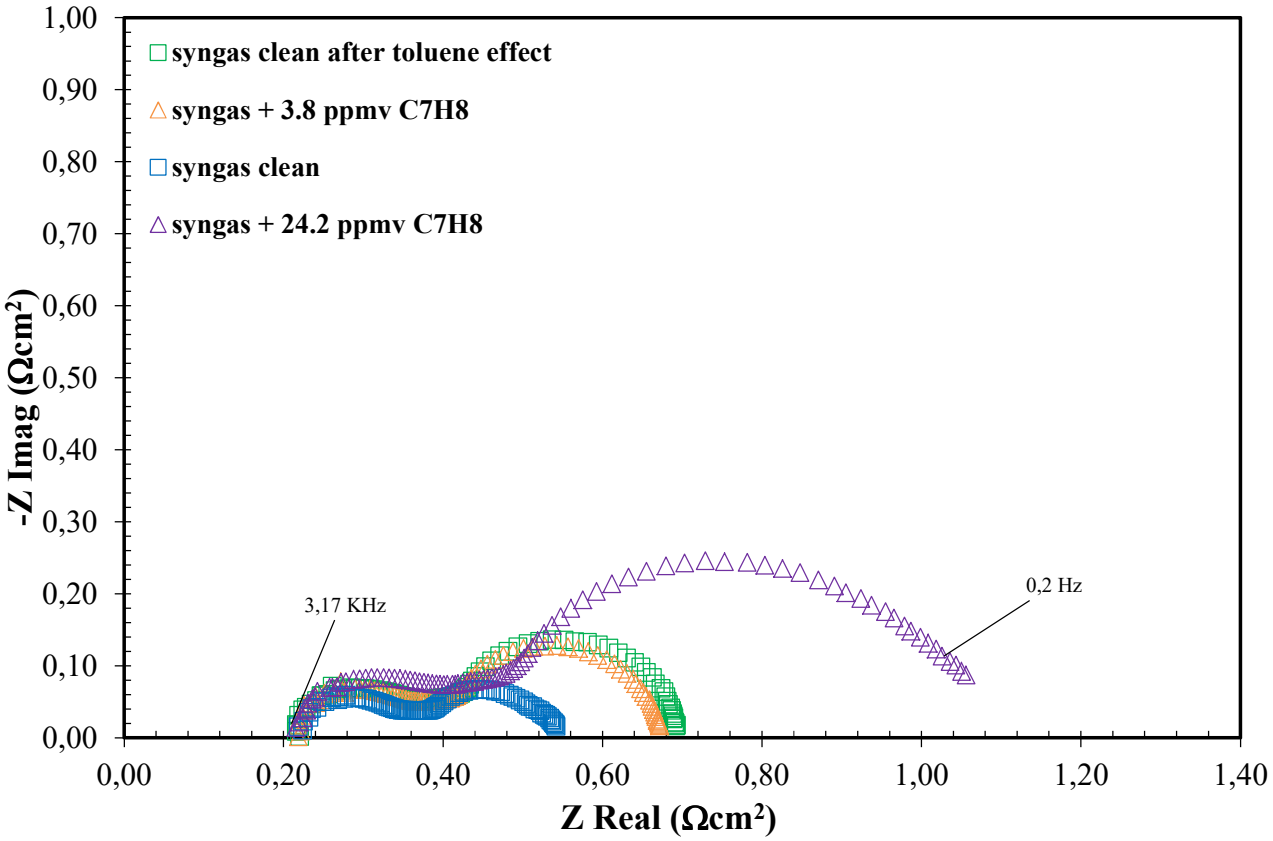

syngas clean after toluene effect
syngas + 3.8 ppmv C7H8
syngas clean
syngas + 24.2 ppmv C7H8
-Z Imag (Ωcm²)
Z Real (Ωcm²)
3,17 KHz
0,2 Hz
1,00
0,90
0,80
0,70
0,60
0,50
0,40
0,30
0,20
0,10
0,00
0,00
0,20
0,40
0,60
0,80
1,00
1,20
1,40

Figure 17

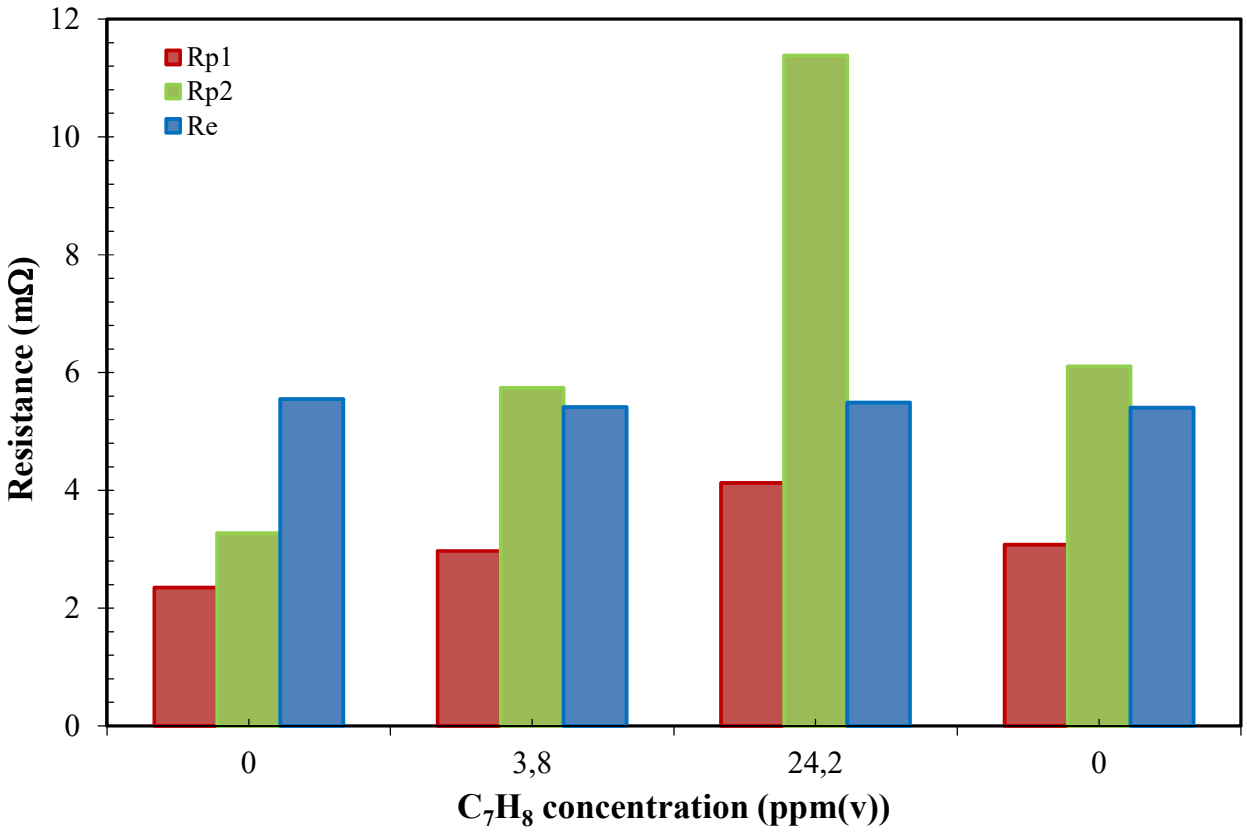

12
10
8
6
4
2
0
Resistance (mΩ)
Rp1
Rp2
Re
0
3,8
24,2
0
C7H8 concentration (ppm(v))

Figure 18

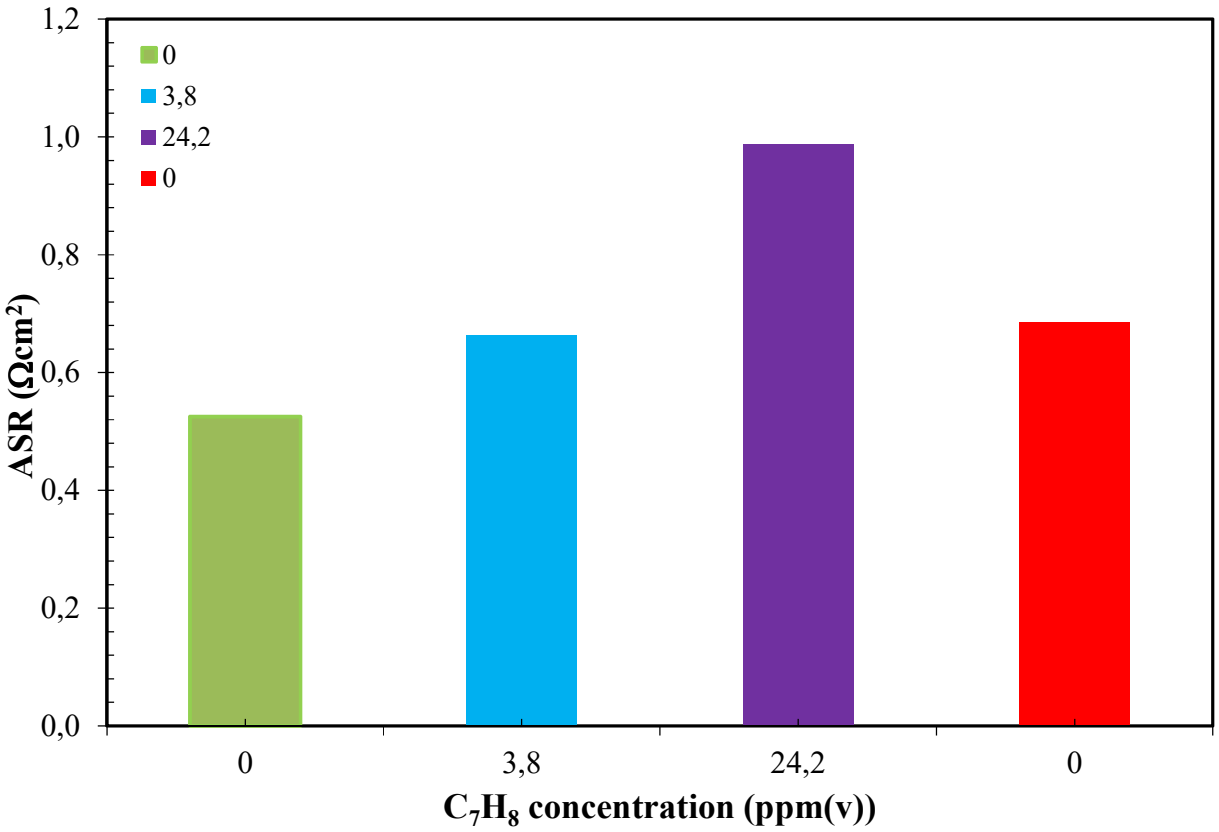

1,2
1,0
0,8
0,6
0,4
0,2
0,0
ASR (Ωcm²)
0
3,8
24,2
0
0
3,8
24,2
0
C7H8 concentration (ppm(v))

Figure 19

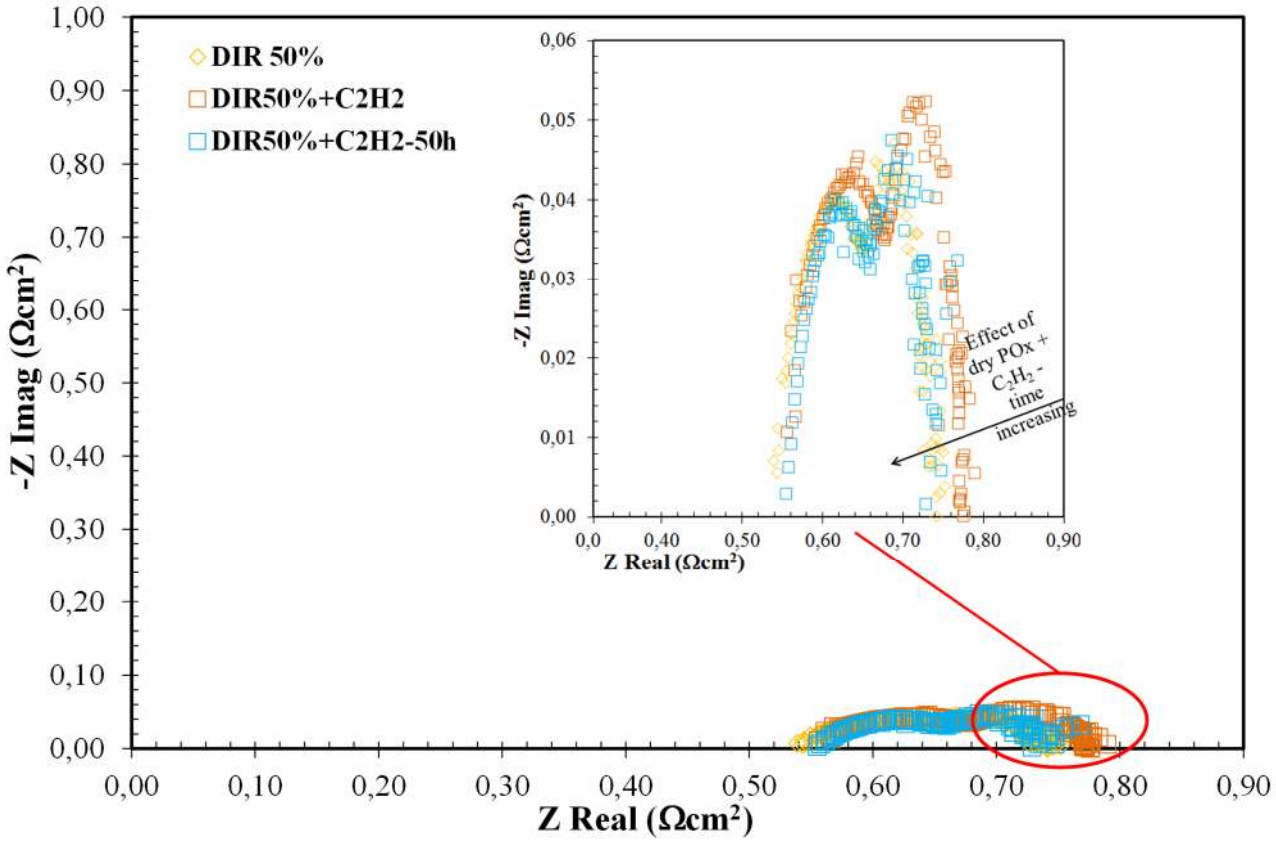

DIR 50%
DIR50%+C2H2
DIR50%+C2H2-50h
-Z Imag (Ωcm²)
Z Real (Ωcm²)
Effect of dry POx + C2H2 - time increasing

Figure 20

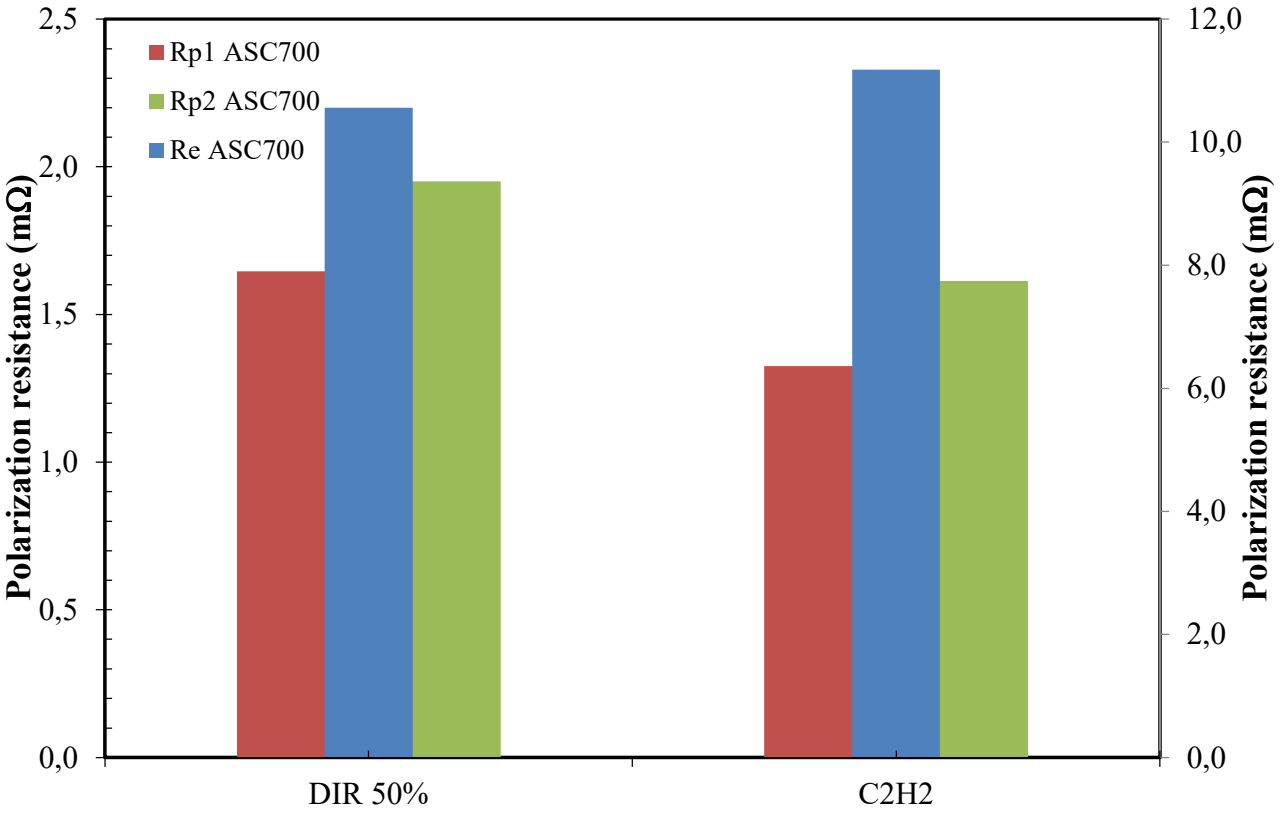

Rp1 ASC700
Rp2 ASC700
Re ASC700
Polarization resistance (mΩ)
Polarization resistance (mΩ)
2,5
2,0
1,5
1,0
0,5
0,0
12,0
10,0
8,0
6,0
4,0
2,0
0,0
DIR 50%
C2H2

Figure 21

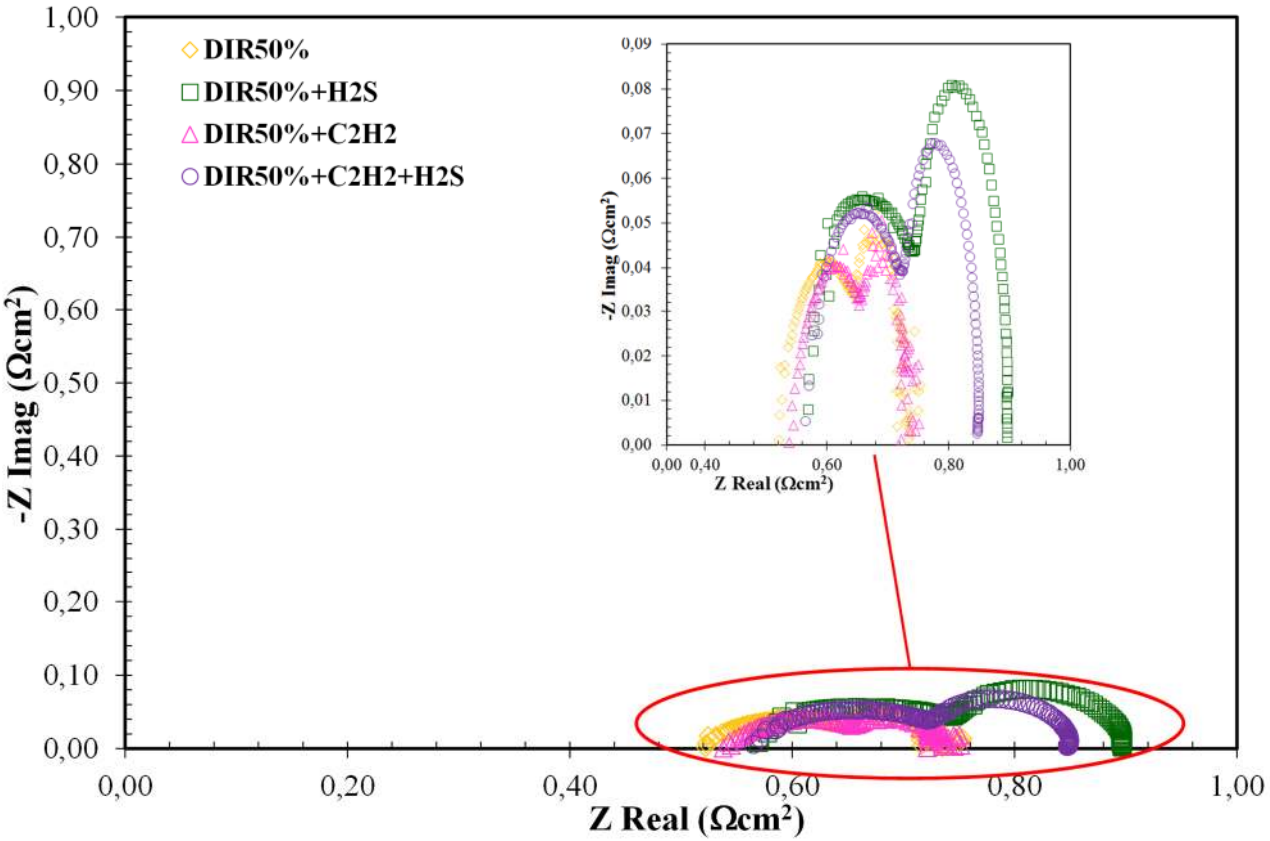

DIR50%
DIR50%+H2S
DIR50%+C2H2
DIR50%+C2H2+H2S
-Z Imag (Ωcm²)
Z Real (Ωcm²)
1,00
0,90
0,80
0,70
0,60
0,50
0,40
0,30
0,20
0,10
0,00
0,20
0,40
0,60
0,80
1,00
0,09
0,08
0,07
0,06
0,05
0,04
0,03
0,02
0,01
0,00

Figure 22

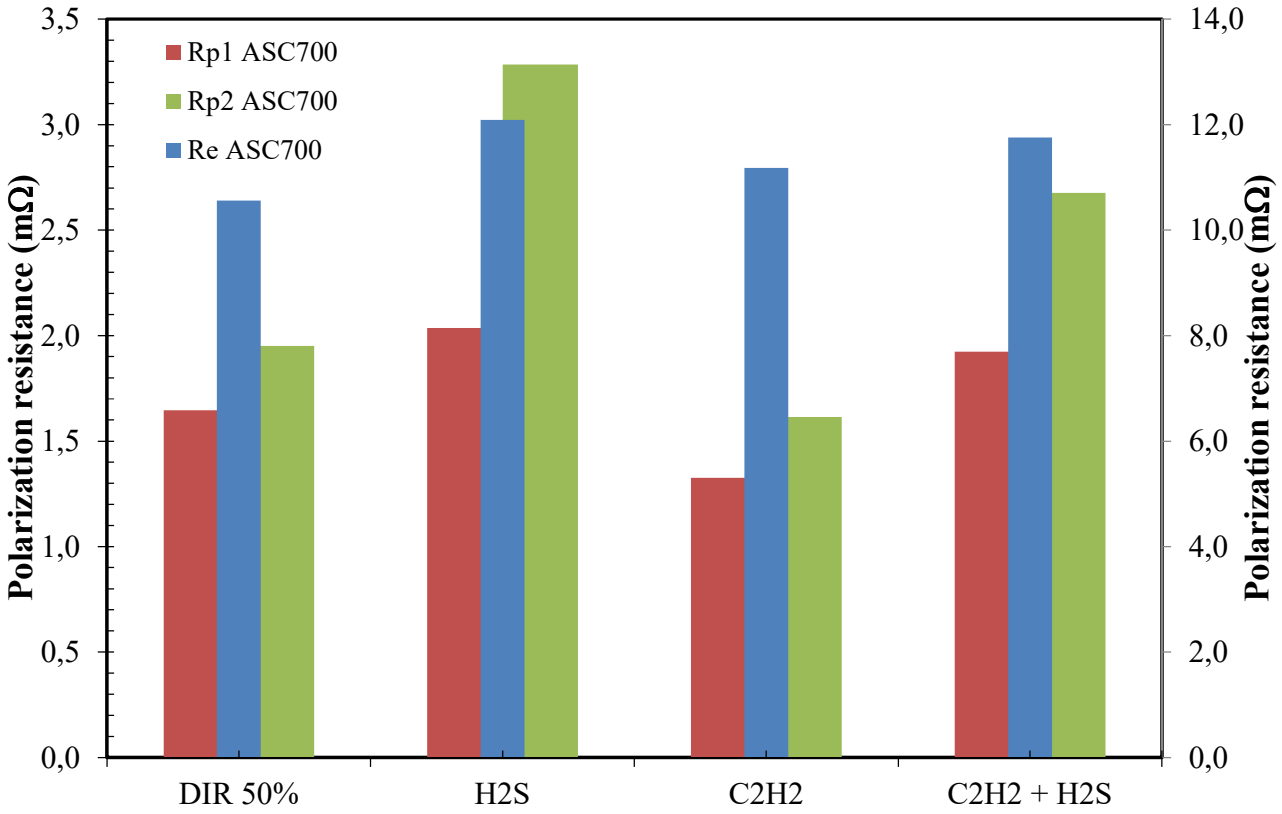

Rp1 ASC700
Rp2 ASC700
Re ASC700
Polarization resistance (mΩ)
Polarization resistance (mΩ)
3,5
3,0
2,5
2,0
1,5
1,0
0,5
0,0
14,0
12,0
10,0
8,0
6,0
4,0
2,0
0,0
DIR 50%
H2S
C2H2
C2H2 + H2S

Figure 23

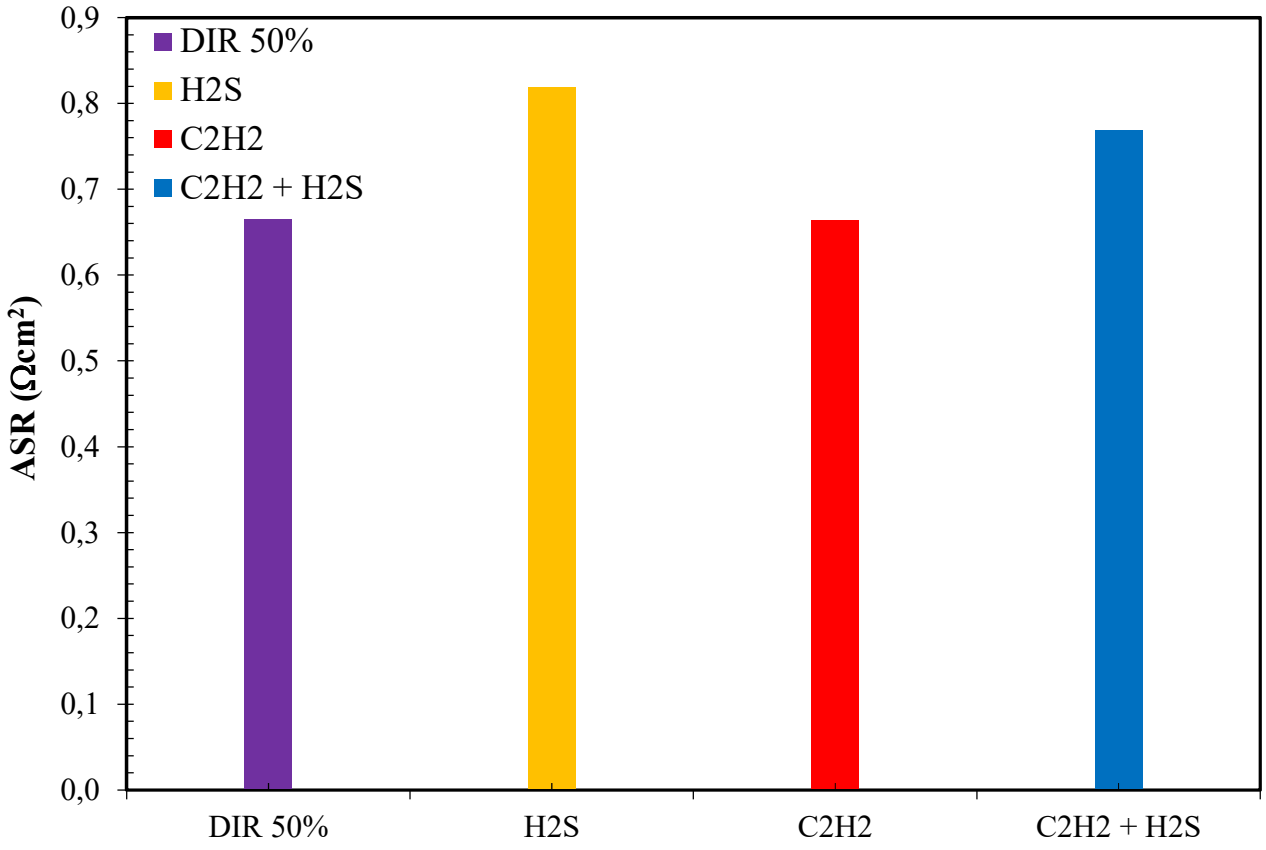

0,9
0,8
0,7
0,6
0,5
0,4
0,3
0,2
0,1
0,0
ASR (Ωcm²)
DIR 50%
H2S
C2H2
C2H2 + H2S
DIR 50%
H2S
C2H2
C2H2 + H2S

Figure 24

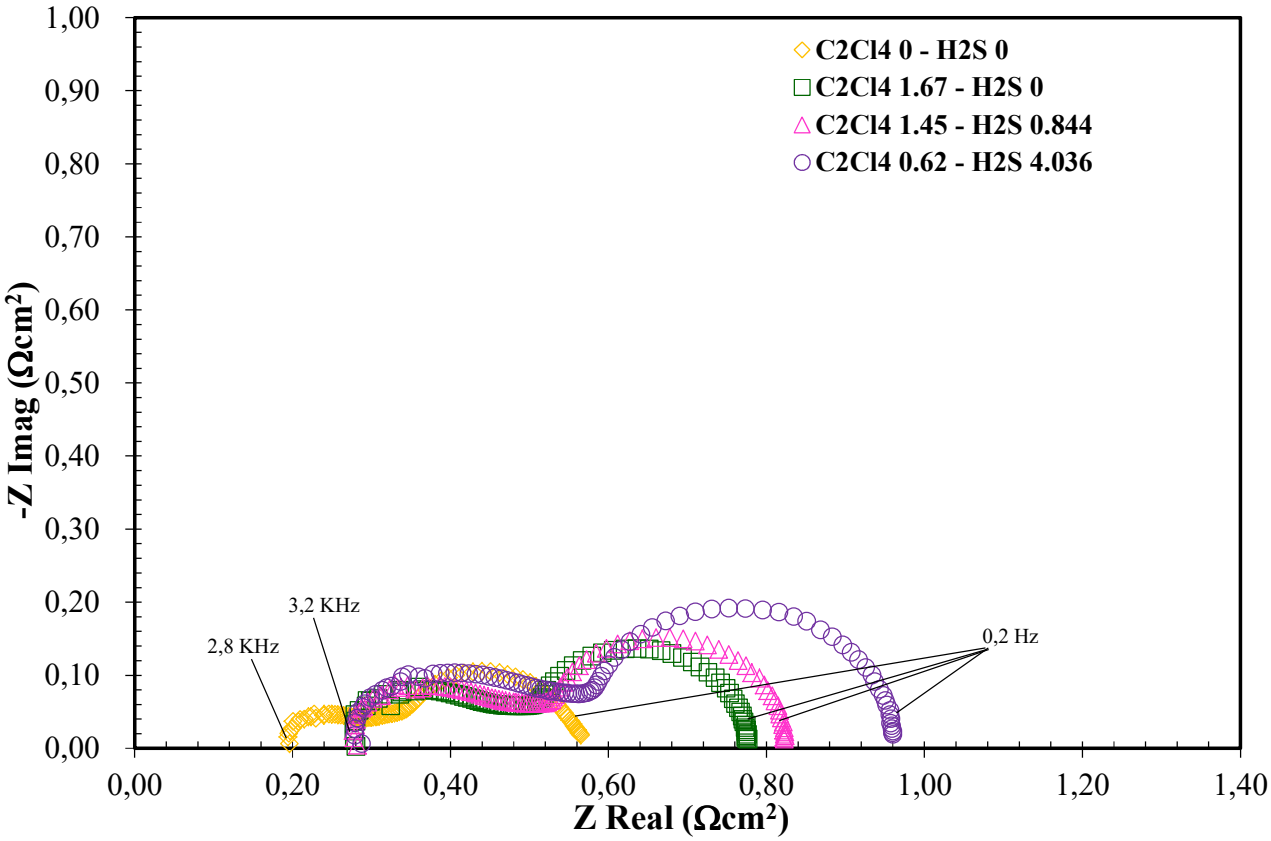
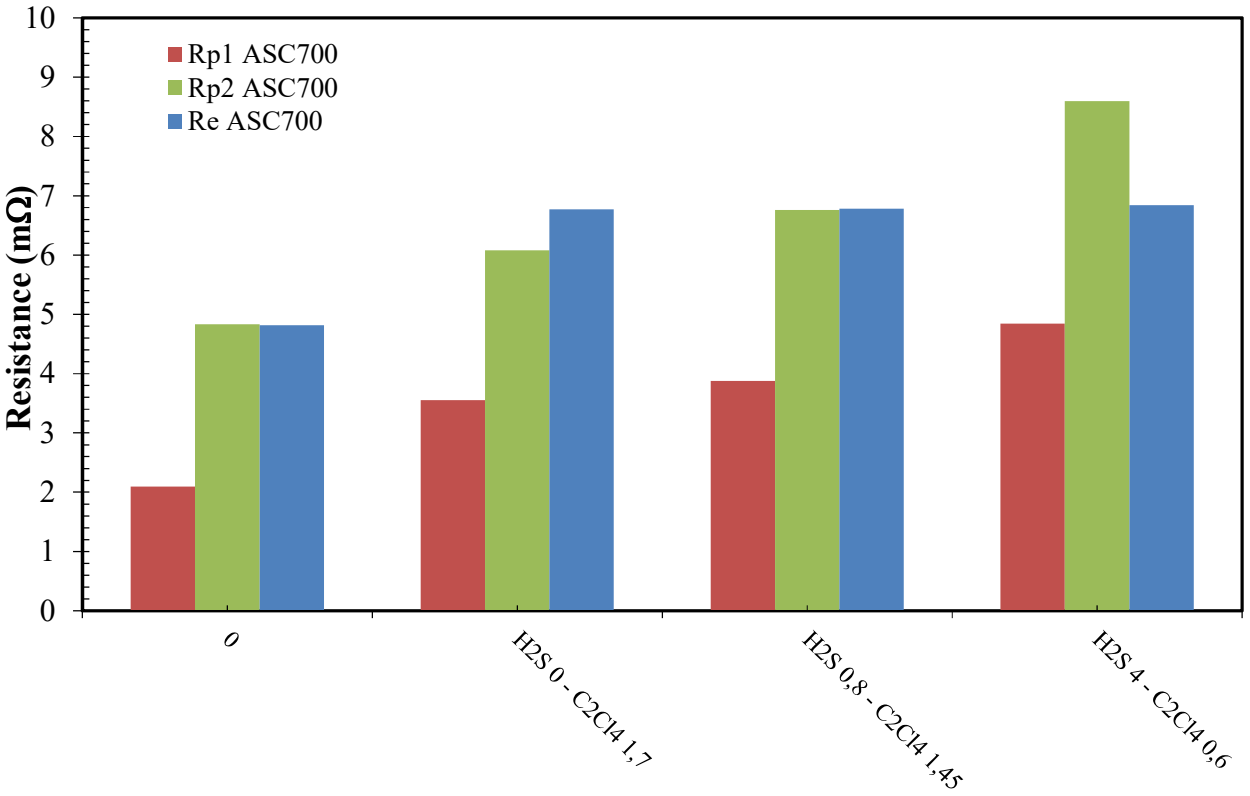
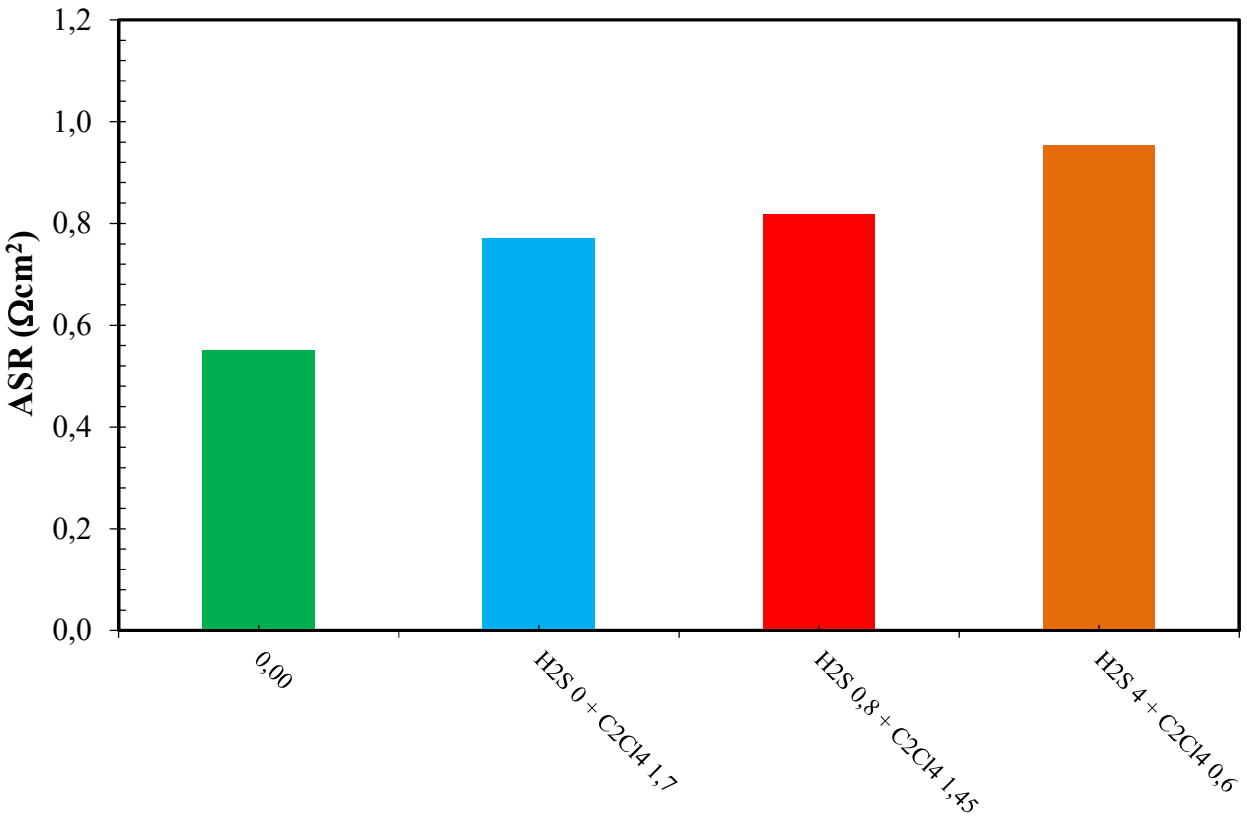

C2Cl4 0 - H2S 0
C2Cl4 1.67 - H2S 0
C2Cl4 1.45 - H2S 0.844
C2Cl4 0.62 - H2S 4.036
-Z Imag (Ωcm²)
Z Real (Ωcm²)
1,00
0,90
0,80
0,70
0,60
0,50
0,40
0,30
0,20
0,10
0,00
0,00
0,20
0,40
0,60
0,80
1,00
1,20
1,40
2,8 KHz
3,2 KHz
0,2 Hz

Figure 25


Rp1 ASC700
Rp2 ASC700
Re ASC700
Resistance (mΩ)
10
9
8
7
6
5
4
3
2
1
0
0
H2S 0 - C2Cl4 1,7
H2S 0,8 - C2Cl4 1,45
H2S 4 - C2Cl4 0,6

331 **Figure 26**



332

333

334

335

336

337

338

339

340

341

Figure 27

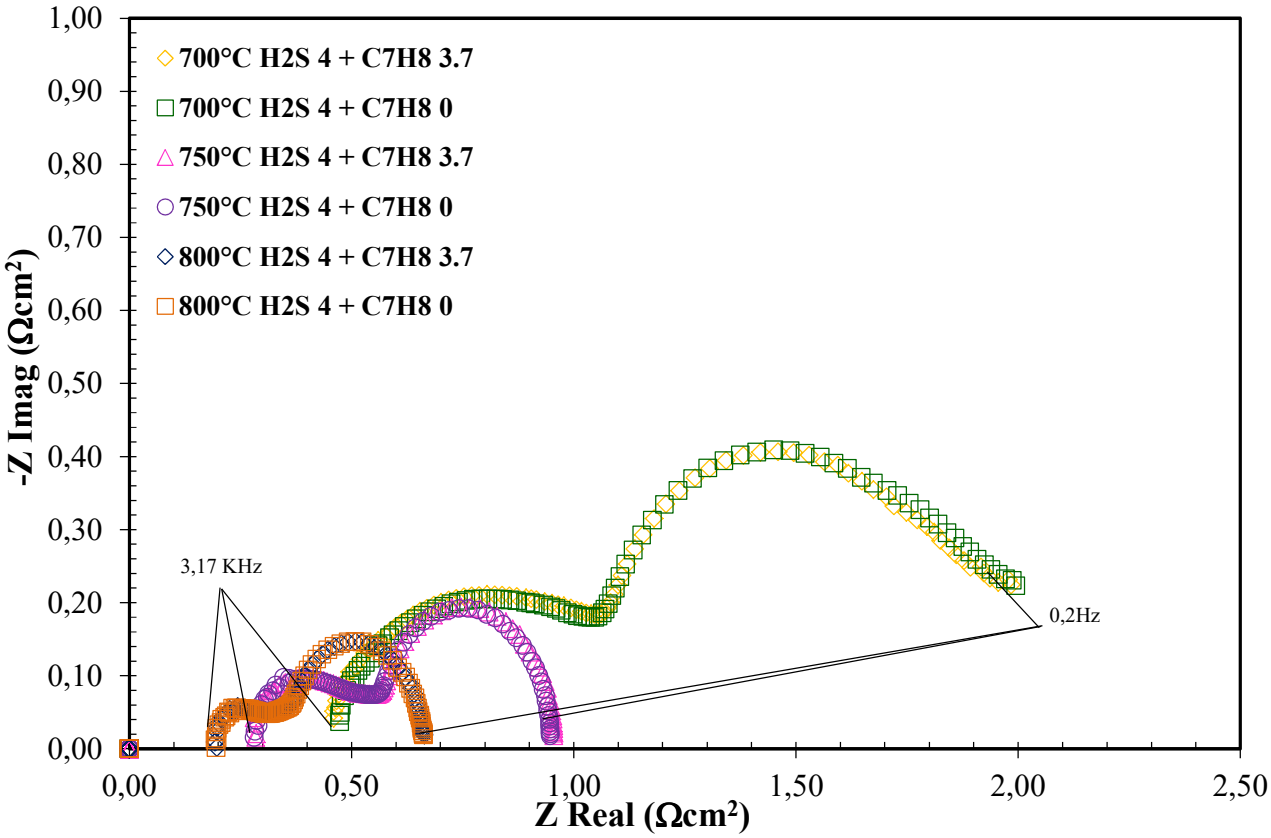

700°C H2S 4 + C7H8 3.7
700°C H2S 4 + C7H8 0
750°C H2S 4 + C7H8 3.7
750°C H2S 4 + C7H8 0
800°C H2S 4 + C7H8 3.7
800°C H2S 4 + C7H8 0
-Z Imag (Ωcm²)
Z Real (Ωcm²)
3,17 KHz
0,2Hz
0,00
0,10
0,20
0,30
0,40
0,50
0,60
0,70
0,80
0,90
1,00
0,00
0,50
1,00
1,50
2,00
2,50

Figure 28

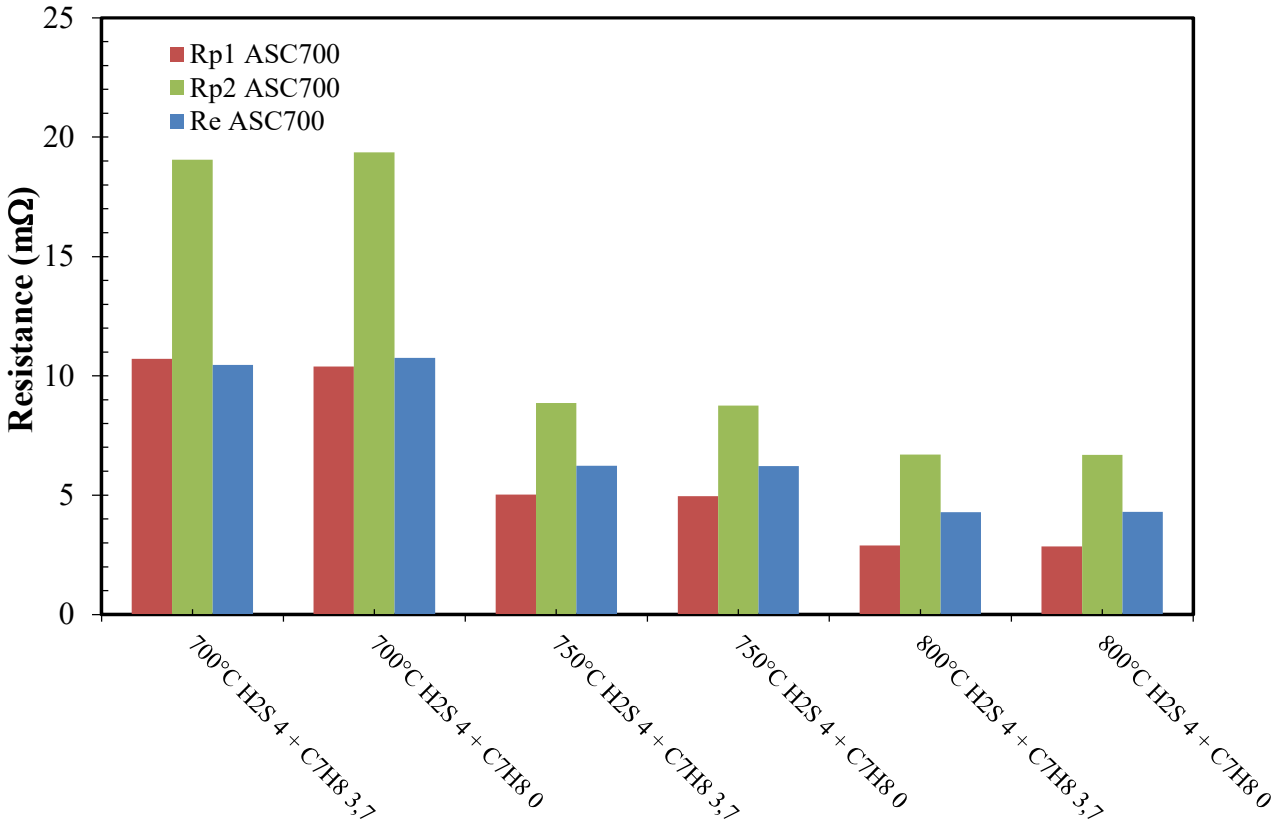
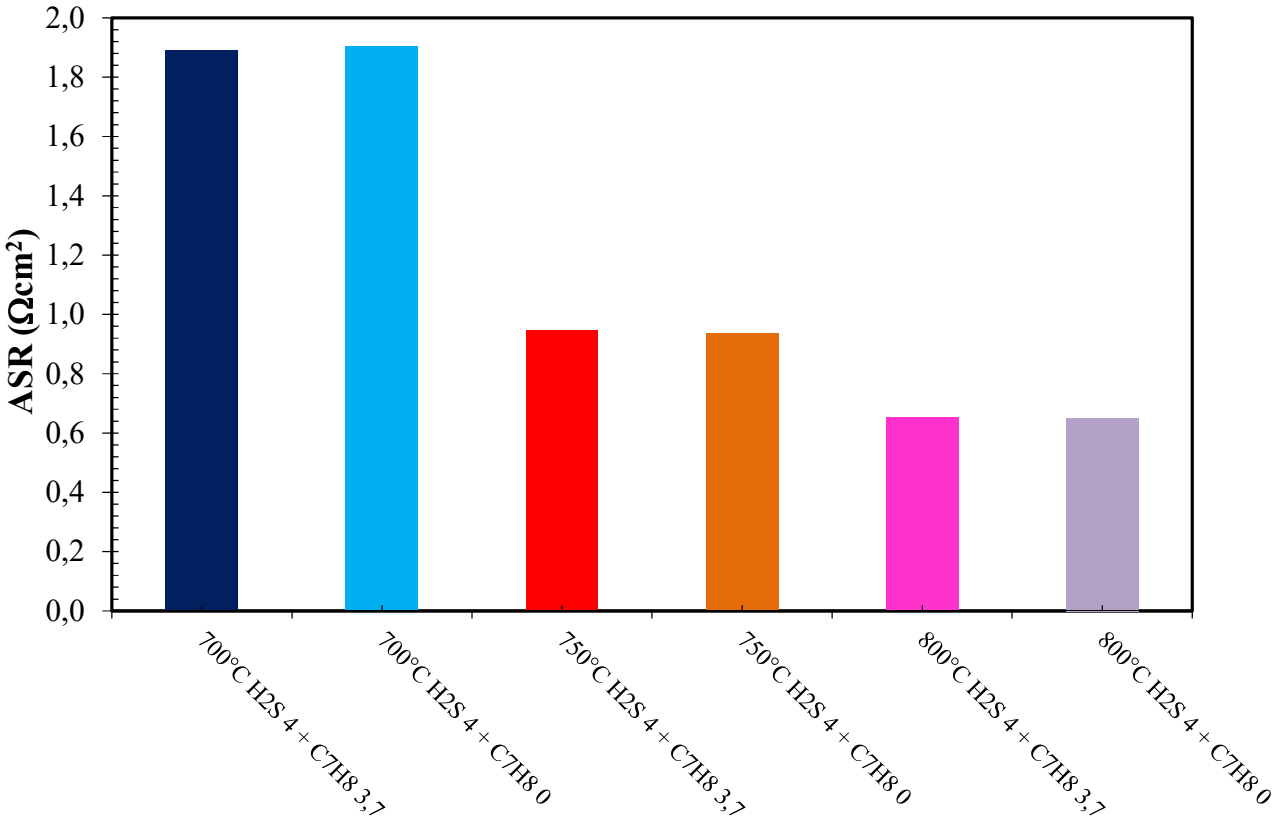

Rp1 ASC700
Rp2 ASC700
Re ASC700
Resistance (mΩ)
25
20
15
10
5
0
700°C H2S 4 + C7H8 3,7
700°C H2S 4 + C7H8 0
750°C H2S 4 + C7H8 3,7
750°C H2S 4 + C7H8 0
800°C H2S 4 + C7H8 3,7
800°C H2S 4 + C7H8 0

Figure 29


ASR (Ωcm²)
2,0
1,8
1,6
1,4
1,2
1,0
0,8
0,6
0,4
0,2
0,0
700°C H2S 4 + C7H8 3,7
700°C H2S 4 + C7H8 0
750°C H2S 4 + C7H8 3,7
750°C H2S 4 + C7H8 0
800°C H2S 4 + C7H8 3,7
800°C H2S 4 + C7H8 0

375

376

377

378